

**BURSA TECHNICAL UNIVERSITY ❖ GRADUATE SCHOOL OF NATURAL
AND APPLIED SCIENCES**

**SYNTHESIS OF ANTIBACTERIAL POLYMERS REDUCING BIOFILM
FORMATION AND THEIR APPLICATION ON HOLLOW FIBER
MEMBRANES**



**Ph.D. THESIS
Fatma DEMİRCİ**

Department of Fiber and Polymer Engineering

OCTOBER 2018

**BURSA TECHNICAL UNIVERSITY ❖ GRADUATE SCHOOL OF NATURAL
AND APPLIED SCIENCES**

**SYNTHESIS OF ANTIBACTERIAL POLYMERS REDUCING BIOFILM
FORMATION AND THEIR APPLICATION ON HOLLOW FIBER
MEMBRANES**



Ph.D. THESIS

**Fatma DEMİRCİ
(141081001)**

Department of Fiber and Polymer Engineering

Thesis Advisor: Assoc. Prof. Dr. Hasan Basri KOÇER

OCTOBER 2018

Fatma Demirci, a Ph.D. student of BTU Graduate School of Natural and Applied Sciences student ID 141081001, successfully defended the thesis entitled “SYNTHESIS OF ANTIBACTERIAL POLYMERS REDUCING BIOFILM FORMATION AND THEIR APPLICATION ON HOLLOW FIBER MEMBRANES”, which she prepared after fulfilling the requirements specified in the associated legislations, before the jury whose signatures are below.

Thesis Advisor : **Assoc. Prof. Dr. Hasan Basri KOÇER**
Bursa Technical University

Jury Members : **Prof. Dr. Behçet BECERİR**
Bursa Uludağ University

Asst. Prof. Dr. Ayşe KALEMTAŞ
Bursa Technical University

Asst. Prof. Dr. Meral AKKOYUN
Bursa Technical University

Asst. Prof. Dr. Halil İbrahim AKYILDIZ.....
Bursa Uludağ University

Date of Defense : 30 October 2018

Director of the Institute: **Assoc. Prof. Dr. Murat ERTAŞ**
Bursa Technical University /...../.....

PLAGIARISM STATEMENT

I hereby declare that all information and results presented in visual, auditory and written form in this thesis has been obtained and presented in accordance with academic rules and ethical conduct. I also declare that, as required by these rules and conduct, I have fully cited and referenced all material and results that are not original to this work, and that I accept all kinds of legal conclusions in the case of the contrary.

Student Name Surname : Fatma DEMİRCİ

Signature :





To my spouse and family,

FOREWORD

There are many people who have been helpful in a variety ways for the completion of this work. First and foremost, I would like to express my deepest gratitude to my supervisor, Assoc. Prof. Dr. Hasan Basri KOÇER for his support, guidance, and suggestions in this thesis research.

I would like to thank the members of my Dissertation committee for their time, constructive input and contributions.

I would like to express my deep thanks to all the members of “Koçer Research Group”. In particular, special thanks to Res. Asst. Ahmet AYDIN, Res. Asst. Büşra ATEŞ and Instructor Zeynep ORDU, for their help, friendship and the nice environment they created not only inside, but also outside the lab.

The author is owed a tremendous appreciation to MSc. Emel TAŞYAKAN from Destek Automotive Supplier company for help to design and produce the hollow fiber spinning line. Thanks to Assoc. Prof. Dr. Onur SARAY and Res. Asst. Mümin YILMAZ for help to design and produce the spinneret. The author also owes a thank to Assoc. Prof. Dr. Mehmet ORHAN for running antibacterial tests.

I would like to thank to my friends, Asst. Prof. Dr. Burçak KAYA ÖZSEL, MSc. Zeynep YAĞAR, Res. Asst. Merve ALTAY and MSc. Betül Merve FAKI ÇAKIR for their moral supports and encouragements.

I also would like to thank my parents who raised me and support me spiritually throughout my life. Without their love, understanding and constant encouragement, I would never have come this far. I would also like to thank my sisters, brother and parents-in-law also for their encouragement and love.

Finally, I would like to express most special thanks to my dear husband, Emre DEMİRCİ for his constant support, love and encouragement throughout the preparation of this thesis.

October 2018

Fatma DEMİRCİ

TABLE OF CONTENTS

	<u>Page</u>
FOREWORD	v
TABLE OF CONTENTS	vi
ABBREVIATIONS	ix
SYMBOLS	x
LIST OF TABLES	xi
LIST OF FIGURES	xii
SUMMARY	xv
ÖZET	xvi
1. INTRODUCTION	1
1.1 Aim and Scope of the Thesis.....	3
1.2 Literature Review	3
1.2.1 An overview to membrane science and technology	3
1.2.1.1 Historical developments of membranes	3
1.2.1.2 Types of membranes	4
1.2.1.3 Membrane separation processes	7
1.2.2 Ultrafiltration membranes	8
1.2.2.1 Structure of ultrafiltration membranes	8
1.2.2.2 Membrane configurations and modules	9
1.2.2.3 Applications of ultrafiltration membranes	11
1.2.2.4 Ultrafiltration membranes for water treatments	12
1.2.2.5 Membrane fouling.....	12
1.2.3 Antibacterial agents.....	14
1.2.3.1 Common biocides	15
1.2.3.2 <i>N</i> -halamines.....	17
1.2.4 Antibacterial HFMs.....	18
1.2.5 <i>N</i> -halamine added antibacterial HFMs	19
2. SYNTHESIS OF <i>N</i>-HALAMINE POLYMERS AND THEIR INCORPORATION INTO PVDF ULTRAFILTRATION MEMBRANE STRUCTURE	20
2.1 Introduction	20
2.2 Experimental	21
2.2.1 Materials.....	21
2.2.2 Synthesis of <i>N</i> -halamine monomer and its polymers.....	22
2.2.3 Preparation of the ternary phase diagrams	23
2.2.4 Polymer blends and flat sheet membrane production	23
2.2.5 Chlorination of the produced membranes	24
2.2.6 Permeability tests of the produced membranes.....	25
2.2.7 Characterization of the produced membranes.....	26
2.3 Results and Discussion.....	27
2.3.1 Characterization of the synthesized monomer and polymers	27

2.3.2 Ternary phase diagram of the polymer/NMP/water system	29
2.3.3 Filtration and BSA rejection performance of the produced membranes...	30
2.3.4 FTIR and XPS characterization of the produced membranes	34
2.3.5 Thermal properties of the produced membranes.....	36
2.3.6 Morphology of the produced membranes	37
2.3.7 Biocidal performance of the produced membranes	39
2.4 Conclusion.....	41
3. PRODUCTION OF PVDF ULTRAFILTRATION MEMBRANES EXHIBITING ANTIBACTERIAL PROPERTY BY THE INCORPORATION OF NOVEL N-HALAMINE COPOLYMERS	43
3.1 Introduction	43
3.2 Experimental	43
3.2.1 Materials.....	43
3.2.2 Synthesis of the novel <i>N</i> -halamine copolymers	44
3.2.3 Preparation of ternary phase diagram	44
3.2.4 Polymer blends and flat sheet membrane production	46
3.2.5 Chlorination of the produced membranes	46
3.2.6 Permeability tests of the produced membranes.....	46
3.2.7 Characterization of the produced polymers and membranes	48
3.3 Results and Discussion.....	49
3.3.1 Characterization of the new synthesized polymers.....	49
3.3.2 Characterization of the produced membranes.....	53
3.3.2.1 Ternary phase diagrams of polymer / NMP / water systems	53
3.3.2.2 Filtration and BSA rejection performances of the produced membranes	55
3.3.2.3 FTIR and XPS characterization of the produced membranes.....	56
3.3.2.4 Morphology of the produced membranes	58
3.3.2.5 Biocidal performance of the produced membranes	60
3.4 Conclusion.....	63
4. ESTABLISHMENT OF A HOLLOW FIBER SPINNING UNIT AND PRODUCTION OF HOLLOW FIBER MEMBRANES WITH ADDITION OF ANTIBACTERIAL N-HALAMINE COPOLYMERS	65
4.1 Introduction	65
4.2 Experimental	66
4.2.1 Materials.....	66
4.2.2 Design and production of the hollow fiber spinning spinneret.....	66
4.2.3 Design and establishment of the hollow fiber spinning unit.....	67
4.2.4 Preparation of the dope solutions.....	68
4.2.5 Spinning of the HFMs.....	68
4.2.6 Chlorination of the HFMs	69
4.2.7 Preparation of the hollow fiber test modules	69
4.2.8 Permeability tests of the HFMs.....	70
4.2.9 Characterization of the HFMs.....	71
4.3 Results and Discussion.....	72
4.3.1 Morphologies of the produced HFMs	72
4.3.2 Filtration and BSA rejection performances of the HFMs	75
4.3.3 Biocidal performances of the produced HFMs	77
4.4 Conclusion.....	78
5. CONCLUSIONS AND RECOMMENDATIONS.....	80
REFERENCES.....	82

APPENDICES	91
CURRICULUM VITAE.....	94



ABBREVIATIONS

BN	: Sterlitech BN475
BSA	: Bovine serum albumin
CP	: Poly(N-(2-methyl-1-(4-methyl-2,5-dioxoimidazolidin-4yl)propan-2-yl)acrylamide-co-2-Acrylamido-2-methyl-1-propanesulfonic acid sodium salt)
DA	: N-(1,1-Dimethyl-3-oxobutyl)acrylamide
DSC	: Differential scanning calorimeter
FTIR	: Fourier-transform infrared
HA	: N-(2-methyl-1-(4-methyl-2,5-dioxoimidazolidin-4yl)propan-2-yl)acrylamide
HP	: Poly(N-(2-methyl-1-(4-methyl-2,5-dioxoimidazolidin-4yl)propan-2-yl)acrylamide)
HCl	: Hydrochloric acid
HFM	: Hollow fiber membrane
MF	: Microfiltration
NaOCl	: Sodium hypochlorite
NF	: Nanofiltration
NMP	: N-Methyl-2-pyrrolidone
NIPAAm	: N-Isopropylacrylamide
NNDMAAm	: N,N-Dimethylacrylamide
NTBAAm	: N-tert-Butylacrylamide
PBS	: Phosphate buffer solution
PPS	: Potassium persulfate
PVDF	: Poly(vinylidene fluoride)
PVP	: Polyvinylpyrrolidone
PWF	: Pure water flux
RO	: Reverse osmosis
SA	: 2-Acrylamido-2-methyl-1-propanesulfonic acid sodium salt
SEM	: Scanning electron microscopy
UF	: Ultrafiltration
XPS	: X-ray photoelectron spectra

SYMBOLS

A	: Effective membrane area
Cl⁺	: Weight percent of the oxidative chlorine
C_f	: Feed solution BSA concentration
C_p	: Filtrated solution BSA concentration
J_w	: Pure water flux
N	: Titrant solution concentration
R	: Protein rejection percentage
t	: Filtration time
V_w	: Permeated water volume
V_T	: Titrant solution volume
W	: Sample weight

LIST OF TABLES

	<u>Page</u>
Table 2.1 : Casting solution compositions of the produced membranes.....	24
Table 3.1 : Casting solution compositions of the membranes produced with the incorporation of novel polymers.	47
Table 4.1 : Dope solution compositions of the HFM.....	68
Table 4.2 : Spinning conditions of the HFMs	69



LIST OF FIGURES

	<u>Page</u>
Figure 1.1 : Schematic view of membrane classification according to their morphology (Baker, 2004).....	5
Figure 1.2 : Schematic ternary phase diagram of a three component system (Baker, 2004)	7
Figure 1.3 : Membrane separation processes with different particle and molecule size ("Membrane technology," 2018).....	8
Figure 1.4 : Schematic representation and cross-section images of an asymmetric UF membrane (Porter, 1990; Strathmann, 2001).....	9
Figure 1.5 : Schematic representation of hollow fiber spinneret and dry-jet wet spinning system (Tsai et al., 2006)	10
Figure 1.6 : A commercial hollow fiber module and outside-in filtration mode.....	11
Figure 1.7 : Cross-flow and dead-end filtrations	13
Figure 1.8 : Cell structures of Gram-positive and Gram-negative bacteria.....	14
Figure 1.9 : Regenerable property of <i>N</i> -halamine compounds (Gao and Cranston, 2008)	17
Figure 1.10 : General structure of <i>N</i> -halamines.....	17
Figure 2.1 : Synthesis of the hydantoin acrylamide.....	22
Figure 2.2 : Synthesis of the homopolymer	22
Figure 2.3 : Synthesis of the copolymer	23
Figure 2.4 : Filtration test system	25
Figure 2.5 : The mechanism of the Bucherer-Bergs reaction	27
Figure 2.6 : FTIR spectra of the DA and HA.....	28
Figure 2.7 : FTIR spectra of the synthesized polymers	28
Figure 2.8 : DSC thermograms of the DA, HA, HP, and CP.....	29
Figure 2.9 : Ternary phase diagram of the Polymer (PVDF, HP, and CP)/NMP/Water systems at 30 °C	30
Figure 2.10 : Pure water flux of the commercial, PVP added, and unmodified membranes	31
Figure 2.11 : BSA rejection of the commercial, PVP added, and unmodified membranes	31
Figure 2.12 : Pure water flux of the commercial, PVP added, and HP added membranes	32
Figure 2.13 : BSA rejection of the commercial, PVP added, and HP added membranes	32
Figure 2.14 : Pure water flux of the commercial, HP and CP added membranes	33
Figure 2.15 : Pure water flux of the commercial, HP and CP added chlorinated membranes	34
Figure 2.16 : BSA rejection of the commercial, HP and CP added chlorinated membranes	34
Figure 2.17 : FTIR spectra of the produced membranes.....	35

Figure 2.18 : XPS spectra of the produced membranes	36
Figure 2.19 : DSC thermograms of the produced membranes; (a) during first heating cycle, and (b) during second heating cycle	37
Figure 2.20 : The surface morphology of the unmodified, HP added and chlorinated membranes (a) at 5,000x magnification, (b) at 50,000x magnification	38
Figure 2.21 : The surface morphology of the unmodified, CP added and chlorinated membranes (a) at 5,000x magnification, (b) at 50,000x magnification	39
Figure 2.22 : Biocidal Test 1	40
Figure 2.23 : Biocidal test 2	41
Figure 3.1 : Reaction mechanisms of the novel synthesized copolymers	45
Figure 3.2 : ¹ H NMR spectrum of the P(HA-co-NTBAAm) (solvent: DMSO-d ₆)..	50
Figure 3.3 : ¹ H NMR spectrum of the P(HA-co-NIPAAm) (solvent: DMSO-d ₆) ...	50
Figure 3.4 : ¹ H NMR spectrum of the P(HA-co-NNDMAAm) (solvent: DMSO-d ₆)	51
Figure 3.5 : FTIR spectra of the HP, P(HA-co-NTBAAm), and NTBAAm	51
Figure 3.6 : FTIR spectra of the HP, P(HA-co-NIPAAm), and NIPAAm	52
Figure 3.7 : FTIR spectra of the HP, P(HA-co-NNDMAAm), and NNDMAAm....	53
Figure 3.8 : Ternary phase diagram of Polymer / NMP / Water systems at 30 °C ...	54
Figure 3.9 : Ternary phase diagram of polymer incorporated PVDF / NMP / Water systems at 30 °C	54
Figure 3.10 : Pure water flux performances of the unchlorinated membranes	55
Figure 3.11 : Pure water flux performances of the chlorinated membranes	56
Figure 3.12 : BSA rejection performances of the produced membranes	56
Figure 3.13 : FTIR spectra of the synthesized polymers added membranes	57
Figure 3.14 : XPS spectra of the synthesized polymers added membranes.....	58
Figure 3.15 : The surface and cross-section SEM images of the produced membranes	59
Figure 3.16 : Results of the biocidal tests by using agar diffusion method with 10 ⁵ CFU/mL bacterial concentrations. (Chlorine loading on the chlorinated samples of M-0, M-P(HA-co-NTBAAm), M-P(HA-co-NIPAAm), and M-P(HA-co-NNDMAAm) were 0%, 0.144%, 0.135%, and 0.123%, respectively.).....	61
Figure 3.17 : Results of the biocidal tests by using agar diffusion method with 10 ⁸ CFU/mL bacterial concentrations. (Chlorine loading on the chlorinated samples of M-0, M-P(HA-co-NTBAAm), M-P(HA-co-NIPAAm), and M-P(HA-co-NNDMAAm) were 0%, 0.144%, 0.135%, and 0.123%, respectively.).....	62
Figure 3.18 : Biocidal test results of membranes after microorganism solution filtration. (Chlorine loading on the chlorinated samples of M-0, M-P(HA-co-NTBAAm), M-P(HA-co-NIPAAm), and M-P(HA-co-NNDMAAm) were 0%, 0.144%, 0.135%, and 0.123%, respectively.)	63
Figure 4.1 : Schematic view of the spinneret; (a) isometric, (b) cross-section.....	66
Figure 4.2 : Schematic view of the (a) designed spinning device, (b) spinning device with coagulation bath	67
Figure 4.3 : General view of the hollow fiber spinning system	67
Figure 4.4 : Preparation of the HFM test modules.....	70
Figure 4.5 : HFM module filtration test system.....	71
Figure 4.6 : Surface SEM images of the produced HFMs with a) 5,000x and b)50,000x magnifications.....	73
Figure 4.7 : Cross-section SEM images of the produced HFMs at 175x and 600x magnifications	74
Figure 4.8 : Pure water flux performances of the produced HFMs	76

Figure 4.9 : BSA rejection performances of the produced HFMs	76
Figure 4.10 : Biocidal test against <i>S. aureus</i>	77
Figure 4.11 : Biocidal test against <i>E. coli</i>	78
Figure A.1 : The technical drawings of the spinning device	92
Figure B.1 : The technical drawings of the spinning device.....	93



SYNTHESIS OF ANTIBACTERIAL POLYMERS REDUCING BIOFILM FORMATION AND THEIR APPLICATION ON HOLLOW FIBER MEMBRANES

SUMMARY

Conventional water filtration systems become insufficient to fulfill the standards. Therefore, the demand to advanced filtration processes increases dramatically. Membrane processes are preferred the most, especially the ultrafiltration (UF) membranes. Among the cross-flow and static (dead-end) ultrafiltration methods, static filtration is advantageous by using less energy; however, relatively fast fouling compared to the cross-flow method is one of the main drawbacks of this system. One of the major reasons for fouling is the biofouling caused by the colonization of microorganisms on the surface of membranes. In general, to remove the formed biofilms on the membrane surfaces, chemical backwashings are periodically applied to membranes and these washings decrease the membranes mechanic performances. If the halogens (occur during the backwashing cycles) can be hold for a longer period of time on the surface of membranes, the use-life of membranes can be increased by reducing the number of harmful washing cycles. This assumption can be achieved by using halogen storing *N*-halamine compounds. In this regard, the prepared membranes will be reactivated in each washing-cycle and antibacterial surfaces will be provided without the necessity of various chemicals.

In this study, in order to increase the biodegradability resistance of the ultrafiltration membranes used in water treatments, polymers having high chlorine loading capacity, good solubility in matrix systems, high chlorine stability and not leaching from the material by water were synthesized and added to matrix polymers being used in the production of flat sheet and hollow fiber membranes (HFM). A dry-jet-wet spin line and spinneret was designed and produced. HFMs were successfully manufactured in the established spinning system and packed in module form. The effects of antibacterial polymers on the membrane structures were determined by investigation of ternary phase diagrams, morphological and surface properties of flat sheet and HFMs. The permeability tests and SEM analyzes were used to obtain information about the porosity of the membranes and the improvement of the water flux and protein rejection values of the membranes according to the unmodified membranes. In addition, the produced flat-sheet membranes permeability values were compared with a commercial PVDF membrane and it was found that some of the produced membranes showed higher protein rejection performance than the commercial membrane. Likewise, the water flux of HFMs were very close to the commercial membranes. Finally, the speed and duration of the produced membranes biocidal performances were proven with different test methods.

Keywords: Antibacterial polymer, polymer synthesis, *N*-halamines, ultrafiltration membranes, dry- jet-wet spinning.

BİYOFİLM OLUŞUMUNU AZALTAN ANTİBAKTERİYEL POLİMERLERİN SENTEZİ VE İÇİ BOŞ LİFLERE UYGULANMASI

ÖZET

Klasik su arıtma sistemleri sıkılaştıran standartları sağlamakta yetersiz kalmaktadırlar. Bu sebeple, ileri arıtma proseslerine olan talep gün geçtikçe artmaktadır. Membran prosesleri en çok tercih edilen ileri arıtma prosesleridir. Bu prosesler içerisinde ultrafiltrasyon (UF) membranları yaygın kullanıma sahiptir. UF membranları çapraz-akışlı veya dik-akışlı olarak işletilebilmektedir. Dik-akışlı filtrasyon yöntemi daha az enerji kullandığı için avantajlıdır, ancak zamanla diğer yonteme göre hızlı tıkanması bu sistemin önündeki en büyük engellerdendir. Tıkanmaların en önemli sebeplerinden birisi ise su arıtımı ile filtrelenen mikroorganizmaların membran yüzeyinde oluşturduğu biyofilmlerdir. Genellikle su arıtma tesislerinde, membran yüzeyinde oluşan bu biyofilmleri uzaklaştırmak için membranlara zarar veren sodyum hipoklorit gibi kimyasallar ile periyodik ters(geri)-yıkamalar yapılmaktadır. Bu yıkamalarda ortaya çıkan halojenler bir miktar daha membran yüzeyinde tutulabilirse, yıkama sayıları azaltılabilir ve membran kullanım ömürleri uzatılabilir. Bu varsayım halojenleri depolayabilen *N*-halamin kimyası ile gerçekleştirilebilir. Böylece her yıkama işleminde membran yüzeyleri tekrar aktifleştirilmiş olup, farklı kimyasallar kullanılmadan antibakteriyel yüzeyler elde edilmiş olacaktır.

Bu çalışmada, su uygulamalarında kullanılacak ultrafiltrasyon membranların biyobozunum dirençlerini arttırmak amacıyla, matris polimer ile ortak çözgünde çözülebilen, yüksek klor depolama kapasitesine sahip, klor stabilitesi yüksek ve su ile malzemedan kolayca uzaklaşmayan polimerler sentezlenmiş ve sentezlenen polimerler membran üretiminde kullanılan polimer matrislere katılarak, düz ve içi boş lifler üretilmiştir. İçi boş lif üretimi için bir kuru-jet-yaş çekim hattı ve bir düze tasarlanmış ve üretilmiştir. Kurulan sistemde içi boş lifler başarıyla üretilmiş ve geçirgenlik testleri için modül formunda paketlenmiştir. Membranların üretiminde kullanılan polimerlerin üçlü faz diyagramları ile düz ve içi boş liflerin morfolojik ve yüzey özellikleri incelenerek sentezlenen antibakteriyel polimerlerin yapıya olan etkileri belirlenmiştir. Geçirgenlik testleri ve SEM analizleri yardımıyla membranların gözeneklilikleri hakkında bilgi edinilmiş, katkısız membrana göre membranın su akısı ve protein reddi değerlerindeki iyileşmeler ortaya konulmuştur. Ayrıca elde edilen düz membran geçirgenlik değerleri halihazırda ticari olarak kullanılan bir PVDF membran ile kıyaslanarak, elde edilen protein reddi değerlerinin ticari membrandan dahi yüksek olduğu görülmüştür. Yine benzer şekilde üretilen içi boş lifler ticari kataloglardaki akı değerlerine çok yakın su akısı değerleri göstermiştir. Son olarak üretilen membranların farklı test yöntemleriyle hızlı ve uzun süreli bir antibakteriyel etkinliğe sahip olduğu kanıtlanmıştır.

Anahtar Kelimeler: Antibakteriyel polimer, polimer sentezi, *N*-halamin, ultrafiltrasyon membranları, kuru-jet-yaş lif çekimi.

1. INTRODUCTION

Water has a great importance in our lives, we need water in every part of our lives from food and beverage and cleaning to jobs. Therefore, even reaching clean and fresh water has a vital importance, unfortunately 2.1 billion people worldwide lack of safe drinking water, and more than 4 billion people lack of safe sanitation. According to the 2017 report of the World Health Organization, 842,000 people die every year globally due to clean water shortage. On the other hand, the worldwide problems such as climate change, population growth, urbanization, and industrialization increase the scarcity of clean and fresh water. In this context, wastewater and water treatments are gaining importance as well as the water resources management (WHO, 2017; WWAP, 2012; WWAP 2016).

Membrane technologies, especially pressure driven membrane technologies with hollow fiber form have been used extensively in water treatments due to being more economical and energy effective by decreasing space requirements, energy consumption, and waste production than traditional separation methods (Aryanti et al., 2018; Fakhru'l-Razi et al., 2009; Zhang et al., 2009). In spite of these advantages, the organic/bio-fouling which influence the membrane efficiency limit the application of pressure driven membranes in water treatments (Aryanti et al., 2018; Kang et al., 2016). Between pressure driven membrane processes including microfiltration, ultrafiltration, nanofiltration, and reverse osmosis, ultrafiltration has significant portion of worldwide market in water treatment as it can be applied directly or for pre-filtration before reverse osmosis and nanofiltration (Chang et al., 2014; Zhao et al., 2012).

Poly(vinylidene fluoride) (PVDF) attracts considerable attention in ultrafiltration applications due to its good film forming capability and mechanical properties, outstanding anti-oxidation activities, excellent chemical resistance, strong thermal and hydrolytic stabilities, and good solubility in many organic solvents. In contrast to all these advantages, the hydrophobic character of the polymer limits membrane performance by increasing fouling tendency of ultrafiltration membrane, which

causes a sharp drop in water flux performance of the membrane and has been restricted its usage in water treatments (Wang et al., 2012; Yan et al., 2006; Yuliwati and Ismail, 2011; Zhao et al., 2013). To recover the membrane performances periodic backwashings are applied generally with sodium hypochlorite being one of the most effective cleaning agents for PVDF ultrafiltration membranes. Even if the cleaning efficiency of sodium hypochlorite is greater than 85% in PVDF membrane backwashings, the membrane structure is damaged by these washing cycles (Bogati et al., 2015; Nguyen and Roddick, 2011). Many modifications have been applied to PVDF membranes to reduce backwashing cycles by decreasing organic/bio-fouling on membrane surface and so prolong the membrane lifetime.

Surface modification and blending modification are the two main methods applied to PVDF membranes to improve the hydrophilicity (Liu et al., 2011). Surface modification can be achieved by coating hydrophilic substances (Boributh et al., 2009; Nunes et al., 1995) or grafting hydrophilic substances by high energy irradiation (Yang et al., 2013), plasma (Wang et al., 2002; Zhao et al., 2015), living/controlled polymerization (Chen et al., 2007; Meng et al., 2011) or UV photo irradiation (Chen et al., 2018; Rahimpour et al., 2009). Modifying the membrane surface by these methods is expensive and also it may lose its effectiveness over time due to the partially modification on only membrane surface. Therefore, blending modification is more advantageous method allowing modification during production and providing modification of all membrane structure including even inner side (Liu et al., 2011). Hydrophilic (Fadilah et al., 2016; Fontananova et al., 2006; Ngang et al., 2014; Zuo et al., 2008) or amphiphilic (Liu et al., 2013; Zhao et al., 2008) polymers, and inorganic nanoparticles (Safarpour et al., 2014; Yan et al., 2006) are commonly used additives for blending modification method.

Although hydrophilic additives are effective against organic fouling, antibacterial additives are needed to destroy the biofilm formed by microorganisms on the membrane surface. Quaternary ammonium salts (Kakihana et al., 2017; Zhang, et al., 2016), metal ions (Damador et al., 2009; Shi et al., 2013), and *N*-halamines (Huang et al., 2017; Kang et al., 2016; Wang et al., 2017) are some of the antibacterial agents applied to membrane structure to improve biocidal performance of the membranes. Among these agents, besides the features like long term stability in water and dry air, lack of corrosion of surfaces, effectiveness against a broad spectrum of

microorganisms, non-toxicity to human and environment, especially the two abilities of *N*-halamines; storing the halogens that occurs during backwashings and regenerating by rechlorination make them the most advantageous agent for membrane applications (Hou et al., 2017; Yu et al., 2013). Backwashing can be converted to an added-value with these properties of *N*-halamines. *N*-halamines storing halogens in their structure for a certain period of time and releasing when exposed to microorganism will prevent the formation of biofilm on the membrane surface and thus membrane can be used more actively for a longer time. Therefore, there is a demand for new *N*-halamine polymers being compatible with membrane structure and improving the membrane performance.

1.1 Aim and Scope of the Thesis

The aims of the study are to synthesize antibacterial polymers reducing the biofilm formation on membrane surface during the filtration of microorganism-containing fluids, and to produce PVDF flat-sheet and HF membranes incorporated with the synthesized polymers. In the first section, a general literature review was conducted by examining the historical background and current developments related to the research subject. In the second section, it is aimed to examine the changes in membrane structure caused by the additives made by selecting appropriate polymer structures from literature. In the third section, it is aimed to synthesize novel antibacterial polymers based on the findings obtained in the first section and to investigate the effects of synthesized polymers on membrane properties. In the fourth section, it is first aimed to establish a hollow fiber spinning unit, then to produce hollow fibers by the incorporation of the polymers which improves the membrane properties in the third section, and finally to investigate the effects of these additives on the HFM structure.

1.2 Literature Review

1.2.1 An overview to membrane science and technology

1.2.1.1 Historical developments of membranes

Even if the commercial use of membranes in large scale is a new technology, the history of membrane development dates back to the eighteenth century. In fact that

the phenomenon of osmosis, which is the transport of solvent molecules through a semipermeable membrane into a higher solute concentration region, have already been observed since ancient times (e.g. on the construction of Egyptian pyramids), but have not been described until 1748 (Hammel and Scholander, 1976). As Jean-Antoine Nollet's studies to explain the term of 'osmosis', membrane studies had always been conducted on a laboratory scale until the beginning of the twentieth century (Baker, 2004; "Osmosis," 2018). The first commercial membrane was produced under the sponsorship of the US Army to test the safety of water due to the water problems after the World War II. In consequence of the four main problems of membrane separation; unreliableness, bad selectiveness, slowness, and expensiveness, there was no significant membrane industry until 1960 (Baker, 2004). Loeb-Sourirajan's development of defect-free, high-flux, anisotropic reverse osmosis membranes in 1960, which has an ultrathin selective layer on a much thicker microporous support, was a milestone in the membrane technology (Baker, 2004; Loeb and Sourirajan, 1963). After this development, membrane technology progressed rapidly and membrane processes (microfiltration, ultrafiltration, reverse osmosis and electrodialysis) were established in large areas around the world in 1980 (Baker, 2004). Recently, membranes used in many industrial applications such as water and wastewater treatments, gas separation, environmental and energy areas, food, biotechnology, pharmaceutical, medicine, and etc. (Li et al., 2008; "Membrane technology," 2018).

1.2.1.2 Types of membranes

Membranes can be classified according to their morphologies (symmetrical or anisotropic), thicknesses, transport mechanisms (active or passive), materials (organic or inorganic), origins (biological or synthetic), and etc. Among them the classification made by morphology has a great importance (Mulder, 1996). As seen in Figure 1.1, membranes can be divided into two groups as symmetrical and anisotropic membranes according to their morphology.

Symmetrical membranes can be in microporous structure or as a nonporous dense layer form. While isotropic microporous membranes generally used as microfiltration membranes, nonporous dense membranes used in laboratory studies due to their low flux ratio. Nonporous dense membranes can be produced as a simple

casted film with help of a casting knife or as a melt extruded film. Isotropic microporous membranes are generally produced by one of the phase separation techniques. Track-etch, melt expansion or template leaching are the other methods to produce isotropic microporous membranes (Baker, 2004).

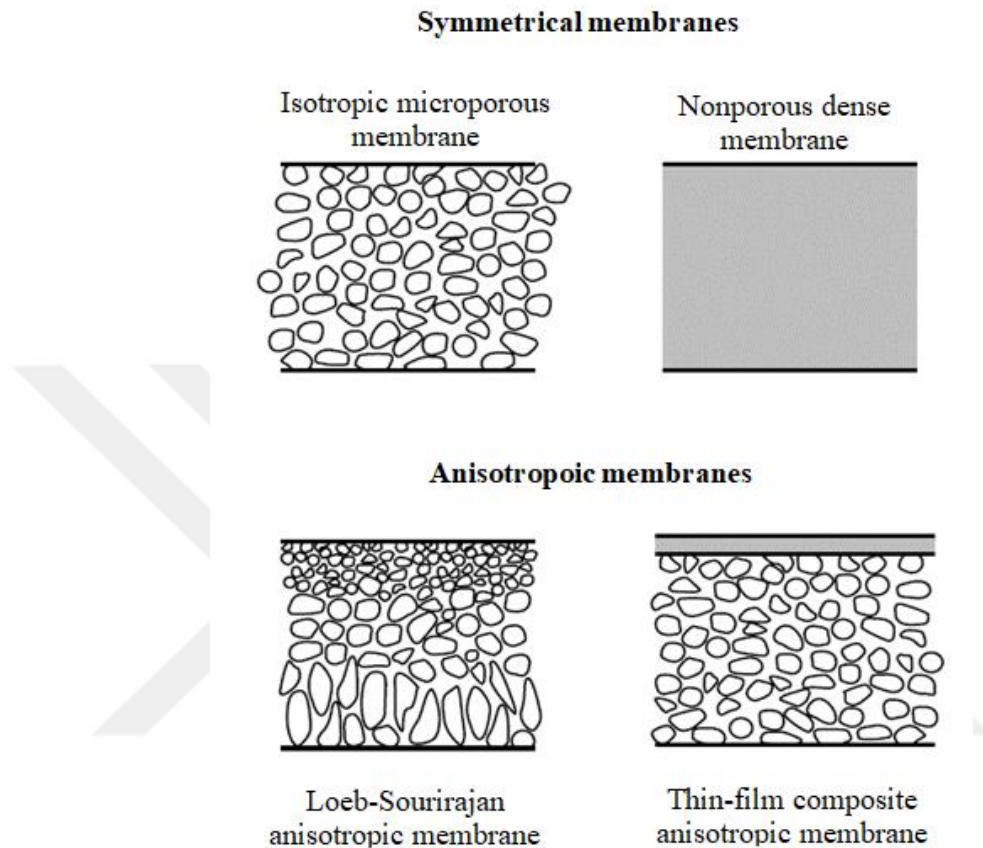


Figure 1.1 : Schematic view of membrane classification according to their morphology (Baker, 2004)

The separation in anisotropic membranes takes place at the very thin top layer (0.1 to 1 μm) supported by the large pores (100 to 200 μm) at the bottom. As the separation process takes place in a very thin layer, very high flux values can be achieved. Phase separation, interfacial polymerization, solution coating, plasma polymerization are some of the methods to produce anisotropic membranes. Among them phase separation has the most common use (Baker, 2004; Porter, 1990).

While preparing a membrane with the phase separation method, a homogeneous polymer solution is prepared, the solution is casted as a film, and the casted film is precipitated by several ways such as immersing in a nonsolvent bath, placing the film in a humid atmosphere to provide water vapor absorption, and evaporating the solvent. During precipitation step one phase homogeneous polymer solution

separates into two phases; a polymer-rich solid phase forming the membrane structure and polymer-poor liquid phase forming the membrane pores. The precipitation at surface occurs more rapidly than the inner and bottom sides of the film that causes a smaller pore formation at the membrane surface (Baker, 2004; Porter, 1990). This instantaneous precipitation at the membrane surface decreases the speed of solvent removing at the inner side of membrane resulting the formation of large finger-like cavities. Thus, the asymmetric membrane structure is formed.

Nonsolvent induced phase separation is one of the most common approaches to obtain porous asymmetric membranes with phase separation process. Nonsolvent induced phase separation is a complex system with at least three components (polymer/solvent/nonsolvent) and double-sided mass transfer. The phase separation mechanism of this three component system can be explained by ternary phase diagram (Idris et al., 2017; Witte et al., 1996). A schematic ternary phase diagram desired to prepare an asymmetric membrane is shown in Figure 1.2. The curve shown as solid line represents the binodal curve dividing the diagram into two principle regions as one-phase region and two-phase region. While all of the components are miscible in one-phase region, polymer solution separates into a polymer-rich (solid) and polymer-poor (liquid) phases in two-phase region. The curve shown as dashed line represents the spinodal curve. The region between the binodal and spinodal curves is metastable region where the polymer solution is not precipitate normally even if being in a thermodynamically unstable region.

For a specific polymer concentration at point A, the composition of ternary system follows the A-D path where a continuous solvent-nonsolvent exchange occurs, and reached the final membrane composition at point D. Until the point B, precipitation is not start for this solution composition. However, after that point casting solution enters a metastable region and during the path the viscosity increases. The point where the precipitated polymer can be considered as solid is shown as C. S and L points on the polymer-nonsolvent line represent the polymer-rich (solid) phase and the polymer-poor (liquid) phase, respectively. The position of the point D on S-L line indicates the porosity of the membrane (Baker, 2004; Porter, 1990; Sadrzadeh and Bhattacharjee, 2013).

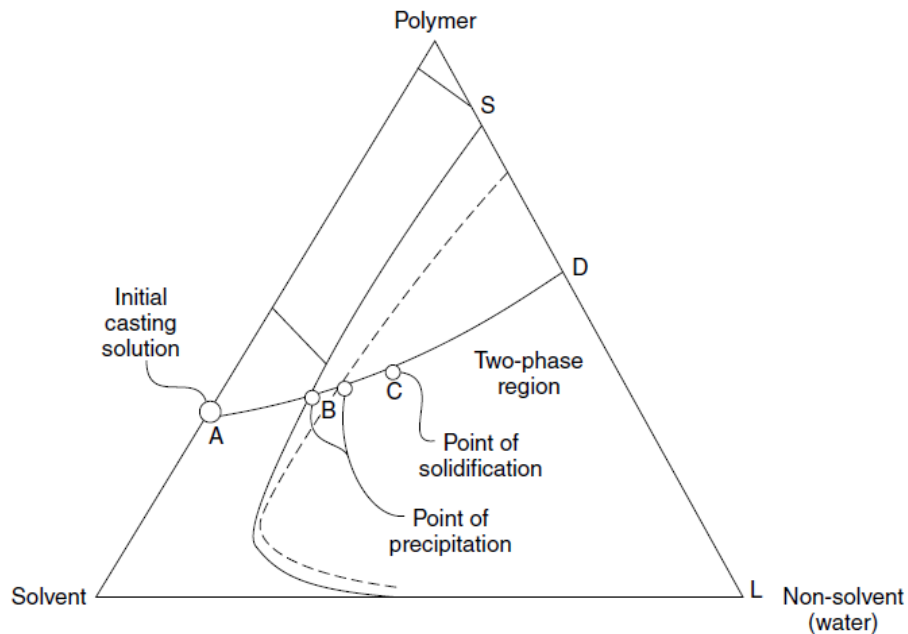


Figure 1.2 : Schematic ternary phase diagram of a three component system (Baker, 2004)

Generally, water is used as a non-solvent instead of organic-based coagulation bath such as methanol or isopropanol due to its higher precipitation ratio that forms more anisotropic membrane structure. Depending on the application area of the membrane, different additions have been made to the membrane structure such as addition of low solubility solvents for more dense structure, hydrophilic polymer additions for more porous membrane structure, antibacterial agents additions to produce membranes with antibacterial properties, and etc. (Baker, 2004; Damodar et al., 2009; Fadilah and Hassan 2016; Zhang et al., 2016; Zuo et al., 2008).

1.2.1.3 Membrane separation processes

As seen in Figure 1.3, four industrial membrane processes have been developed depending on the size of particles and molecules separated; microfiltration (MF), ultrafiltration (UF), nanofiltration (NF), and reverse osmosis (RO). Reverse osmosis membranes can be reject even species with very low molecular weight such as salt ions due to almost dense surface layer where separation occurs with thermal motion of the polymer chains. Reverse osmosis generally used for desalination of seawater (Macedonio et al, 2012). Nanofiltration membranes (with a pore diameter between 10-100 Å) which have a separation feature between ultrafiltration and reverse osmosis membranes are used in many applications such as water and wastewater

treatments, desalination, pharmaceutical, biotechnology, food, and etc. (Mohammad et al., 2015). Recently, ultrafiltration membranes have a great importance as they can be applied as a prefiltration for nanofiltration and reverse osmosis and as a membrane process itself (Susanto and Ulbricht, 2009). While the ultrafiltration membranes can discriminate the dissolved macromolecules (e.g. proteins) from solution, microfiltration membranes having the largest pore diameters of these four separation processes, filters the 0.1 to 10 μm diameter particles such as colloidal particles, and bacteria (Figure 1.3).

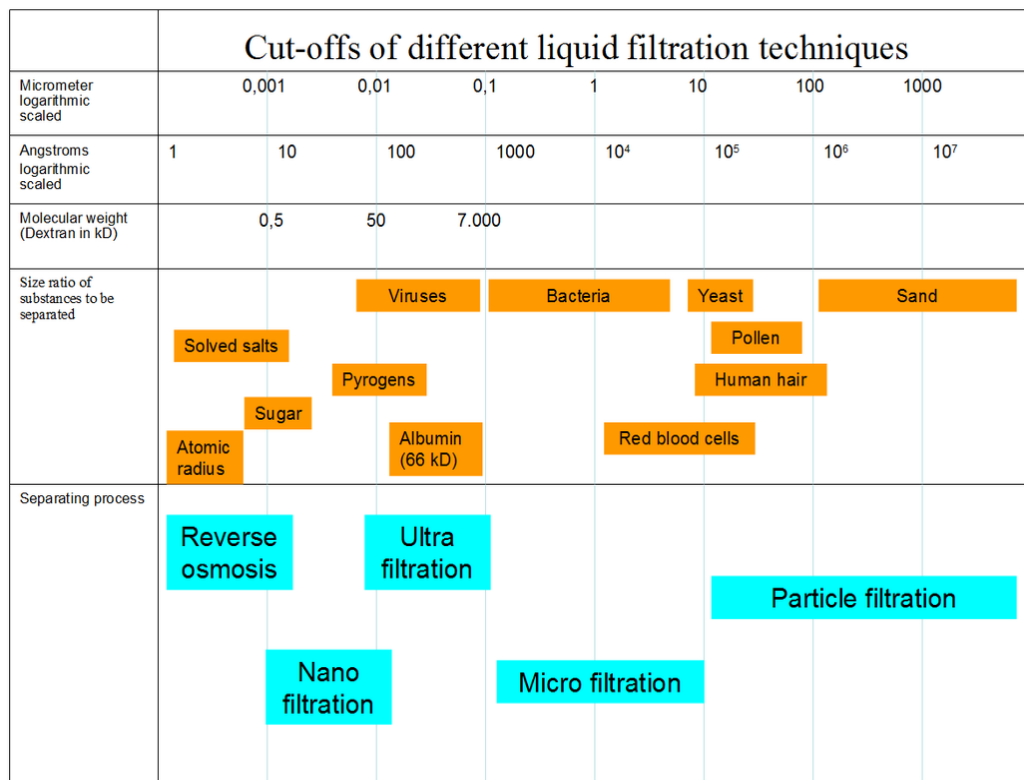


Figure 1.3 : Membrane separation processes with different particle and molecule size ("Membrane technology," 2018)

1.2.2 Ultrafiltration membranes

The term of ‘ultrafilter’ described firstly by Bechhold, is a pressure-driven membrane separation process with fine pores catching the macromolecules and colloids (Baker, 2004; Koros et al., 1996).

1.2.2.1 Structure of ultrafiltration membranes

Ultrafiltration membranes are generally produced in an anisotropic structure with Loeb-Sourirajan process. A schematic representation and cross-section images of

anisotropic membrane structure is given in Figure 1.4. As seen in figure membrane structure consists of a finely porous surface layer (0.1 to 1 μm) performing the separation, and a microporous support layer (approximately 125 μm) providing mechanical strength (Baker, 2004; Porter, 1990; Strathmann, 2001). As the separation takes place in such a thin layer, high flux values can be achieved in the ultrafiltration membrane processes.



Figure 1.4 : Schematic representation and cross-section images of an asymmetric UF membrane (Porter, 1990; Strathmann, 2001)

As mentioned previously, such asymmetric membrane structure is obtained by delaying coagulation of the interior side of membrane due to the rapid coagulation of membrane surface. In the literature, a variety of modifications have been applied to the membranes changing the coagulation behavior of membrane to obtain the desired membrane properties. For example, as explained in literature addition of hydrophilic polymers to the casting solution until a specific concentration triggers the instantaneous demixing causing a more porous membrane surface. On the other hand, extra addition above this concentration increases the viscosity of casting solution and forms a denser top-layer due to the delayed demixing (Ma et al., 2011).

1.2.2.2 Membrane configurations and modules

Membranes have been produced in different geometries such as flat-sheet, tubular, and hollow fiber. Flat sheet membranes are produced easily by casting dope solution

on a support layer with an applicator. However, for large-scale applications, membrane films are obtained by casting the dope solution on a rotating drum or an endless band (Baker, 2004). Tubular membranes are formed on the 0.25-1 inch diameter tube's inner walls. The advantages of this membrane configuration are less fouling and easy cleaning. Despite these advantages, expensive support tubes requirement is the most important limitation of this membrane form (Porter, 1990). Between other geometries, HFMs are very advantageous because they provide high surface area, low pressure losses, high material transfer rate, and easy production (Peng et al., 2012). A schematic representation of hollow fiber spinneret and spinning system are given in Figure 1.5. Polymer solution and a suitable bore-forming liquid (water, oil, etc.) inject from different channels to form hollow fiber structure. The dense surface layer in anisotropic membrane structure can be formed on the outside surface, inside surface or both side surfaces of the fiber, by changing the bore-forming liquid and coagulation bath compositions. The position of dense layer should be adjusted according to the where separation liquid fed, since the separation takes place in this thin dense layer of membrane (Baker, 2004).

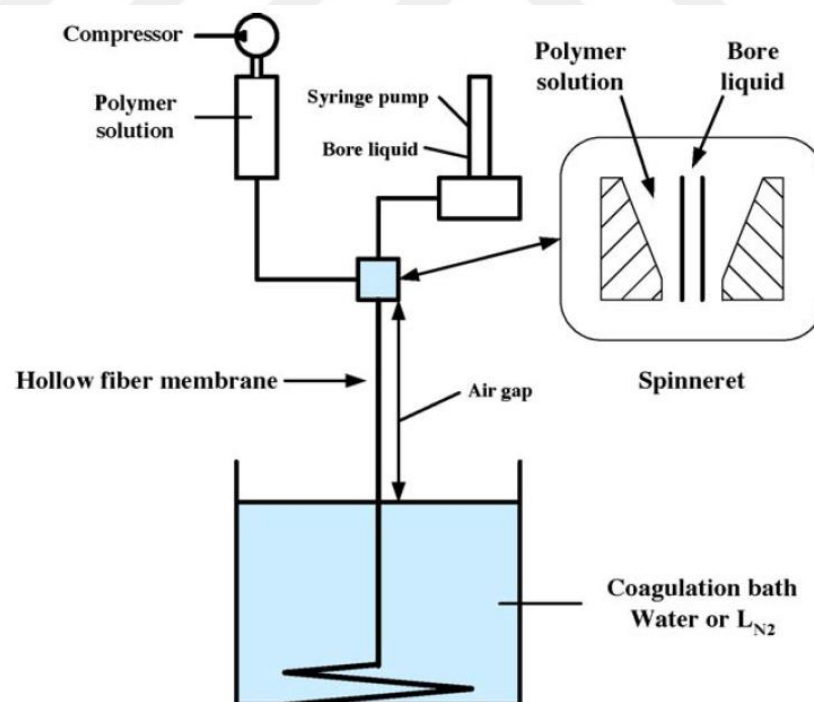


Figure 1.5 : Schematic representation of hollow fiber spinneret and dry-jet wet spinning system (Tsai et al., 2006)

In industrial applications separation processes require hundred thousands of square meters of membrane. Therefore, membranes are packed in modules to obtain

effective separation with large surface area (Ismail et al., 2015). Most commonly used four module types are; plate & frame, spiral wound, tubular, and hollow fiber. Between them, while plate & frame, and spiral wound modules are used to pack the flat-sheet membranes, tubular and hollow fiber modules are used for tube and hollow fiber form membranes, respectively as their names indicate. High surface area to per unit volume which provides high productivity is the most important advantage of the hollow fiber modules. For example, for volume of 0.04 m^3 , the effective membrane area of; HFM, spiral wound flat-sheet membrane, and tubular membrane are 575 m^2 , 30 m^2 , and 5 m^2 , respectively (Moch Jr, 2005).

According to the flow direction, two different flow types are available for hollow fiber modules due to their tubular geometry; inside-out and outside-in. Solution feed through the bore of hollow fiber and permeate is collected from the outside of the membrane in the inside-out flow mode. On the other hand, in the outside-in mode while feeding made from the upper surface of the membrane, the permeate is collected in the fiber bore (Serra et al., 1998). The appropriate flow type is selected according to the application area. In the case of hollow fiber module applications such as water treatments the outside-in mode is used (Figure 1.6) (Li et al., 2004; Li et al., 2008).

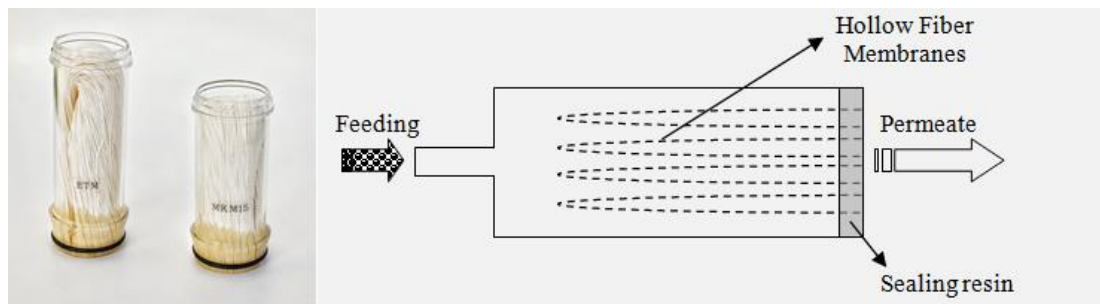


Figure 1.6 : A commercial hollow fiber module and outside-in filtration mode

1.2.2.3 Applications of ultrafiltration membranes

Ultrafiltration membranes used to recover electrocoat paint in automotive plant as first large-scale industrial application, have been used various applications nowadays. Cheese production, clarification of fruit juice, filtration of gelatin, egg white separation, wine and beer productions are some of the examples for ultrafiltration applications in food industry. Ultrafiltration is utilized to harvest the cell, concentrate and purify the enzymes, process the blood plasma, and etc. in

pharmaceutical and biotechnology. In automotive industry additional to the recovery of electrocoat paint, ultrafiltration has been used to separate oil-water emulsions. Except these applications ultrafiltration has a large market in water and wastewater treatments (Baker 2004; Jönsson and Trägårdh, 1990; Li et al., 2008; Porter, 1990).

1.2.2.4 Ultrafiltration membranes for water treatments

Conventional water filtration systems are inadequate to remove undesired particles and molecules such as microorganisms, suspended and colloidal particles, natural organic matters, and etc. (Li et al., 2008). Therefore, the demand for advanced treatment processes increases dramatically. Membrane technologies, especially pressure driven membrane technologies began to be used extensively in water treatments due to being more economical and energy effective by decreasing space requirements, energy consumption, and waste production than traditional separation methods (Aryanti et al., 2018; Fakhru'l-Razi et al., 2009; Zhang et al., 2009;). Between pressure driven membrane processes (reverse osmosis, nanofiltration, ultrafiltration, and microfiltration), ultrafiltration has a significant portion of worldwide market in water treatment as it can be applied both in filtration and prefiltration before nanofiltration and reverse osmosis processes (Chang et al., 2014; Zhao et al., 2012). The increase in shortage of clean and fresh water due to the worldwide problems such as population growth, climate change, industrialization, and urbanization triggers the use of UF membranes as a pretreatment to RO allowing to production of freshwater from nonconventional sources. The development of HFM form and dead-end filtration method increased the UF membrane applications in water treatments (Li et al, 2008; WWAP, 2012).

1.2.2.5 Membrane fouling

Separated colloidal and macromolecular materials in membrane processes accumulate on the membrane surface and form a gel layer called as fouling. This fouling layer causes a sharp decline in water flux of the membrane. Especially in dead-end filtration a faster fouling is present according to the cross-flow filtration due to the vertical feed on the membrane surface (Figure 1.7). Despite the faster fouling problem, dead-end filtration providing 70% energy saving per cubic meter of water has been used widely in recent years (Bennett et al., 2012; Serra et al., 1998).

Fouling on the membrane surface can be examined as inorganic fouling, colloidal fouling, microbial fouling, and organic fouling according to the type of fouling material. The most important factors that prevent the use of HFMs in filtration system are colloidal cake and biofilm formation on the membrane surface formed by organic and microbial fouling materials, respectively (Puspitasari et al., 2010; Regula et al., 2013). One of the most important problems encountered in dead-end filtration is biodegradation by microorganisms. Microorganisms that are prevented from passing through the membrane, form biofilms on the membrane surface by clustering (Hilal et al. 2004; Pearce, 2010). As seen in Figure 1.7 the microorganism colonization on the membrane surface reduces the fluid flow rate of the membrane and increases the pressure on the membrane. Biofilm formation generally exponentially increases after module replacement or cleaning.

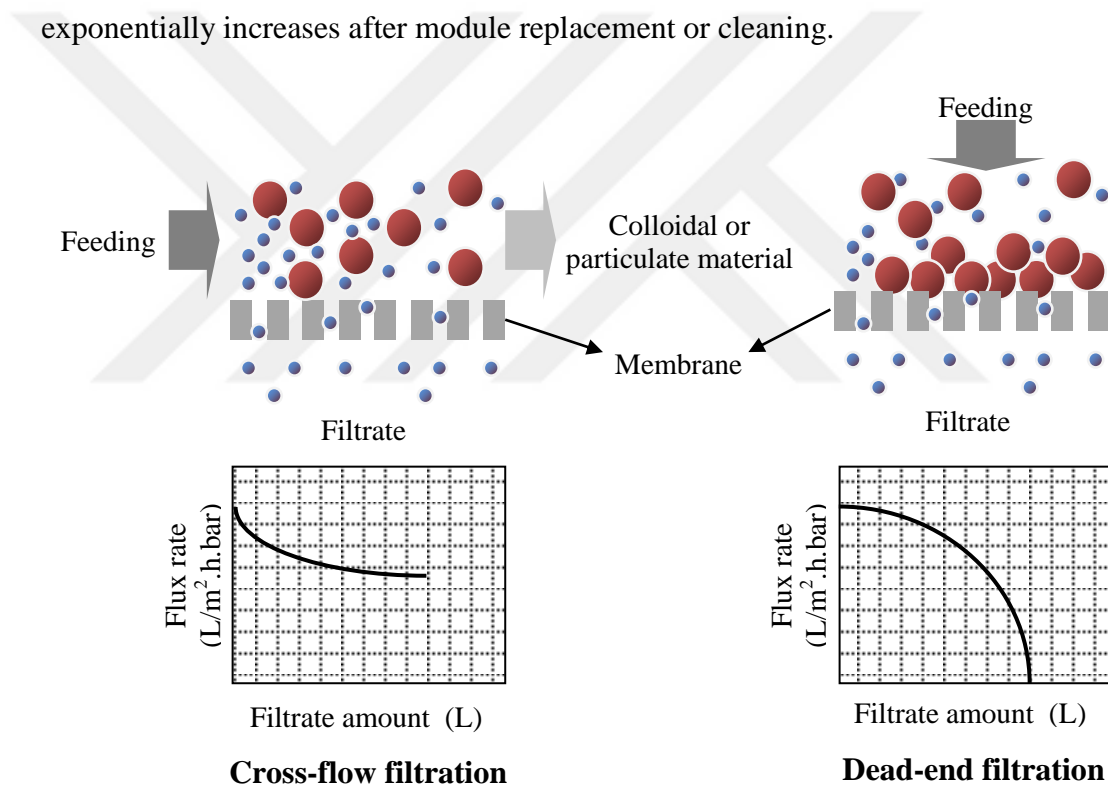


Figure 1.7 : Cross-flow and dead-end filtrations

To prevent the membrane clogging caused by organic and microbial pollutants, periodic backwashings are applied to the membranes at regular intervals. However, with these backwashings, it is very hard to prevent biofouling and chemical backwashing should be performed after several backwashes. Even these strong washings are not enough to clean all members of the colony. For this purpose, shock washing is carried out with high concentrations of chlorine approximately 1 per

week. All these washings to remove organic/bio-foulings reduce the membrane performance, and more importantly, shorten the membrane life (Avlonitis et al., 1992; Ettori et al., 2011; Li et al., 2008). Many modifications have been applied to membranes to reduce backwashing cycles by decreasing organic/bio-foulings on membrane surface and so prolong the membrane lifetime. Generally, hydrophilic (Fadilah and Hassan, 2016; Fontananova et al., 2006; Liang et al., 2013; Liu et al., 2013; Lv et al., 2018; Meyer and Ulbricht, 2018; Ngang et al., 2014; Safarpour et al., 2014; Yan et al., 2006; Zhao et al., 2016; Zuo et al., 2008) and antibacterial agents (Damodar et al., 2009; Huang et al., 2017; Kakihana et al., 2017; Kang et al., 2016; Shi et al., 2013; Wang et al., 2017; Zhang et al., 2016) have been added to membrane structure to reduce organic/bio-foulings, respectively.

1.2.3 Antibacterial agents

Gram-positive and Gram-negative bacteria are the two main groups of the bacteria according to staining with gram. As seen in Figure 1.8, even though the inner structures of them are similar, Gram-positive bacteria has a thick peptidoglycan cell membrane with teichoic acid, Gram-negative bacteria has a thin peptidoglycan cell membrane without teichoic acid. Therefore, while Gram-positive bacteria stain in purple, Gram-negative bacteria stain in pink during gram staining ("Gram stain," 2018). The thin peptidoglycan layer of Gram-negative bacteria is surrounded by outer membrane layer that provides extra resistance to the cell by limiting the concentration of biocide reaching the target sites (Russel, 1999).

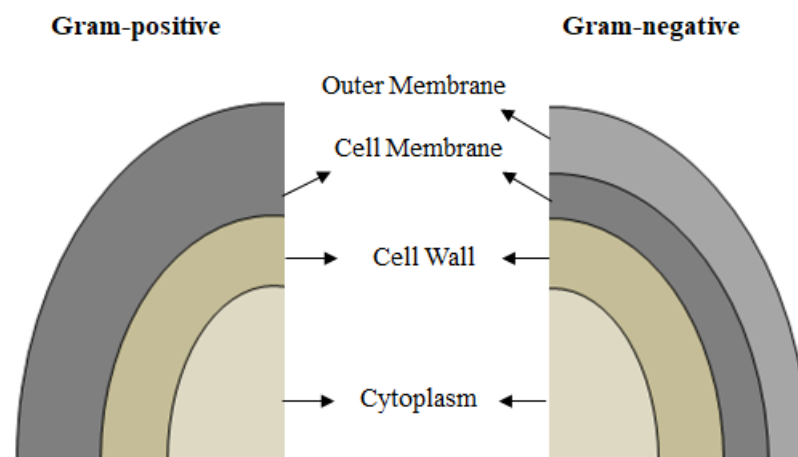


Figure 1.8 : Cell structures of Gram-positive and Gram-negative bacteria

To inactivating the bacteria firstly biocides accumulate on the cell surface, then passage and concentrate on target and finally interact and damage the target site. The final attack can occur with physical or chemical interactions of biocide and bacteria (Denyer, 1995). As physical interactive agents damage the cell membrane integrity of bacteria, they are referred as membrane active agents. Quaternary ammonium salts, biguanids, alcohols, and phenols are the examples of membrane active agents (Chapman 2003; Denyer, 1995; McDonnell and Russell, 1999). For chemical interactive agents, a chemical interaction between the biocide and the cytoplasmic constituents of bacterial cell occurs, in order to stop the growth of bacteria or inactive it (Denyer and Stewart 1998; Maillard, 2002). Oxidants such as halogen and peroxides, inorganic ions such as copper and silver, and organic biocides such as formaldehyde are the members of chemical interactive agents (Chapman, 2003).

1.2.3.1 Common biocides

Biocide is a general term including various substances such as preservatives, disinfectants, pesticides, and antimicrobials ("Biocide," 2018). Between them antimicrobials are the agents inhibiting growth of the microorganism or killing them. According to that activation type, they are named as biostatic and biocidal, respectively (Block, 2001; McDonnell and Russell, 1999). In this study, antimicrobial agents used to define the agents that destroy the microorganisms on non-living materials. In this respect, biguanides, heavy metals, peroxides, quaternary ammonium salts, alcohols, and halogens are the most common antimicrobial agents.

Biguanides are the cationic amines demonstrating good biocidal activity by distributing cell membrane. Chlorhexidine and poly(hexamethylenebiguanide) are the most common used biguanide and polymeric biguanide, respectively. Poly(hexamethylenebiguanide) demonstrates much greater antimicrobial activity according to monomeric and dimeric biguanides (De Paula et al., 2011; McDonnell and Russell, 1999; Simoncic and Tomsic, 2010). Biguanides are effective against bacteria, fungi, viruses, and parasites (Chindera et al., 2016). Antimicrobial soaps, antiseptic hand gels, contact lens cleaning solutions, wound dressing, and cosmetics are some of the usage area of biguanides.

Heavy metals such as copper, silver, zinc, cobalt, and their salts are inexpensive and effective agents, but they are toxic to human being except silver and copper. Their

antimicrobial activity occurs by cleavage of the disulfide bonds within proteins (Capelli, 1990; Gao and Craston, 2008; Yoshimura and Minami, 1998).

Peroxides as a chemical interactive agent oxidize the thiol groups of enzymes and proteins to inactivate microorganisms. Peroxides are used in various applications such as sterilants for medical devices, wound cleaners, and etc. due to their effectiveness against wide range of microorganisms including bacteria, bacterial spores, and viruses (McDonnell and Russell, 1999).

Quaternary ammonium salts (QASs) are cationic membrane active agents demonstrating biocidal activity by an electrostatic interaction of N^+ site of salt with the negatively charged cell surface, and the penetration of the long alkyl chain through cell wall (McBain, et al., 2004; McDonnell and Russell, 1999). For an effective biocidal performance the length of the alkyl chain at the nitronium site which is usually between 12-18 carbon atoms is very important (Dizman, et al., 2004; Gao and Cranston, 2008; Windler, et al., 2013).

Alcohols demonstrate fast action but short-term stability due to their low boiling points. Despite the most of alcohol are used as antiseptics, short chain alcohols such as ethanol and isopropanol are used as disinfectant. Inactivation mechanism of alcohols occurs by damaging the cell membrane and denaturing the proteins. As the water increases the diffusion to the cell membrane, the aqueous solutions of alcohols (60-90 wt%) have higher antimicrobial activity. Alcohols are often used as disinfecting sprays in hotels and in hand hygiene or a disinfectant material for thermometer, stethoscope, and etc. They are effective against viruses, fungi, and vegetative bacteria (Block, 2001; Fraise, 1999; McDonnell and Russell, 1999; Rahimi et al., 2012; Wu, 2004).

Halogens are cheap agents with broad spectrum antimicrobial effectiveness. Water solutions of halogens such as Cl_2 , Br_2 , $NaOCl$, and ClO_2 form chloric and iodic acids and then oxidize the amino groups of bacteria protoplasm proteins by releasing atomic oxygen and haloids (Block, 2001; Morato et al., 2003; Wu, 2004). While chlorine uses for disinfection of inanimate objects, swimming pool, drinking water, and etc., iodine generally uses in health related areas such as skin disinfestations ("Antimicrobial Agents I," 2018; "Oxidizing Agents," 2018).

1.2.3.2 *N*-halamines

Halogens are effective against broad spectrum of microorganisms; however their instability in water and on surfaces limits their use. This disadvantage of the halogens can be eliminated by *N*-halamines. As seen in Figure 1.9, *N*-halamines can stabilize an oxidative halogen on their structure by temporary covalent bonds and release the halogen when encountered with a microorganism. The lethal action of *N*-halamines occurs with the transfer of the oxidative chlorine to the acceptor regions (thiol or amino groups in proteins) of microorganisms (Simoncic and Tomsic, 2010; Sun et al., 2010; Timofeeva and Kleshcheva, 2011). Long term stability in water and dry air, being non-corrosive for surface and non-toxic for human and environment, effectiveness against a broad spectrum of the bacteria make *N*-halamines one of the most efficacious biocidal agent (Hou et al., 2017; Yu et al., 2013).

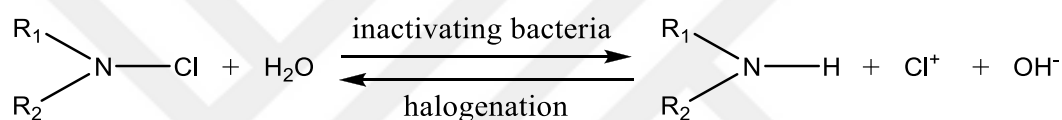


Figure 1.9 : Regenerable property of *N*-halamine compounds (Gao and Cranston, 2008)

Figure 1.10 demonstrates the three types of *N*-halamines; amine, amide, and imide. The N-Cl bond dissociation constants of amine, amide, and imide are $<10^{-12}$, $<10^{-9}$, and $<10^{-4}$, respectively. There is an inverse relationship between the bond length and bond dissociation energy. Even though the length of imide bond is shorter than amide one, its ionic character causes more-rapid hydrolysis of imide bond. So, imide *N*-halamines kill bacteria more rapidly than the other *N*-halamines, but it is the least stable one (Akdag et al., 2006; Kou, 2009).

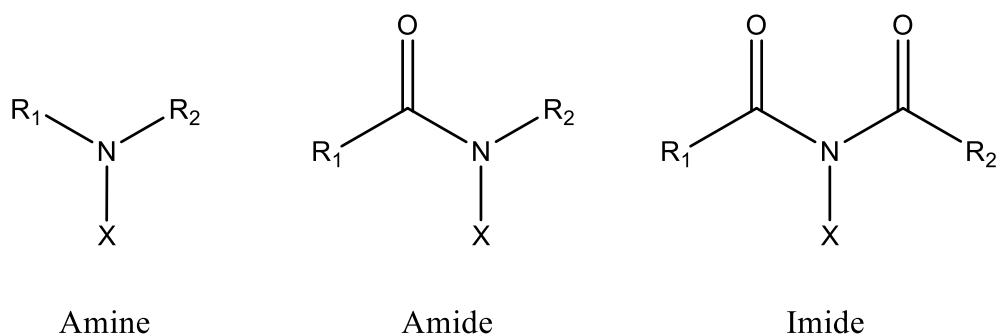


Figure 1.10 : General structure of *N*-halamines

To inhibiting the reestablishment of the microorganisms the stability of *N*-halamine compounds is important. Cyclic *N*-halamine compounds that lack of an α -hydrogen (the hydrogen bonded to carbon atom adjacent to N-X moiety) are the most stable and applicable *N*-halamines. α -hydrogen can cause double bond formation which inhibits the re-chlorination of *N*-halamine compounds (Kaminski et al., 1976).

1.2.4 Antibacterial HFMs

Nano-silver, titanium dioxide, quaternary ammonium salts, and *N*-halamine compounds are generally used in the production of antibacterial membranes to remove the biofilm on the membrane surface. These materials are generally applied by direct addition of the agent to polymer dope solution or by graft polymerization on the HFM surface.

Chou et al. (2005) produced nano-silver added cellulose acetate HFMs. The produced membranes reduced the biodegradation; however, the nano-silver loaded on the membrane lost efficiency in a short span of time like five days. Similarly, in many studies in the literature, the difficulty of regenerating silver atoms is a major disadvantage for nano-silver added systems (Booshehri, et al., 2013; Gunawan et al., 2011; Mansouri et al., 2009; Sawada et al., 2012).

Yuliwati et al. (2011) produced antibacterial poly(vinylidene fluoride) (PVDF) HFMs by addition of titanium dioxide (TiO₂). Since the difficulty of dispersing nano-TiO₂ in polymer mixtures, Resosudarmo et al. (2011) coated the HFM surface with the nano-TiO₂. TiO₂ added systems are not suitable particularly for compact water treatment systems due to the requirement of UV light to activate the TiO₂ (e.g. Li et al., 2004; Rahimpour et al., 2011; Zhang et al., 2014).

Yao et al. (2008) produced antibacterial polypropylene HFMs by grafting quaternary ammonium salts on membrane surface. The obtained membranes showed anti-fouling properties by inactivating the bacteria. However, the very long time requirement (approximately 60 min) to inactivate bacteria and the inability of quaternary ammonium salts to inactivating a wide range of bacteria are the disadvantages of this system.

1.2.5 *N*-halamine added antibacterial HFMs

Even though the biodegradability is reduced by the above methods, chemical backwashings are applied to membranes at regular intervals to prevent biodegradability and generally halogenated oxidants (Cl_2 , Br_2 , I_2 , NaOCl , and ClO_2) are used during these washings (Puspitasari et al., 2010; Regula et al., 2013). In drinking water industry, the membranes are generally disinfected by a 1 min backwashing with chlorine 10 mg/L for every hour and a 15-30 min backwashing with 400 mg/L chlorine for every week (Regula et al., 2013). Therefore, optimizing and improving this disinfection process will be an important step in extending the membrane life.

As mentioned before halogens are inexpensive and very effective agents, but they are not very stable in water. *N*-halamine chemistry is used to make the halogens more stable by forming temporary stable covalent bonds with them (e.g. chlorine and bromine). Chlorine based chemical washing used in water treatment can be converted to an added value by using *N*-halamines. By holding the halogens on membrane structure, the number of washings can be reduced and thus membrane life can be prolonged.

In this regards, Kang et al. (2016) produced antibacterial PVDF ultrafiltration HFMs by addition of *N*-halamine grafted carbon nanotubes to membrane structure. This study requires a two-step processes so direct incorporation of *N*-halamine to membrane structure will be more effective and easier.

2. SYNTHESIS OF *N*-HALAMINE POLYMERS AND THEIR INCORPORATION INTO PVDF ULTRAFILTRATION MEMBRANE STRUCTURE

2.1 Introduction

As mentioned in literature review section, membrane processes are increasingly becoming important for water treatment industry. The major problem of membranes in this industry is membrane organic/bio-fouling, which increases the feed pressure on a membrane and decrease the clean water flux through the membrane. Therefore, it is necessary to apply periodic backwashings to membranes, which deteriorates the membrane structure. To decrease the number of backwashing cycles, it is essential to add hydrophilic and antibacterial agents to membrane structure.

To overcome organic fouling problem, there are many studies suggesting utilization of hydrophilic additives into membrane structure (Liang et al., 2013; Lv et al., 2018; Meyer et al., 2018). Although the organic fouling problem is substantially solved by hydrophilic additives, it is essential to use antibacterial additives to prevent biofouling. In antibacterial applications, the selection of the accurate antibacterial agent depending on the application area is of great importance. In water-treatment applications backwashings are generally applied with halogen sourced oxidizers such as Cl₂, Br₂, I₂, NaOCl, and ClO₂ (Puspitasari et al. 2010; Regula et al., 2013). In general, halogens are not very stable in water so that using an antibacterial agent taking the halogen on its structure would increase the time between backwashings and decrease the biofilm formation on membrane structure. Because of their halogen holding properties, *N*-halamines are the most suitable antibacterial agents for this study. Due to its both good stability and antibacterial activity a hydantoin ring with amide and imide moieties on it; a hydantoin acrylamide (HA) monomer and its various polymers synthesized by Kocer et al. (2011a) was preferred for this study.

The hypothesis of this section of the thesis is “The incorporation of the selected *N*-halamine polymers into the flat sheet PVDF membranes would reduce the biofilm

formation on the membrane surface and improve the filtration performance of the membranes without the need of hydrophilic substances.”

In this part of the study, a hydantoin acrylamide monomer and its homo- and copolymers were synthesized and characterized with FTIR and DSC analysis. Then, a hydrophilic substance (PVP) and synthesized polymers were incorporated into the membrane structure by blending technique. The effects of hydrophilic and antibacterial additions on membrane water flux and BSA rejection performances were investigated and the results were compared with a commercial membrane. The presence of antibacterial additive in membrane structure was characterized by FTIR and XPS analysis. The thermal properties and surface morphology of produced membranes were characterized with DSC and SEM analyses, respectively. The improvement of produced membranes biocidal performance with addition of synthesized polymers was proven.

2.2 Experimental

2.2.1 Materials

For synthesis of N-(2-methyl-1-(4-methyl-2,5-dioxoimidazolidin-4-yl)propan-2-yl)acrylamide (HA), N-(1,1-Dimethyl-3-oxobutyl)acrylamide (DA) (Aldrich), potassium cyanide (Merck) and ammonium carbonate (Sigma-Aldrich) were used. To polymerizing HA, potassium persulfate (PPS) (Acros) was used as initiator. A 9:1 copolymer of HA and 2-Acrylamido-2-methyl-1-propanesulfonic acid sodium salt (SA) (Aldrich) was synthesized.

Polyvinylidene fluoride (PVDF) (Alfa Aesar) and N-Methyl-2-pyrrolidone (NMP) was used as based polymer and solvent in membrane casting solution, respectively. Polyvinylpyrrolidone (PVP) K30 ($M_n=40,000$ g/moles, TCI) was added to the membrane dope solution as a pore former. Sterlitech BN475 (BN) being a commercial PVDF UF membrane was used to compare water flux and BSA rejection performances of the produced membranes. Disodium phosphate ($Na_2HPO_4 \cdot 2H_2O$) (Merck) and sodium dihydrogen phosphate (NaH_2PO_4) (Merck) were used for the preparation of protein feed solution. Bovine Serum Albumin (BSA) (Fisher Scientific) was used for the estimation of protein rejection performance of the produced membranes.

2.2.2 Synthesis of *N*-halamine monomer and its polymers

The HA monomer was prepared according to a procedure described in Kocer et al. (2011b). As seen in Figure 2.1, while producing HA, 17.093 g (100 mmol) *N*-(1,1-Dimethyl-3-oxobutyl)acrylamide (DA), 13.565 g (200 mmol) potassium cyanide, and 57.654 g (600 mmol) ammonium carbonate was reacted in a solvent mixture of water and ethanol (1:1 by volume) for one week at room temperature. After evaporation of ethanol, the crude products were isolated by treating with dilute HCl and filtrated.

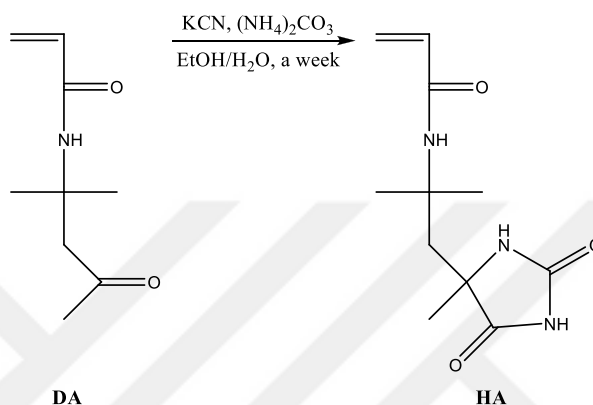


Figure 2.1 : Synthesis of the hydantoin acrylamide

HA monomer was polymerized by free radical polymerization. The HA (8.4 mmol) was dissolved in water with 0.004 g of initiator, potassium persulfate. By nitrogen bubbling for 15 min dissolved oxygen was removed and the reaction was continued under nitrogen atmosphere by stirring at 75 °C for 4 h. The obtained polymer was filtered as white powder form. The reaction mechanism of the homopolymer (HP) was given in Figure 2.2.

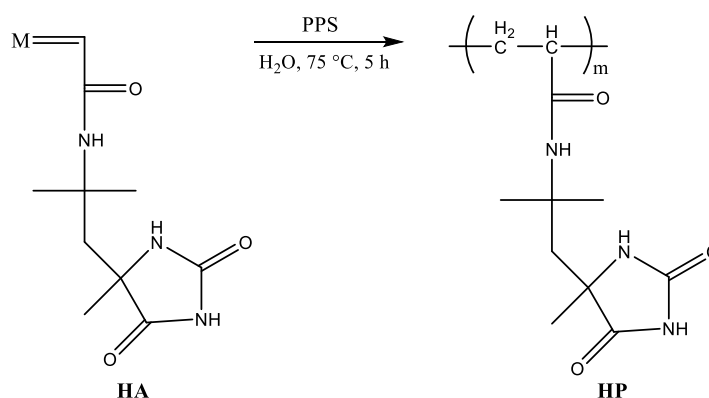


Figure 2.2 : Synthesis of the homopolymer

The 9 mmol HA was copolymerized with 1 mmol 2-Acrylamido-2-methyl-1-propanesulfonic acid sodium salt (SA) by free radical polymerization. 2.15 g of HA

and 0.46 g of SA was dissolved in 50 mL distilled water together with 0.01 g potassium persulfate. By nitrogen bubbling for 15 min dissolved oxygen was removed and the reaction was continued under nitrogen atmosphere by stirring at 75 °C for 4 h. The water was removed by evaporation to take the synthesized polymer. The reaction mechanism of copolymer (CP) was given in Figure 2.3.

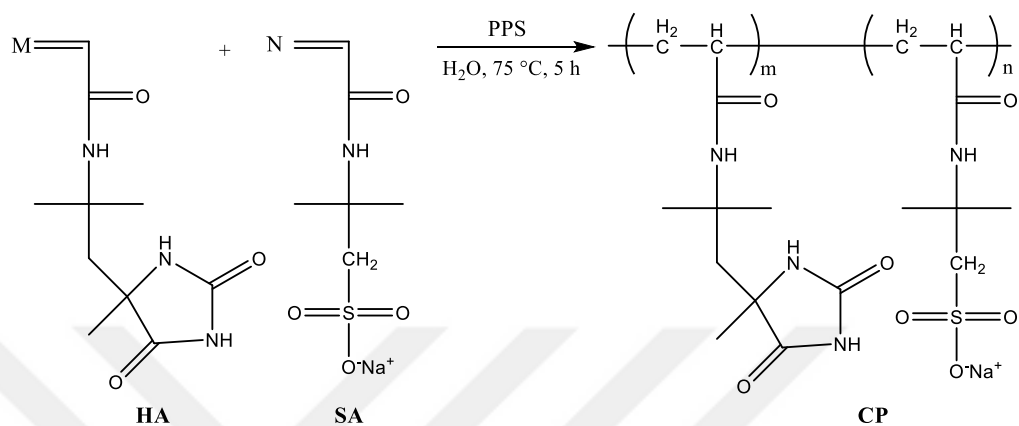


Figure 2.3 : Synthesis of the copolymer

2.2.3 Preparation of the ternary phase diagrams

Ternary phase diagrams of polymer/solvent/nonsolvent systems were drawn to take information about thermodynamic stability and phase separation behavior of the polymers. Ternary diagrams were drawn according to the cloud point test. Nonsolvent (water) was dropwise added to the polymer dope solution stirring at 30 °C. The addition of nonsolvent was stopped when the appearance of dope solution turn to milky-like structure for low concentration solutions and local precipitation was observed and not disappeared for a specific time for high concentration polymer solutions. For low concentration solution after turbidity occurred, stirring was continued for further 30 min to observe the turbidity is disappear or not disappear. If the solution turns to clear, more nonsolvent addition was made to the solution, otherwise the found point is saved as cloud point and composition of the ternary point was calculated according to the polymer, solvent, and nonsolvent weights.

2.2.4 Polymer blends and flat sheet membrane production

Phase inversion method was used to prepare membranes. Pristine PVDF (M-0), just PVP added (M-P30, M-P35, M-P40, M-P45), both PVP and HP added (M-P35-HP1, M-P35-HP3, and M-P35-HP5), just polymer added (M-HP1, M-HP3, M-CP3, and M-CP5) added membranes were prepared as summarized in Table 2.1. While

preparing membrane dope solutions, firstly, HP or CP was dissolved in NMP by stirring at 60 °C for 2 h, then PVDF (and PVP) was added and stirring was continued for extra 4 h, and the mixture was stirred overnight at 40 °C to obtain a homogeneous solution. 200 µm films were produced on a glass sheet with the help of a film applicator. The coagulation of films was made in a tap water bath at 30 °C, and then the produced films were kept in distilled water at 30 °C.

Table 2.1 : Casting solution compositions of the produced membranes.

Membranes	Component Compositions				
	PVDF (wt%)	PVP (wt%)	HP (wt%)	CP (wt%)	NMP (wt%)
M-0	18.00	-	-	-	82.00
M-P30	18.00	0.30	-	-	81.70
M-P35	18.00	0.35	-	-	81.65
M-P40	18.00	0.40	-	-	81.55
M-P45	18.00	0.45	-	-	81.65
M-P35-HP1	17.82	0.35	0.18	-	81.65
M-P35-HP3	17.46	0.35	0.54	-	81.65
M-P35-HP5	17.10	0.35	0.90	-	81.65
M-HP1	17.72	-	0.18	-	82.00
M-HP3	17.46	-	0.54	-	82.00
M-CP1	17.72	-	-	0.18	82.00
M-CP3	17.46	-	-	0.54	82.00

2.2.5 Chlorination of the produced membranes

For chlorination 10% aqueous solution of 6% sodium hypochlorite (household bleach) was prepared and the pH of the solution was adjusted to 7 with 6 N HCl. After the produced membranes were kept in this solution for 1 h, the unbonded chlorine on membrane was removed by washing with tap and distilled water, and 1 h drying at 45 °C. Iodometric/thiosulfate titration was applied to determine the loaded chlorine concentration onto the samples (Kocer et al., 2010). A solution of ethanol with 0.1 N acetic acid (90/10; v/v) was prepared and 0.25 g potassium iodide was dissolved in this solution, then the dried membrane sample was added to the solution. Titration was made with 0.005 N sodium thiosulfate solution until the color of the solution is yellow to clear. The weight percent of the loaded chlorine (Cl^+) on the membrane samples were calculated according to the equation given below:

$$Cl^+ \% = \left[\frac{N \times V_T \times 35.45}{2 \times W} \right] \times 100 \quad (2.1)$$

where Cl^+ , N , V_T , and W refer to weight percent of the oxidative chlorine on the membrane samples, titrant solution concentration (mol/L), titrant solution volume (L), and sample weight (g), respectively.

2.2.6 Permeability tests of the produced membranes

All produced membranes were kept in distilled water for seven days and the membrane pores were opened by wetting isopropanol before the permeability tests. Water flux tests were applied two times for HP and CP added membranes, before and after chlorination.

Dead-end filtration method was used to determine water flux performance of the membranes. The schematic and real images of the installed dead-end filtration system with HP4750 Sterlitech stirred cell were given in Figure 2.4. The effective membrane filtration area of the system was 14.6 cm^2 . Water filtration experiments were performed under three different constant pressures of 1, 3, and 5 bars.

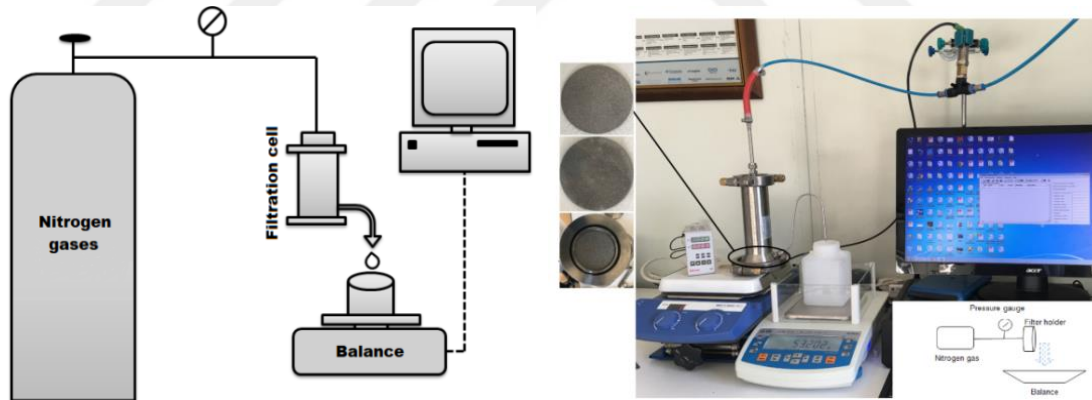


Figure 2.4 : Filtration test system

The pure water fluxes ($\text{L/m}^2\text{h}$) of the produced membranes were calculated according to the equation given below:

$$J_w = \frac{V_w}{A \times t} \quad (2.2)$$

where J_w , V_w , A , and t refer to pure water flux (PWF), permeated water volume (L), effective membrane area (m^2), and filtration time, respectively.

A phosphate buffer solution (0.1 M, pH 7) containing 1 g/L BSA was prepared to perform BSA rejection tests. The protein content in filtrated solution after one hour filtration was determined with UV-Visible spectrophotometer at 280 nm wavelength. Scinco-NEOSYS200 UV-Visible spectrophotometer was used for analysis and the rejection ratios of the produced membranes were calculated according to the equation given below:

$$R(\%) = \frac{C_f - C_p}{C_f} \times 100 \quad (2.3)$$

where R , C_f , and C_p refer to protein rejection percentage (%), feed solution BSA concentration, and filtrated solution BSA concentration, respectively. For the pure water flux and BSA rejection performances, the membranes were tested at least three times and the results were given as mean value along with the standard deviations.

2.2.7 Characterization of the produced membranes

Attenuated total reflectance Fourier-transform infrared (ATR-FTIR) spectroscopy (Thermo Nicolet, IS50) was used to characterize the produced monomer, polymers (HP and CP), and membranes. While recording the spectra 16 scans were made at 4 cm^{-1} spectral resolution and the scanning range was from 400 to 4000 cm^{-1} .

Thermal properties of the produced monomer and polymers were characterized with Perkin Elmer DSC 8000. Experiments were carried out under nitrogen atmosphere. Thermal transitions of samples were taken by heating the samples to 300 °C with 10 °C/min heating rate.

Thermo Scientific, K-Alpha spectrometer with a monochromated Al K α (1486.6 eV) X-ray source was used to take X-ray photoelectron spectra (XPS) measurements. All binding energy corrections were made according to the carbon photo electron signal at 284.6 eV.

Thermal properties of the produced membranes were characterized with TA Instrument, Q2000 differential scanning calorimeter (DSC). Firstly, thermal history on membrane samples (7-8 mg) were erased by heating the sample to 250 °C from 50 °C with a 10 °C/min heating rate, then the sample was cooled to 50 °C and heated to again 250 °C with 10 °C/min heating rate under nitrogen atmosphere.

The morphologies of the membranes were characterized with FEI, QUANTA 200F Field Emission scanning electron microscope. Images of gold-palladium coated (10 nm) membranes were obtained at 5,000x and 50,000x magnifications.

Biocidal performances of the produced membranes were determined according to ASTM E 2149. *Staphylococcus aureus* (ATCC 6538) and *Escherichia coli* (ATCC 35218) bacteria were used for tests. Bacteria suspension with 5×10^5 CFU/mL concentration were treated to the chlorinated (M*) and unchlorinated membrane samples. The 1 g of membrane samples were put in 50 mL bacteria suspension and shaken for four different contact times as 5 min, 15 min, and 60 min. Then serial dilutions with phosphate buffer solution were prepared and spread onto Muller-Hilton II agar plates. Before colonies were counted, the agar media was waited at 37 °C for 24 h and the bacterial reduction was determined as logarithmic.

2.3 Results and Discussion

2.3.1 Characterization of the synthesized monomer and polymers

As seen in Figure 2.1 hydantoin ring was formed from ketone moiety of DA. The formation of hydantoin ring from a ketone moiety occurs via Bucherer-Bergs reaction as seen in Figure 2.5 (Kou, 2009).

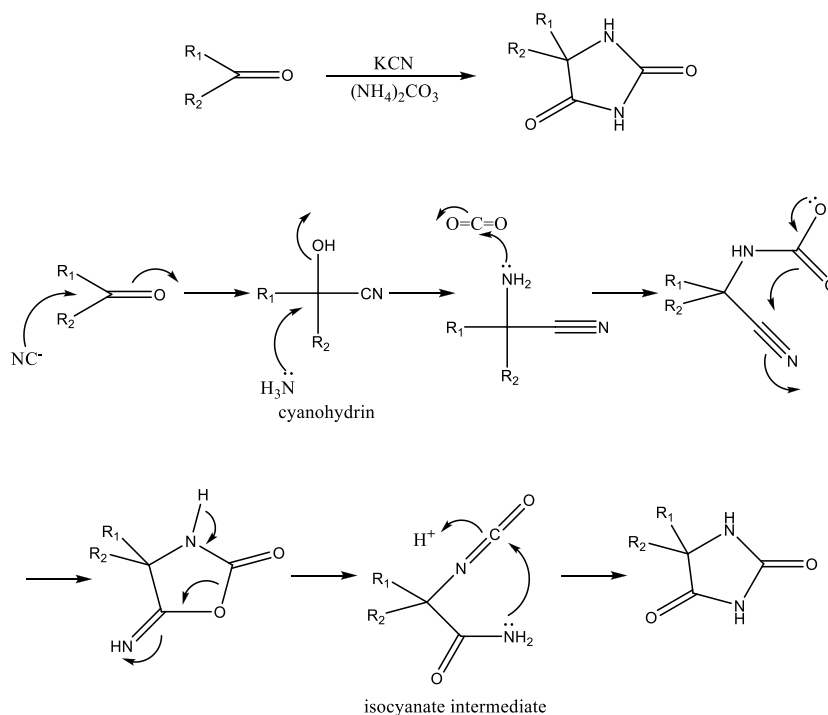


Figure 2.5 : The mechanism of the Bucherer-Bergs reaction

The FTIR spectrum of DA and synthesized HA was demonstrated in Figure 2.6. The formation of hydantoin ring was confirmed by the new bands stretching at 3202 cm^{-1} , 1760 cm^{-1} , and 1707 cm^{-1} . The band at 3202 cm^{-1} was corresponding to additional N-H stretching of HA. The other two bands at 1760 cm^{-1} and 1707 cm^{-1} are amide and imide carbonyl stretching on the hydantoin ring, respectively.

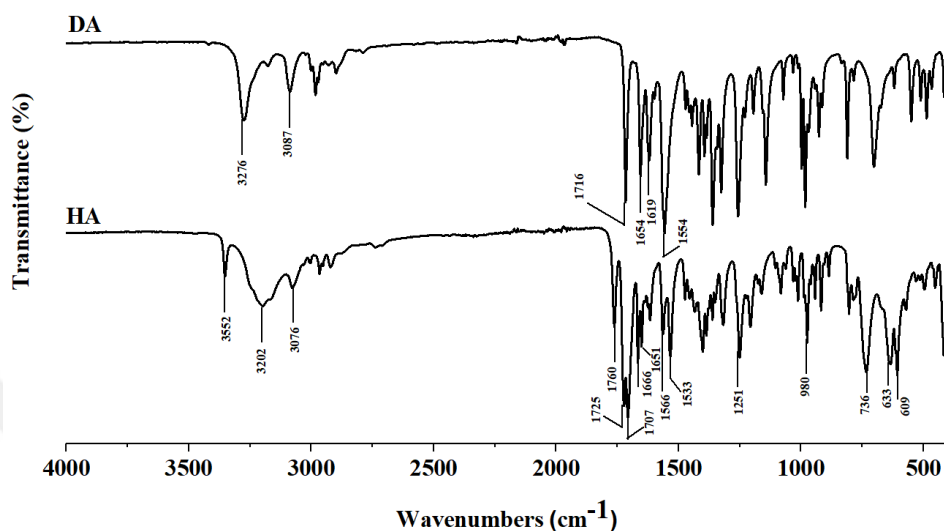


Figure 2.6 : FTIR spectra of the DA and HA

FTIR spectrum of the synthesized homopolymer and copolymers are shown in Figure 2.7. The lack of vinyl bond stretching at 1630 cm^{-1} (overlapped for HA) and the broadening of the bands confirmed the formation of polymerization. On the other hand, the new bands at 1177 cm^{-1} and 1039 cm^{-1} being characteristic for SO_3^- group asymmetric and symmetric stretching demonstrated the SA presence in the copolymer structure.

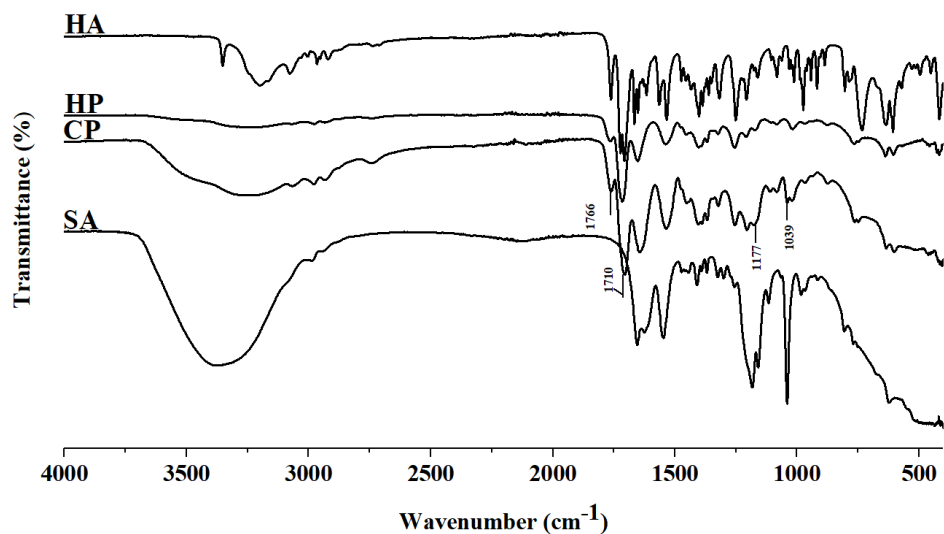


Figure 2.7 : FTIR spectra of the synthesized polymers

DSC thermograms of the DA and HA were given in Figure 2.8. Because of the hydantoin ring formation which increases the H-bonding sites in structure, there was approximately 100 °C increase in melting point of HA according to DA. However, there was no meaningful change observed in HP and CP thermograms between 40 °C and 300 °C.

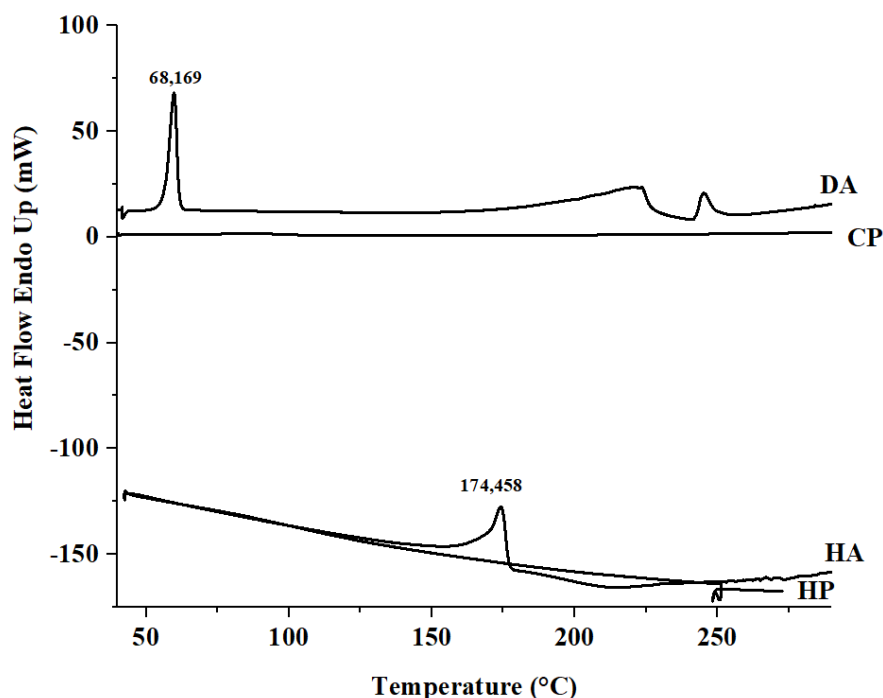


Figure 2.8 : DSC thermograms of the DA, HA, HP, and CP

2.3.2 Ternary phase diagram of the polymer/NMP/water system

Ternary phase diagram of polymer/solvent/nonsolvent at 30 °C were determined in order to understand the thermodynamic behavior of membrane formation process. Thermodynamic analysis informed the effect of our synthesized polymers addition to the demixing process. The binodal curve determined with cloud point test is a measure of thermodynamic stability of the membrane casting solution. As the distance between the binodal curve and the solvent axis increases, the thermodynamic stability of the solution increases. Therefore, more nonsolvent is required for coagulation. According to Figure 2.9 the thermodynamic stabilities of the polymers were ranked from highest to lowest as CP, HP, and PVDF. This ranking showed that the thermodynamic stability of the solution is directly proportional to the hydrophilicity of the polymer. This means that the nonsolvent requirement for precipitation is higher for the hydrophilic polymers. The precipitation behavior

difference of PVDF and the synthesized polymers deteriorate membrane surface structure, as evidenced by SEM surface images of the membranes.

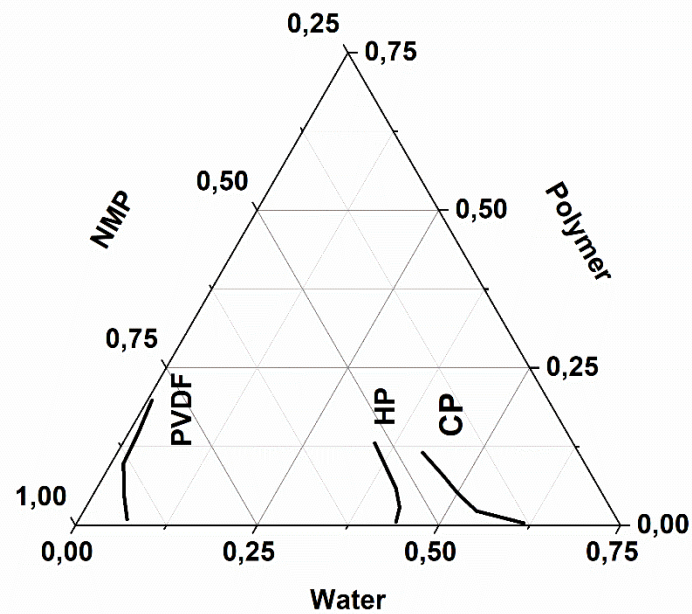


Figure 2.9 : Ternary phase diagram of the Polymer (PVDF, HP, and CP)/NMP/Water systems at 30 °C

2.3.3 Filtration and BSA rejection performance of the produced membranes

To control the organic membrane fouling and increase the membrane water flux, addition of hydrophilic substances such as PVP has been studied in various recent study in literature (Fadilah and Hassan, 2016; Zuo et al., 2008). The pure water flux and BSA rejection performances of commercial and produced membranes were given in Figure 2.10 and Figure 2.11, respectively. As seen in Figure 2.10 PVP addition increased both the pure water flux and BSA rejection performances of the membranes. However, despite this increase, the water flux values of the produced membranes were very low compared to the commercial membrane. On the other hand, contrary to the low water flux performance of the produced membranes, M-P30 and M-P35 membranes demonstrated good BSA rejection performances being even higher than the BN. Although the BSA rejection values were almost same for M-P30 and M-P35, since the M-P35 had higher water flux performance, the HP addition was applied to M-P35 membrane recipe in the next part of the study.

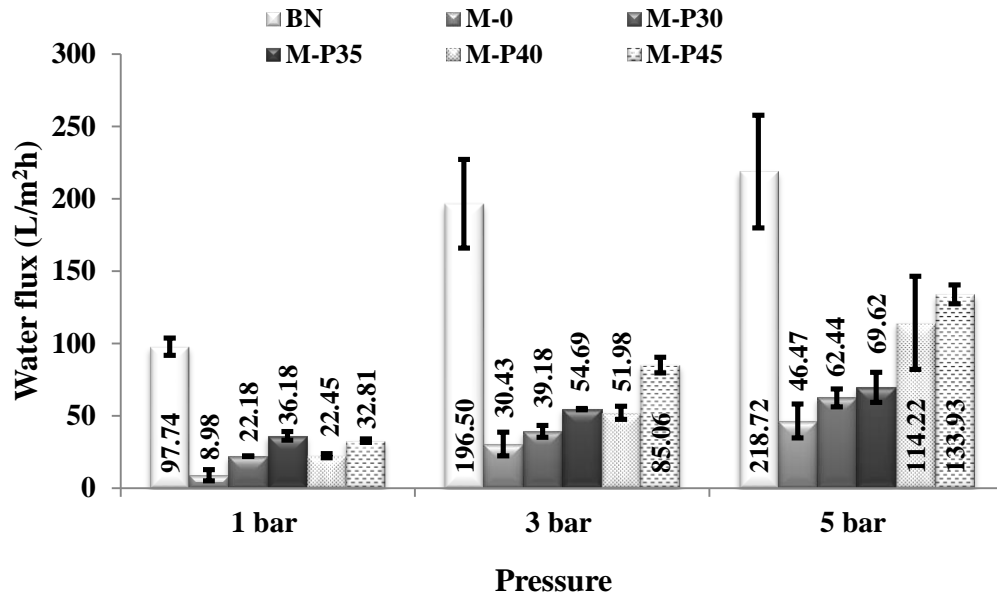


Figure 2.10 : Pure water flux of the commercial, PVP added, and unmodified membranes

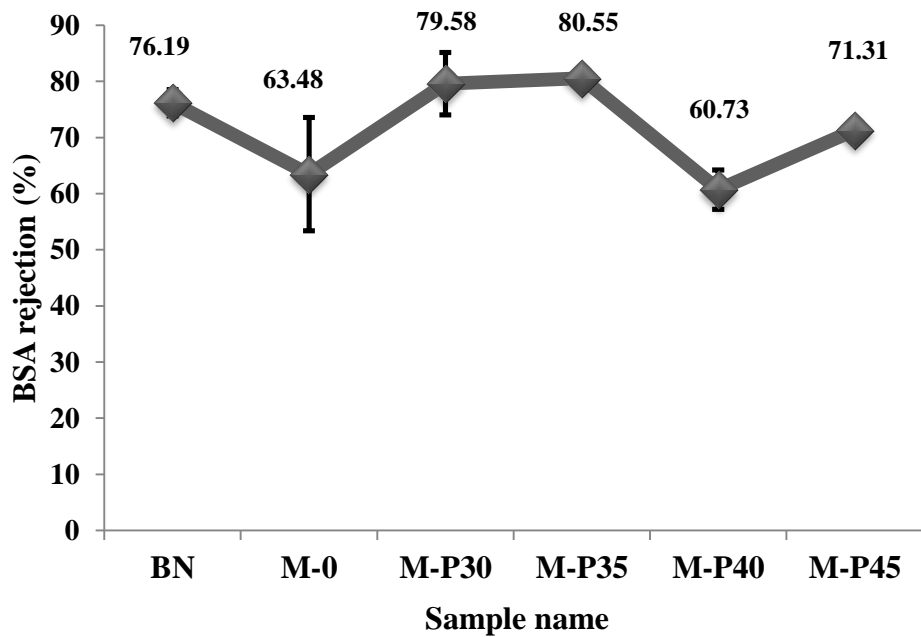


Figure 2.11 : BSA rejection of the commercial, PVP added, and unmodified membranes

In that part of the study, the effect of HP addition on membrane flux and BSA rejection performances was investigated by making various amount of HP addition in determined PVP added recipe (M-P35). Figure 2.12 demonstrated that the addition of HP cause a dramatic increase in water flux values of the membranes. Although the water flux values of HP added membranes were higher than the BN (especially at 3

and 5 bar pressures), BSA rejection ratio of the HP added membranes decreased by about 20% to 30% as seen in Figure 2.13.

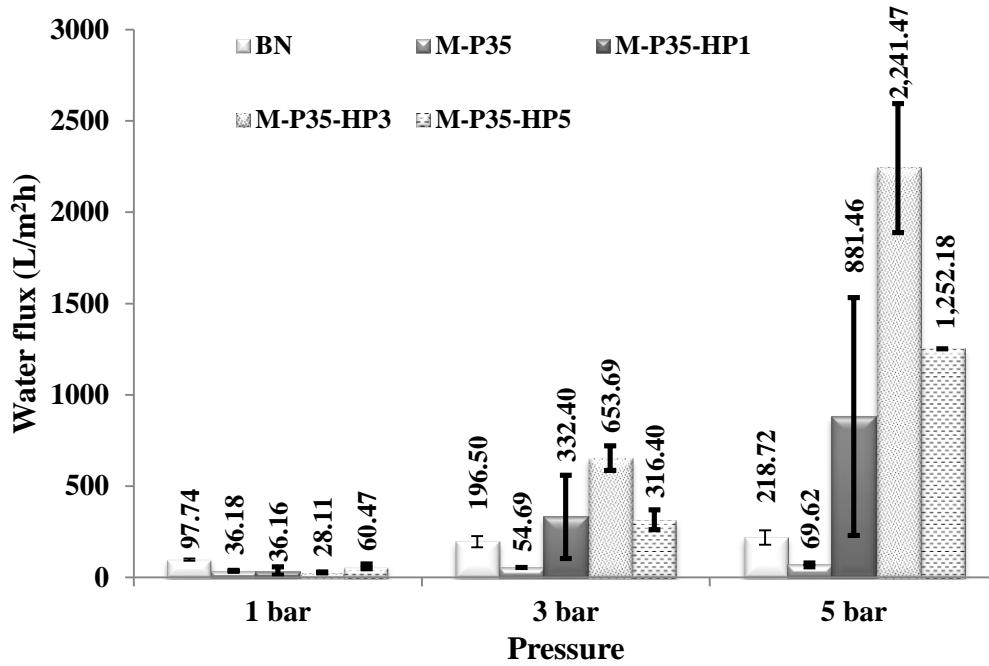


Figure 2.12 : Pure water flux of the commercial, PVP added, and HP added membranes

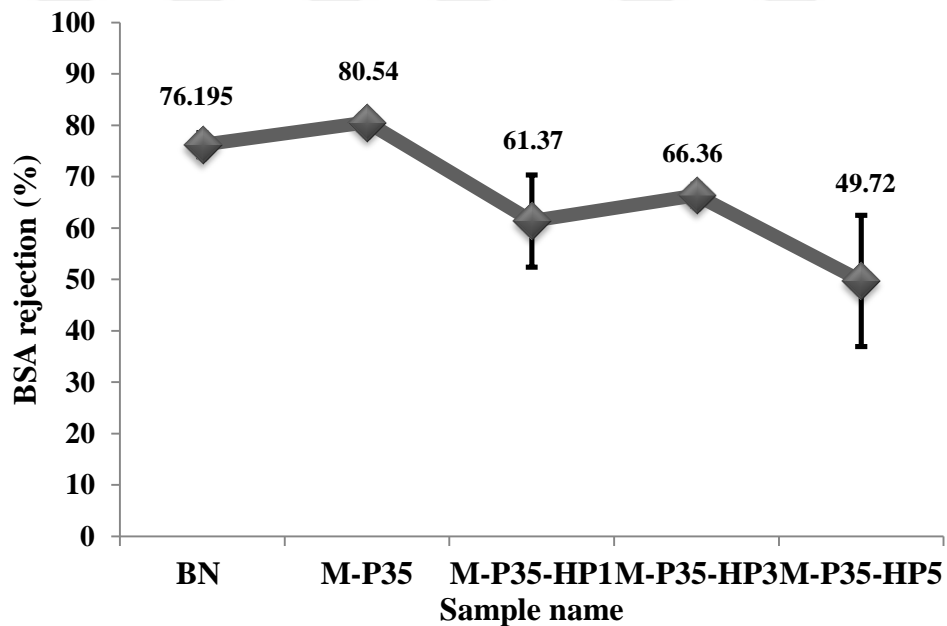


Figure 2.13 : BSA rejection of the commercial, PVP added, and HP added membranes

High water flux obtained by the addition of HP in the membrane structure showed that the membrane flux can be increased without hydrophilic additives such as PVP or PEG in contrast to that done in many studies. In addition, Causserand et al. (2015),

Hanafi et al. (2014), and Pellegrin et al. (2013) showed that PVP in membrane structure is degraded during sodium hypochlorite backwashings and decreases the resistance of the membrane. During these backwashings, the removal of PVP from the membrane structure decreases the hydrophilicity of the membrane. On the other hand, the formation of gaps with leaching of PVP in the inner parts of the membrane decreases the mechanical resistance of the membrane (Causserand et al., 2015; Pellegrin et al., 2013). In this context, the production of membrane without adding PVP could be extended the membrane lifetime. Therefore, in that stage of the study only the synthesized polymers (HP and CP) additions were made to the membrane structure.

As previously mentioned, backwashings are carried out with chlorine in industrial applications and chlorination is required in order to activate our polymers (HP and CP). Therefore, at this stage of the study, water flux tests were applied to HP and CP added membranes both before and after chlorination. The water flux tests results, Figure 2.14 and Figure 2.15, demonstrated that chlorination caused an increase in the water flux performances of membranes. When this result was evaluated together with the SEM images, this increase observed in the water flux values was probably related to the cleaning of the membrane surface. Although the water flux performances of the membranes produced by the addition of HP or CP were not as good as the membranes produced with HP and PVP addition, as seen in Figure 2.16 the BSA rejection of M-HP1 was close to M-P35 and also higher than the BN.

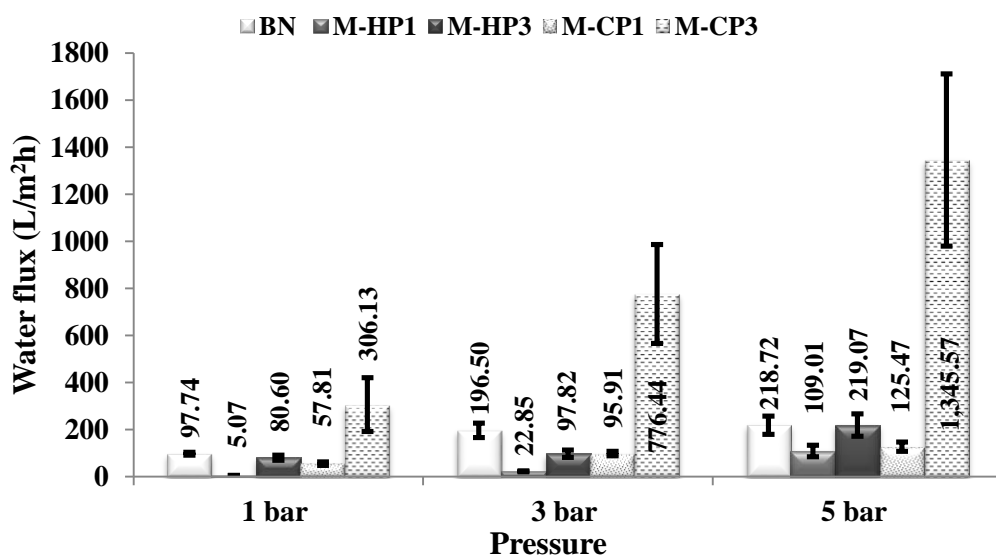
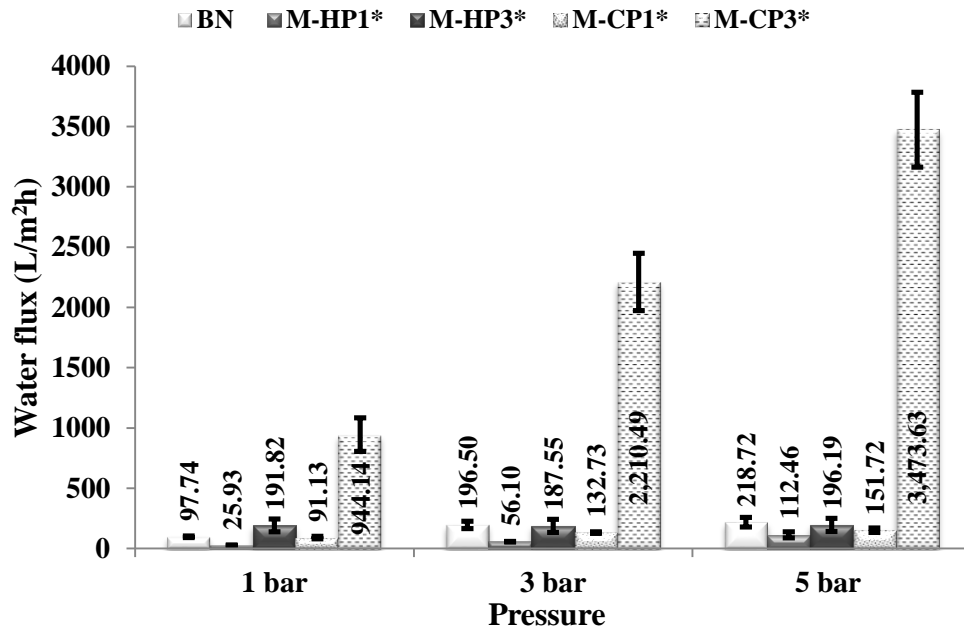
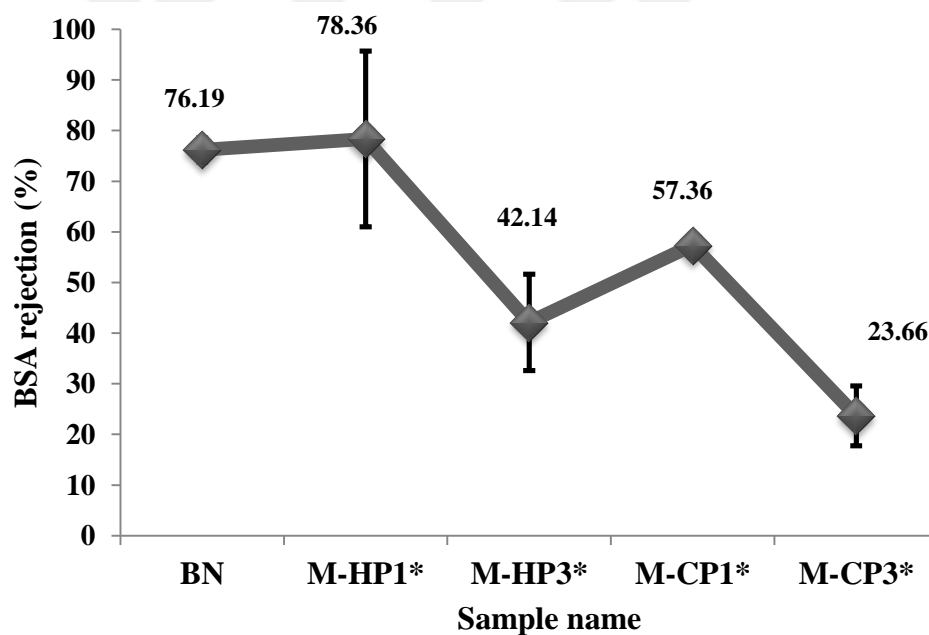


Figure 2.14 : Pure water flux of the commercial, HP and CP added membranes



*Chlorinated membranes

Figure 2.15 : Pure water flux of the commercial, HP and CP added chlorinated membranes



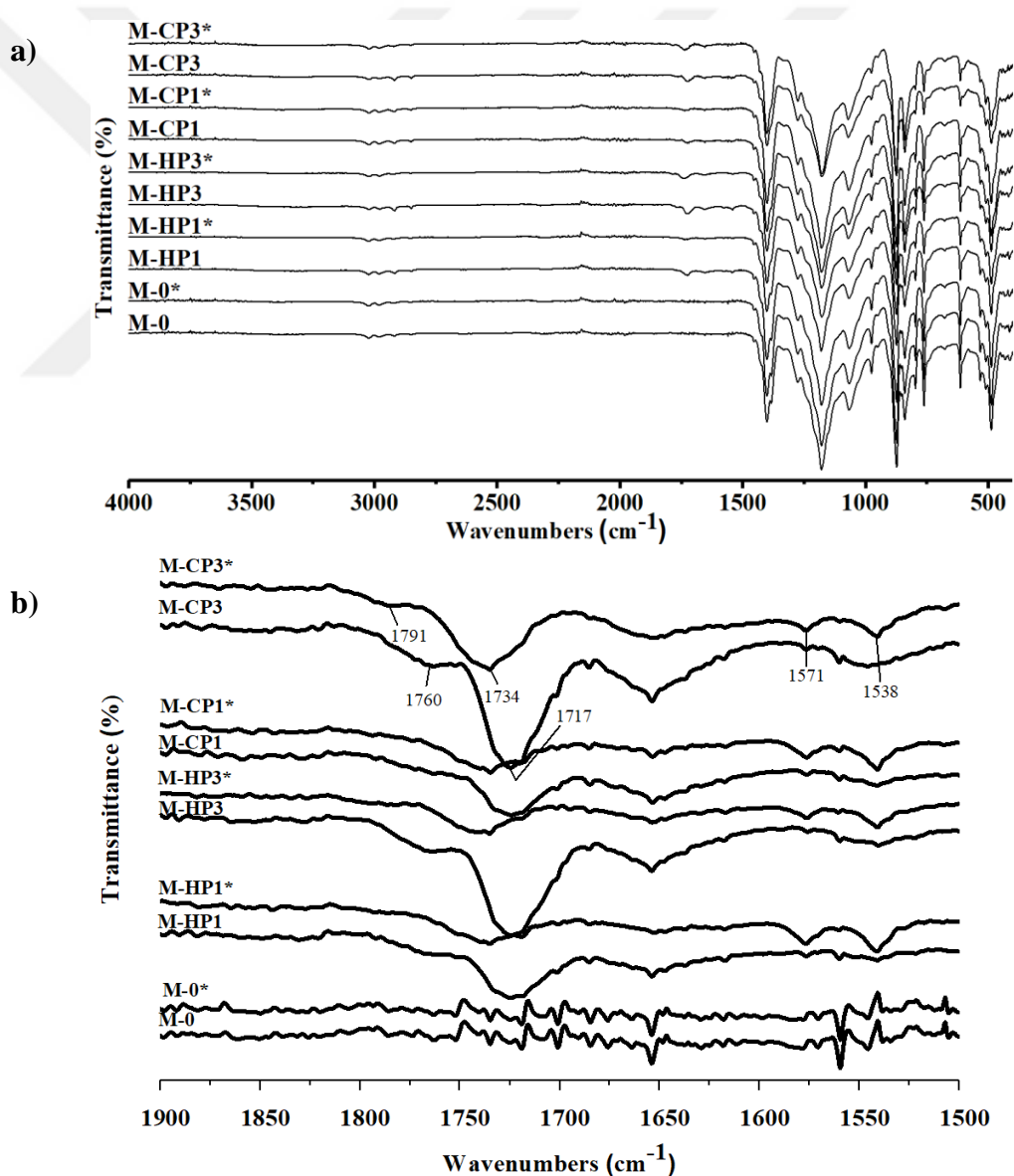
*Chlorinated membranes

Figure 2.16 : BSA rejection of the commercial, HP and CP added chlorinated membranes

2.3.4 FTIR and XPS characterization of the produced membranes

FTIR spectra of the produced membranes both for chlorinated and unchlorinated were given in Figure 2.17a, with full scale spectrum between 400 cm⁻¹ and 4000 cm⁻¹ wavenumbers and in Figure 2.17b, by focusing on the region between 1500 cm⁻¹ and 1900 cm⁻¹ wavenumbers. In HP and CP added membranes spectra, M-HP1, M-HP3,

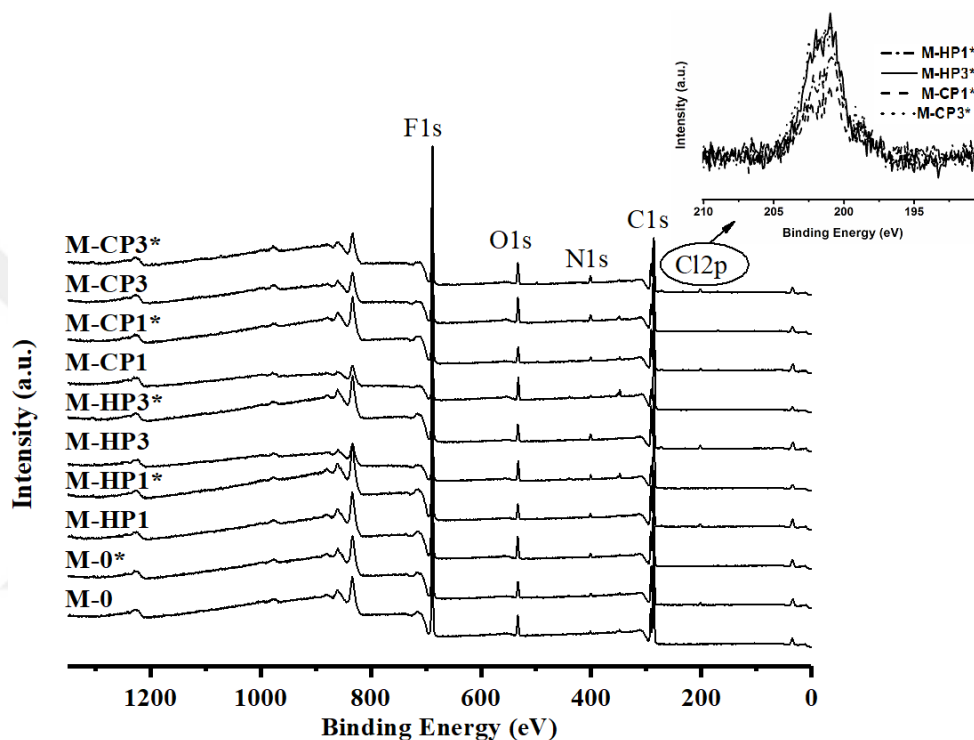
M-CP1, and M-CP3, there were two additional bands at 1717 cm^{-1} and 1760 cm^{-1} corresponding to amide and imide carbonyl stretching of the hydantoin ring. As seen more clearly in Figure 2.17b, as the HP and CP addition rates in the membrane structure increased, the intensity of these two bands also increased. With chlorination, the bond between N-H converts to N-Cl and this conversion causes disruption of hydrogen bonding (N-H...O=C). This bond breakage caused by chlorination was clearly seen in Figure 2.17b by the shift of the bands at 1717 cm^{-1} to 1734 cm^{-1} and 1760 cm^{-1} to 1791 cm^{-1} . This indicated that the HP and CP added membranes could retain chlorine in their structure. At the same time, similar to the literature, after chlorination the broad amide band at 1535 cm^{-1} formed two separate bands at 1538 cm^{-1} and 1571 cm^{-1} .



*Chlorinated membranes

Figure 2.17 : FTIR spectra of the produced membranes

The HP, CP addition and chlorination effects on the membrane surface chemical structure were determined with XPS analysis. The XPS spectra of the produced membranes were given in Figure 2.18. There was an additional peak at about 200 eV corresponding to Cl2p in chlorinated membranes spectra demonstrated the N-Cl bond formation and confirmed the FTIR results. On the other hand, with addition of the synthesized polymers (HP and CP) to the membrane structure the intensities of the bands corresponding to N1s (400 eV), and O1s (532 eV) were increase.

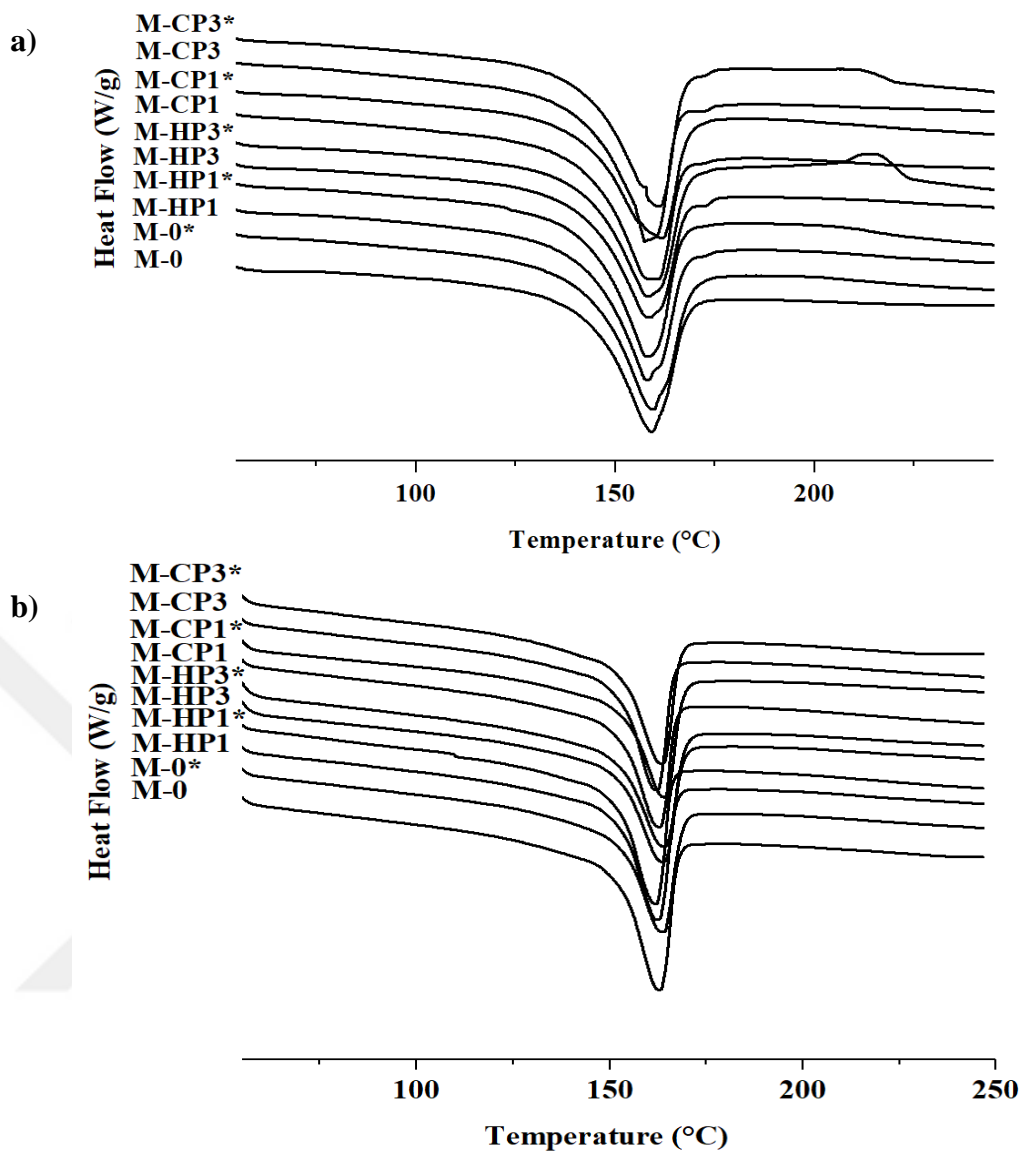


*Chlorinated membranes

Figure 2.18 : XPS spectra of the produced membranes

2.3.5 Thermal properties of the produced membranes

Thermal properties of the produced membranes were determined with DSC analysis including two heating cycles as shown in Figure 2.19. While the melting point of the membranes in the first heating cycle was at around 158 °C, the melting peak shifted to 162 °C in the second cycle. The 4 °C difference between the first and second heating cycles resulted from the mechanical stretching history on the membranes in the first heating cycle. The presence of chlorine in chlorinated membrane structure was also confirmed by DSC analysis. As seen in Figure 2.19a, synthesized polymers added and chlorinated membranes, M-HP1, M-HP3, M-CP1, and M-CP3 showed an additional peak at around 220 °C. This new exothermic peak represented the thermal decomposition of N-Cl bond.



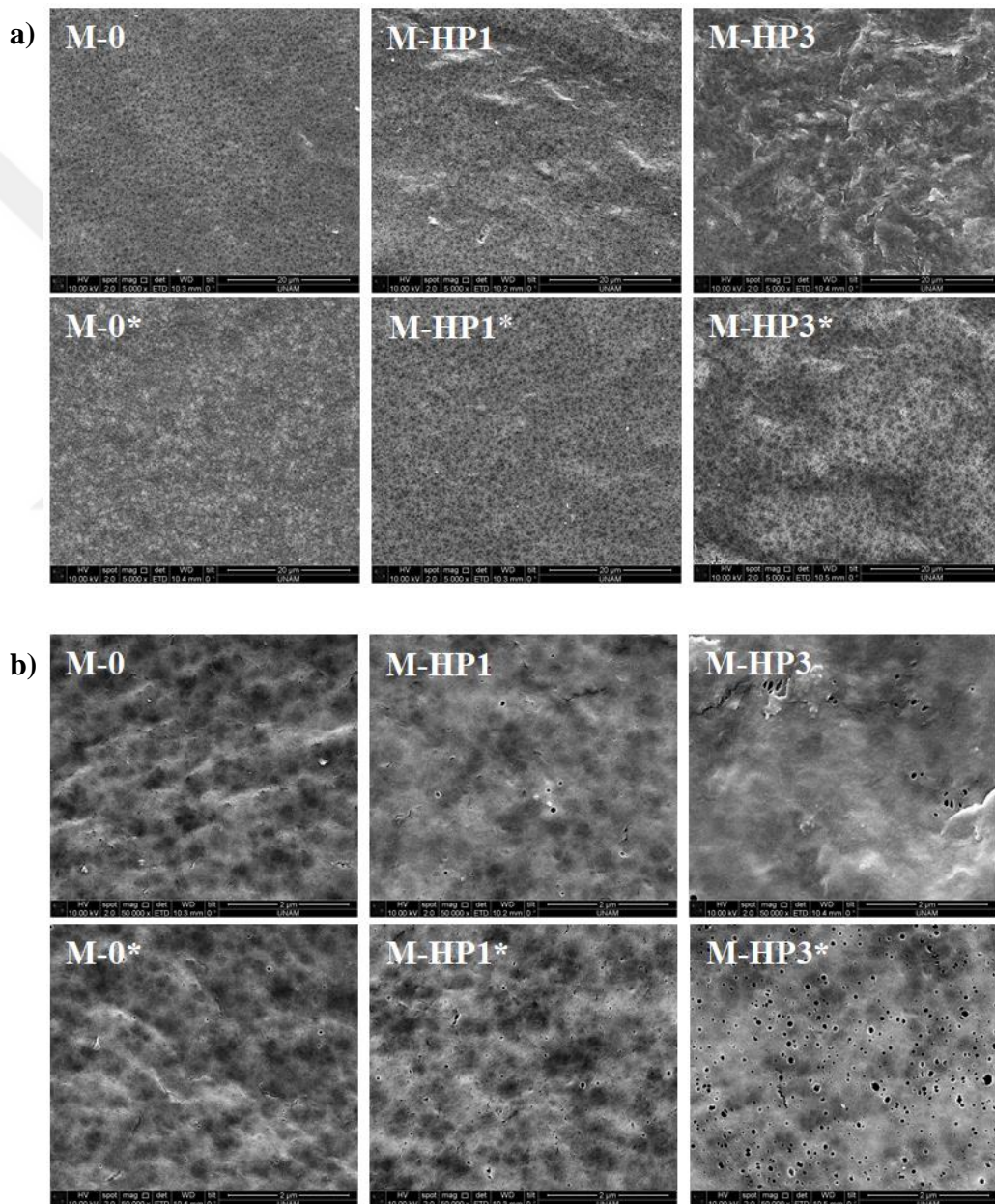
*Chlorinated membranes

Figure 2.19 : DSC thermograms of the produced membranes; (a) during first heating cycle, and (b) during second heating cycle

2.3.6 Morphology of the produced membranes

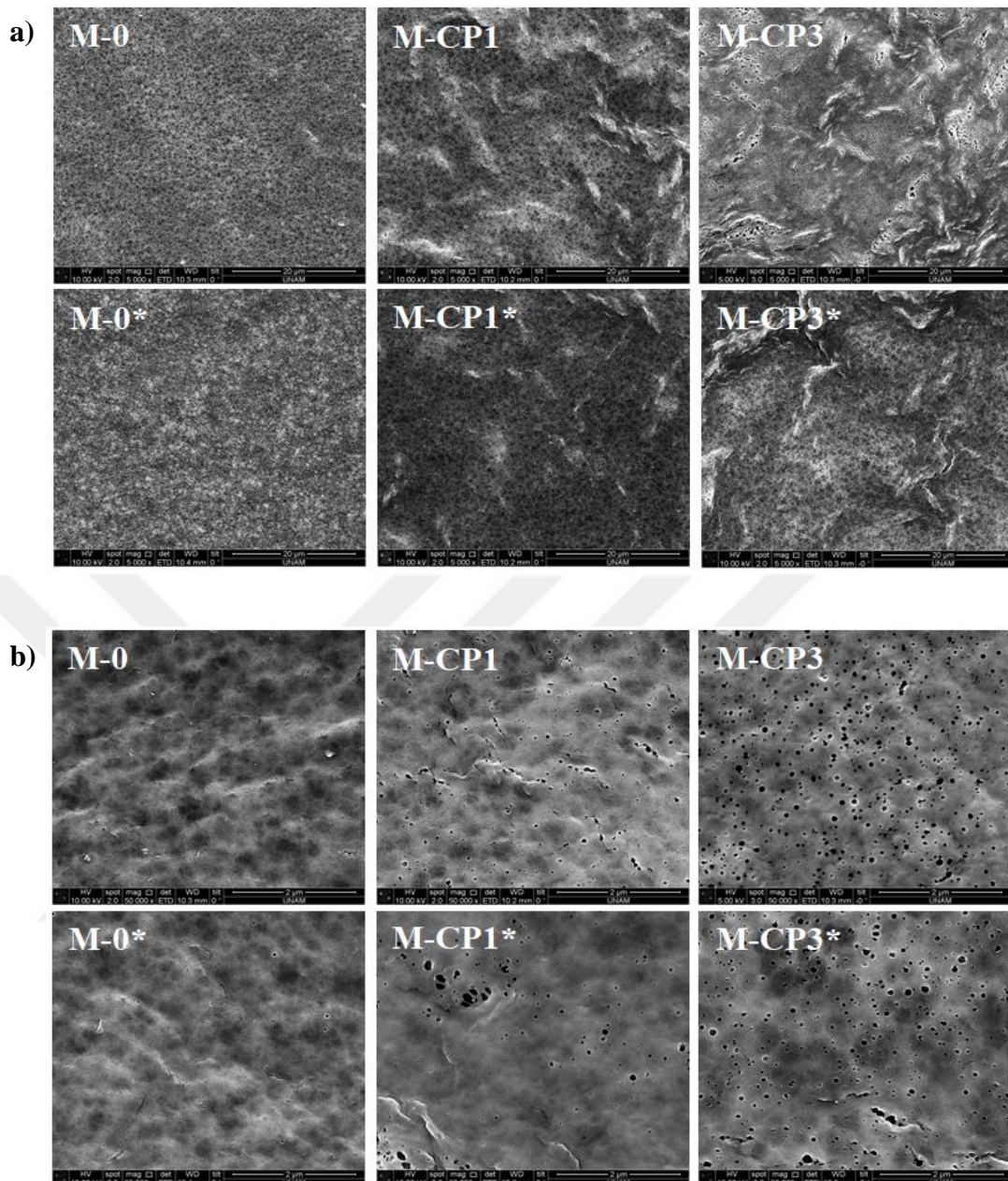
The effects of the additions on membrane surface morphology were investigated with SEM analyses as seen in Figure 2.20 and 2.21. The SEM images were taken with 5,000x and 50,000x magnifications. SEM images demonstrated that chlorination was cleaned the surface of the membranes and increase the membrane water flux values as mentioned in section 2.3.3. It was observed that the addition of synthesized polymers (HP and CP) to membrane structure both increase the porosity and pore size of the membranes. However, especially the high amount addition of HP and CP to the membrane structure cause a huge surface deterioration, a wider pore size distribution, and large cracks formation on the membrane surface. That deformation

on the membrane surface could be caused by the very different phase separation behavior of PVDF and synthesized polymers as explained in ternary phase diagrams. The delayed demixing of solvent – nonsolvent in synthesized polymers deteriorates the smooth membrane surface formed by the rapid precipitated PVDF. The relationship between the membrane surface deterioration and polymer phase separation behavior was proven with more deteriorated surface of M-CP3* according to M-HP3*, the additive of M-HP3* had a smaller thermodynamic stability difference with PVDF than M-CP3* one.



*Chlorinated membranes

Figure 2.20 : The surface morphology of the unmodified, HP added and chlorinated membranes (a) at 5,000x magnification, (b) at 50,000x magnification



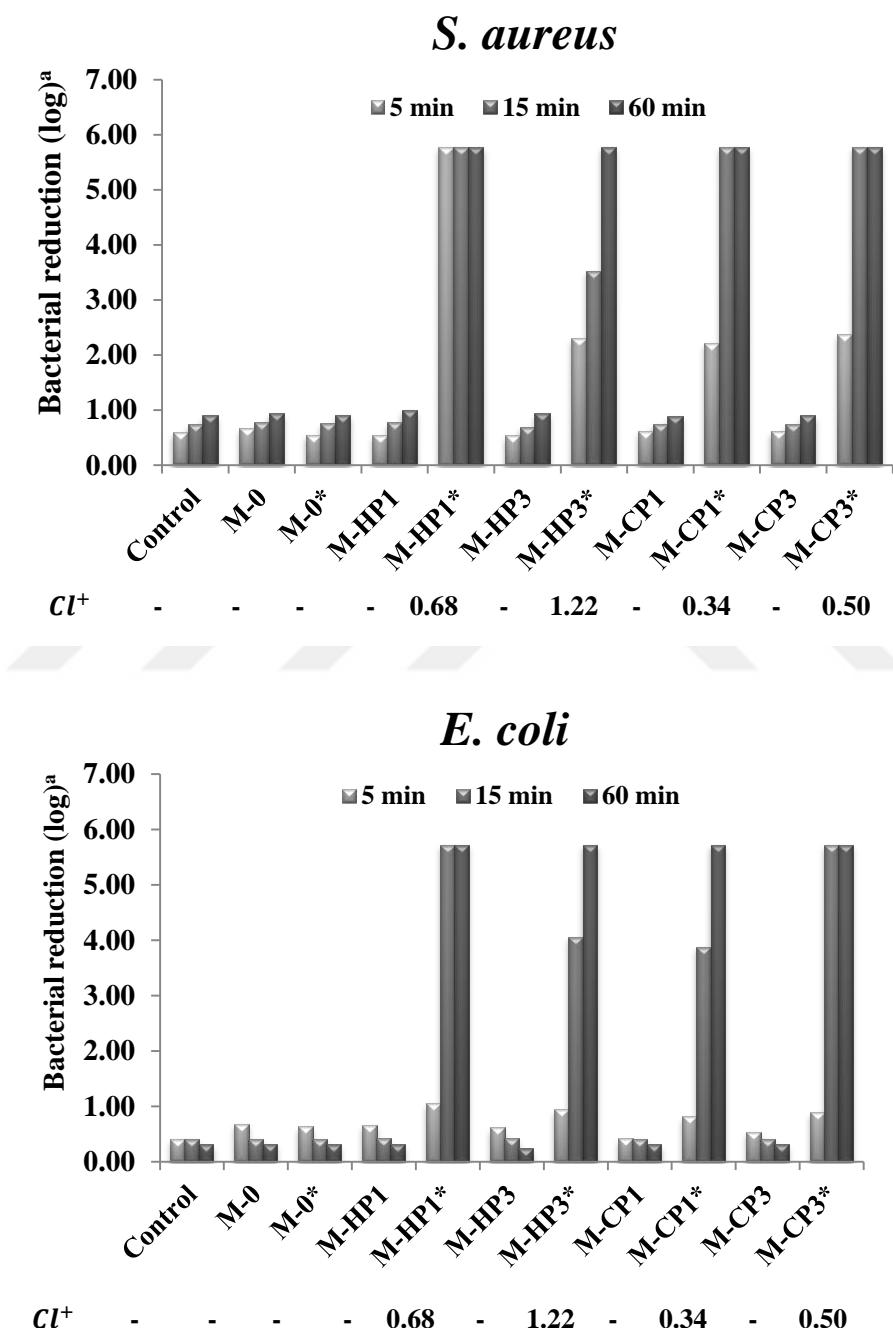
*Chlorinated membranes

Figure 2.21 : The surface morphology of the unmodified, CP added and chlorinated membranes (a) at 5,000x magnification, (b) at 50,000x magnification

2.3.7 Biocidal performance of the produced membranes

The biocidal performances of the produced membranes (both chlorinated and unchlorinated samples) were tested against *S.aureus* and *E.coli* at concentration of about 10^5 CFU/mL, for various contact times as 5 min, 15 min, and 60 min. As seen in Figure 2.22, the control sample that was not include any membrane, unchlorinated samples (M-0, M-HP1, M-HP3, M-CP1, M-CP3), and the chlorinated sample of the pristine PVDF membrane (M-0*) did not show inactivation even at the end of the 60 min. The chlorine loading effect on the biocidal performance was determined by

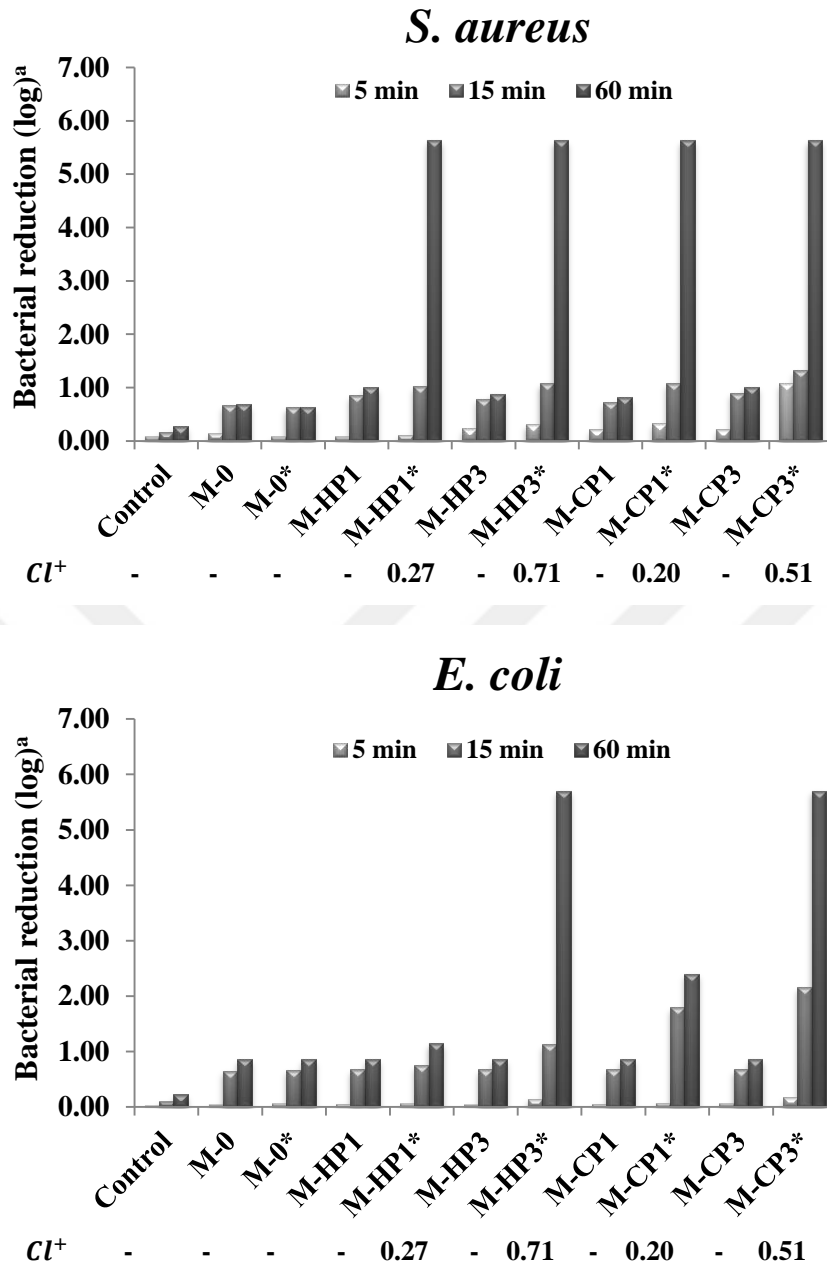
using lower chlorine loaded samples in the second tests as seen in Figure 2.23. All samples biocidal activity against *S. aureus* and *E.coli* for lower contact times (5 min and 15 min) decreased in second test due to the lower chlorine loadings. Even for lower chlorine loadings, the M-HP3* and M-CP3* exhibited complete inactivation against both type of bacteria in a contact time of 60 min.



^aThe inoculum concentrations were 5.78 log and 5.72 log for *S.aureus* (ATCC 6538) and *E.coli* (ATCC 35218), respectively.

*Chlorinated membranes

Figure 2.22 : Biocidal Test 1



^aThe inoculum concentrations were 5.63 log and 5.70 log for *S.aureus* (ATCC 6538) and *E.coli* (ATCC 35218), respectively.

*Chlorinated membranes

Figure 2.23 : Biocidal test 2

2.4 Conclusion

A series of *N*-halamine polymers, HP and CP, were synthesized and added to the membrane dope solution in order to improve the permeation performances of the membranes and reduce the biolayer formation on the membrane surface. The water flux and BSA rejection performances of the produced membranes were compared with a commercial flat sheet PVDF ultrafiltration membrane (BN). In the first stage

of the that part of the study, various amount of PVP (between 0.30 to 0.45 wt%) additions were made to the membrane structure and the best membrane was selected according to the water flux and BSA rejection performances. Then, the HP was added to chosen membrane solution (M-P35). The additions of HP to M-P35 membrane structure caused a huge increase in water flux performance, but decrease the BSA rejection. Because of this huge increase in water flux performance of the membrane, and as the PVP contribution decreases the mechanical resistance of the membrane by leaching during backwashing, only HP and CP added membranes were produced in the last part of this study. The membranes produced with HP and CP additions did not show water flux performances as good as the BN and both PVP and HP included membranes. But on the other hand, the BSA rejection performance of the HP added membrane was even higher than BN.

FTIR and XPS analyses were performed to show the presence of the HP and CP in the membrane structure. Addition of these polymers to the membrane structure did not alter the melting point as demonstrated by DSC analysis. The relationship between polymer coagulation rate and membrane surface structure was explained with ternary phase diagram of the polymer solutions and SEM images of the produced membranes. The biocidal test results showed that the antibacterial properties of the produced membranes were greatly improved by addition of HP and CP to the membrane structure. As a result, most importantly, this antibacterial property being renewed in every backwashing will greatly increase the added value of this washings and will reduce the number of the washings since it prevents the formation of biofilm for a longer time. However, new additives need to be developed to improve the membrane performance without destroying the membrane structure.

3. PRODUCTION OF PVDF ULTRAFILTRATION MEMBRANES EXHIBITING ANTIBACTERIAL PROPERTY BY THE INCORPORATION OF NOVEL *N*-HALAMINE COPOLYMERS

3.1 Introduction

As mentioned earlier, in order to increase the biodegradability resistance of the ultrafiltration membranes used in water treatments, polymers having high chlorine loading capacity, good solubility in matrix systems, high chlorine stability, not leaching from the material by water should be synthesized. In this context, suitable polymer structures were selected and added to the membrane structure in the previous section. The changes in membrane structures resulted by these polymers additions were investigated and it was judged that the membrane surface is deteriorated as the thermodynamic stability difference between the base and additive polymer increases. Therefore, polymers having similar phase separation behavior with PVDF are needed. The hypothesis of this section of the thesis is “Membrane performance would be improved without deteriorating the membrane surface by the incorporation of novel *N*-halamine copolymers having similar thermodynamic stability to PVDF.”

The characterizations of the synthesized polymers were made with ¹H NMR and FTIR analysis. The presence of the synthesized polymers in produced membrane structure was proven with FTIR and XPS analyses. The surface and cross-section images of the produced membranes were investigated. The effects of the additives on membrane water flux and BSA rejection performances were examined. And finally, the speed and duration of biocidal performance of the produced membranes were proven with different biocidal test methods.

3.2 Experimental

3.2.1 Materials

For the synthesis of novel *N*-halamine copolymers, *N*-tert-Butyrylamide (TCI) (NTBAAm), *N*-Isopropylacrylamide (TCI) (NIPAAm), and *N,N*-

Dimethylacrylamide (TCI) (NNDMAAm) were used. Potassium persulfate (Acros) was used as initiator for polymerizations.

Polyvinylidene fluoride (PVDF) (Alfa Aesar) and N-Methyl-2-pyrrolidone (NMP) was used as based polymer and solvent in membrane casting solutions, respectively. Polyvinylpyrrolidone (PVP) K30 ($M_n=40,000$ g/moles, TCI) was added to the membrane dope solution as a pore former. Disodium phosphate ($\text{Na}_2\text{HPO}_4 \cdot 2\text{H}_2\text{O}$) (Merck) and sodium dihydrogen phosphate (NaH_2PO_4) (Merck) were used for the preparation of protein feed solution. Bovine Serum Albumin (BSA) (Fisher Scientific) was used for the estimation of protein rejection performance of the membranes.

3.2.2 Synthesis of the novel *N*-halamine copolymers

Novel copolymers of HA (7:3 mmol) with NTBAAm, NIPAAm, and NNDMAAm were synthesized by free radical polymerization. The copolymers were synthesized by dissolving 1.67 g (7 mmol) HA, and 0.39 g (3 mmol) NTBBAm, 0.35 g (3 mmol) NIPAAm or 0.30 g (3 mmol) NNDMAAm in 50 mL distilled water together with potassium persulfate (Acros) (PPS). By nitrogen bubbling for 15 min dissolved oxygen was removed and the reaction was continued under nitrogen atmosphere by stirring at 75 °C for 4 h. The precipitated copolymers were filtered. The reaction mechanisms of the new copolymers were given Figure 3.1.

3.2.3 Preparation of ternary phase diagram

Ternary phase diagrams of polymer/solvent/nonsolvent systems were drawn to take information about thermodynamic stability and phase separation behavior of the polymers. Ternary diagrams were drawn according to the cloud point test. Nonsolvent (water) was dropwise added to the polymer dope solution stirring at 30 °C. The addition of nonsolvent was stopped when the appearance of dope solution turn to milky-like structure for low concentration solutions and local precipitation was observed and not disappeared for a specific time for high concentration solutions. For low concentration solution after turbidity occurred, stirring was continued for further 30 min to observe the turbidity is disappear or not disappear. If the solution turns to clear, more nonsolvent addition was made to the solution, otherwise the found point is saved as cloud point and composition of the ternary point was calculated according to the polymer, solvent, and nonsolvent weights. In

this section ternary phase diagrams of synthesized polymer solutions were studied both single and by mixing with PVDF.

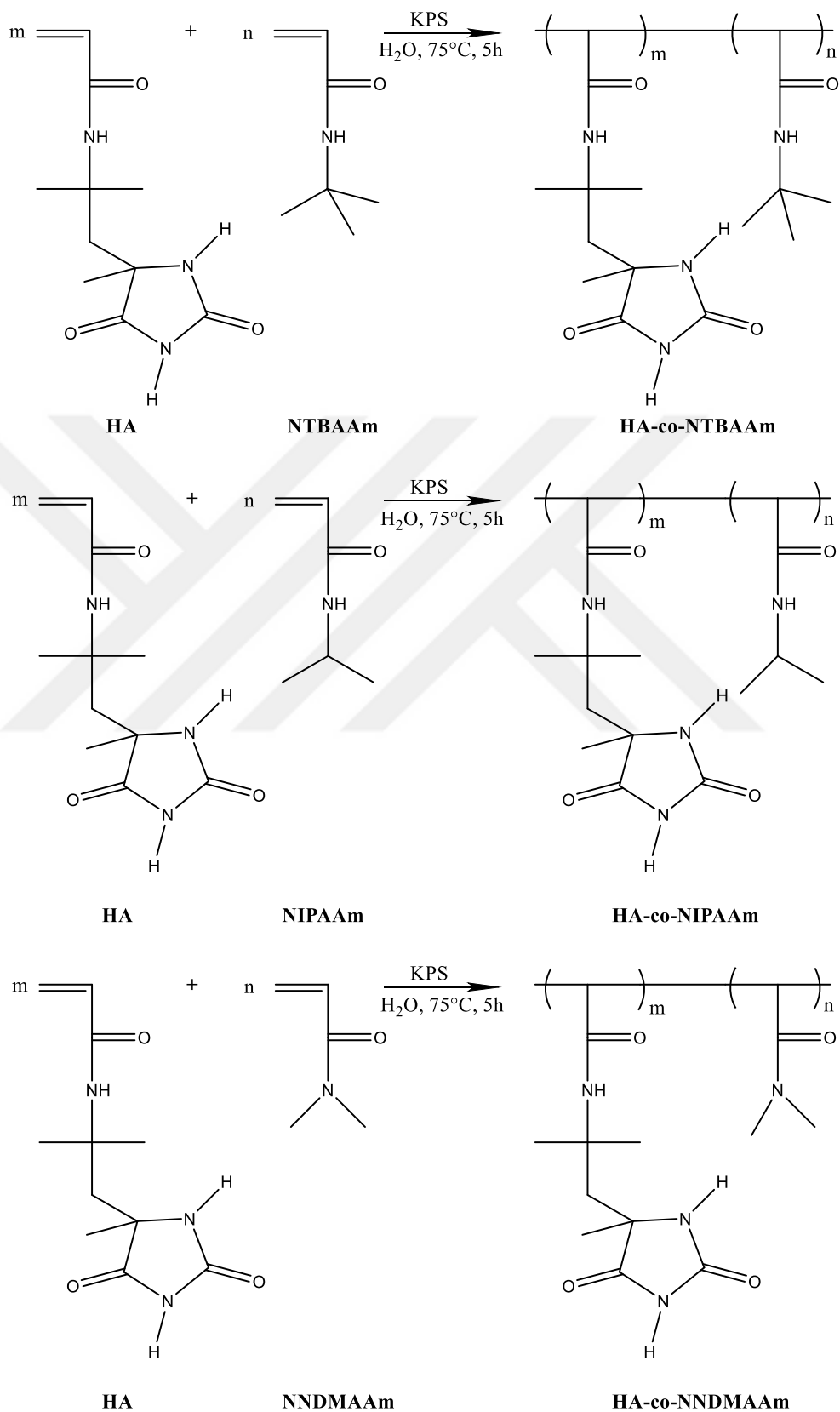


Figure 3.1 : Reaction mechanisms of the novel synthesized copolymers

3.2.4 Polymer blends and flat sheet membrane production

Phase inversion method was used to prepare membranes. Pristine PVDF (M-0), both PVP and polymer added (M-P(HA-co-NTBAAm)-PVP, M-P(HA-co-NIPAAm)-PVP and M-P(HA-co-NNDMAAm)-PVP), just polymer added (M-P(HA-co-NTBAAm), M-P(HA-co-NIPAAm) and M-P(HA-co-NNDMAAm)) membranes were prepared as seen in Table 3.1. While preparing membrane dope solutions; firstly the copolymers were dissolved in NMP by stirring at 60 °C for 2 h, then PVDF (and PVP) were added and stirring was continued for an extra 4 h, and then the mixture was stirred overnight at 40 °C to obtain a homogeneous solution. 200 µm films were produced on a glass sheet with the help of a film applicator. The coagulation of the films was made in a tap water bath at 30 °C, and then the produced films were kept in distilled water at 30 °C.

3.2.5 Chlorination of the produced membranes

A 10% aqueous solution of 6% sodium hypochlorite (household bleach) was prepared and the pH of the solution was adjusted to 7 with 6 N HCl. After the produced membranes were kept in this solution for 1 h, the unbonded chlorine on the membrane was removed by washing with tap and distilled water, and 1 h drying at 45 °C. Iodometric/thiosulfate titration was applied to determine the loaded chlorine concentration onto the samples (Kocer et al., 2010). A solution of ethanol with 0.1 N acetic acid (90/10; v/v) was prepared and 0.25 g potassium iodide was dissolved in this solution, then the dried membrane sample was added to the solution. Titration was made with 0.005 N sodium thiosulfate solution until the color of the solution is yellow to clear. The weight percent of the loaded chlorine (Cl^+) on the membrane samples were calculated according to the equation 2.1.

3.2.6 Permeability tests of the produced membranes

All produced membranes were kept in distilled water for seven days, and the membrane pores were opened by wetting isopropanol before the permeability tests. Water flux tests were applied two times for the polymer added membranes, before and after chlorination.

Table 3.1 : Casting solution compositions of the membranes produced with the incorporation of novel polymers.

Membranes	Component Compositions						
	PVDF (wt%)	PVP (wt%)	P(HA-co-NTBAAm) (wt%)	P(HA-co-NIPAAm) (wt%)	P(HA-co-NNDMAAm) (wt%)	NMP (wt%)	
M-0	18.00	-	-	-	-	82.00	
M-P(HA-co-NTBAAm)	17.82	-	0.18	-	-	82.00	
M-P(HA-co-NTBAAm)-PVP	17.82	0.35	0.18	-	-	81.65	
M-P(HA-co-NIPAAm)	17.82	-	-	0.18	-	82.00	
M-P(HA-co-NIPAAm)-PVP	17.82	0.35	-	0.18	-	81.65	
M-P(HA-co-NNDMAAm)	17.82	-	-	-	0.18	82.00	
M-P(HA-co-NNDMAAm)-PVP	17.82	0.35	-	-	0.18	81.65	

Dead-end filtration method was used to determine water flux performance of the membranes. The schematic and real images of the installed dead-end filtration system with HP4750 Sterlitech stirred cell was given in Figure 2.4. The effective membrane filtration area of the system was 14.6 cm^2 . Water filtration experiments were performed under three different constant pressures of 1, 3, and 5 bars. The pure water fluxes (L/m²h) of the produced membranes were calculated according to the equation 2.2.

A phosphate buffer solution (0.1 M, pH 7) containing 1 g/L BSA was prepared to perform BSA rejection tests. The protein content in filtrated solution after one hour filtration was determined with UV-Visible spectrophotometer at 280 nm wavelength. Scinco-NEOSYS200 UV-Visible spectrophotometer was used for analysis and the rejection ratios of the produced membranes were calculated according to the equation 2.3.

For the pure water flux and BSA rejection performances, the membranes were tested at least three times and the results were given as mean value along with the standard deviations.

3.2.7 Characterization of the produced polymers and membranes

Attenuated total reflectance Fourier-transform infrared (ATR-FTIR) spectroscopy (Thermo Nicolet, IS50) was used to characterize the synthesized polymers and the produced membranes. While recording the spectra 16 scans were made at 4 cm^{-1} spectral resolution and the scanning range was from 400 to 4000 cm^{-1} .

NMR analyses were made with 400 MHz Jeol-ECS spectrometer. NMR spectra of the produced polymers recorded with 32 (¹H) scans.

Thermo Scientific, K-Alpha spectrometer with a monochromated Al K α (1486.6 eV) X-ray source was used to take X-ray photoelectron spectra (XPS) measurements. All binding energy corrections were made according to the carbon photo electron signal at 284.6 eV.

The surface morphology and cross-section of the membranes were characterized with FEI, QUANTA 200F Field Emission scanning electron microscope. Images of gold-palladium coated (10 nm) membranes were obtained at 800x and 3,000x magnifications for cross-section, and 50,000x magnification for surface.

The biocidal performances of the produced membranes were investigated both with agar diffusion method and by filtering the bacterial suspension. A Gram-positive and a Gram-negative bacteria were used as test microorganisms. For agar diffusion test both cultures were grown overnight and 10^8 and 10^5 CFU/mL bacterial suspensions of them were prepared. 100 μ L of the bacterial suspension were spread on the Muller-Hilton II and bloody agars with 10^8 and 10^5 CFU/mL bacteria concentrations, respectively. All produced of the membranes (both chlorinated, M*, and unchlorinated) were cut as 25 mm diameter circular disks and put on the inoculated agar plates for incubation at 37 °C for 24 h. Since the *N*-halamines are contact active antibacterial agents, the membranes were removed from the agar plate to determine antibacterial efficacy.

Secondly, a countable result was obtained with filtration test. In the filtration test after 2 mL of phosphate buffer solution (PBS) was filtered to soak the membranes, 3 mL of a known concentration (10^5 CFU/mL) of bacterial suspension was filtered through the both chlorinated (M*) and unchlorinated membrane samples. Following the filtration of bacterial suspensions, the membranes (with 25 mm diameter) were divided into four equal parts. Then three parts of each membrane were placed in 10 mL PBS after 5, 15, and 30 min time intervals, and the suspension were shaken for 30 sec, then 100 μ L of the bacterial suspension was taken and their serial dilutions with PBS were prepared and spread onto Muller-Hilton II agar plates. Before colonies were counted, the agar media was waited at 37 °C for 24 h and the bacterial reduction was determined as logarithmic.

3.3 Results and Discussion

3.3.1 Characterization of the new synthesized polymers

The synthesized polymers structures were confirmed by NMR and FTIR analyses. The primary evidence for the polymer formations is the absence of the vinyl proton signals between 5.5 and 6.5 ppm. For the P(HA-co-NTBAAm), the signals at 1.25 ppm, 7.89 ppm, 10.63 ppm can be attributed to the protons of the methyl groups and the protons of hydantoin ring amide and imide groups, respectively. ^1H NMR spectrum of the P(HA-co-NTBAAm) was given in Figure 3.2.

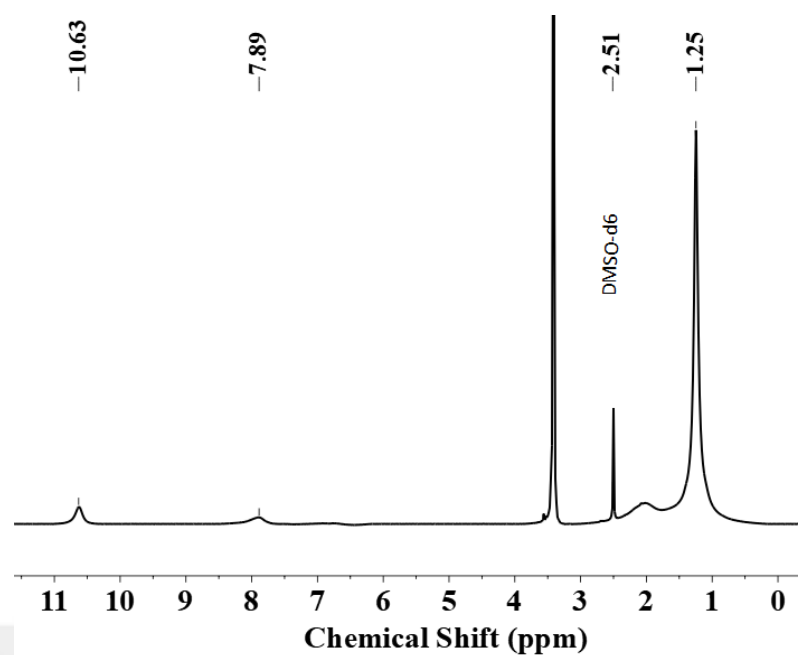


Figure 3.2 : ^1H NMR spectrum of the P(HA-co-NTBAAm) (solvent: DMSO-d₆)

In the spectrum of the P(HA-co-NIPAAm), two new signals appeared at around 3.84 and 1.04 ppm, owing to the methanetriyl and methyl groups of the NIPAAm comonomer, respectively. ^1H NMR spectrum of the P(HA-co-NIPAAm) was given in Figure 3.3.

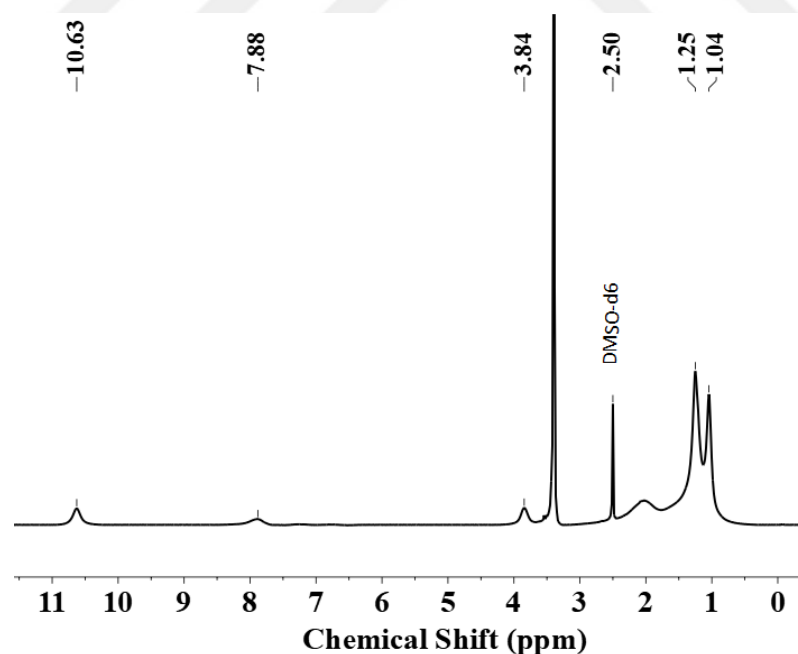


Figure 3.3 : ^1H NMR spectrum of the P(HA-co-NIPAAm) (solvent: DMSO-d₆)

^1H NMR spectrum of the P(HA-co-NNDMAAm) was given in Figure 3.4. The new signal at 2.80 ppm in the P(HA-co-NNDMAAM) originated from the protons of the methyl groups bonded to the nitrogen atom in the comonomer structure.

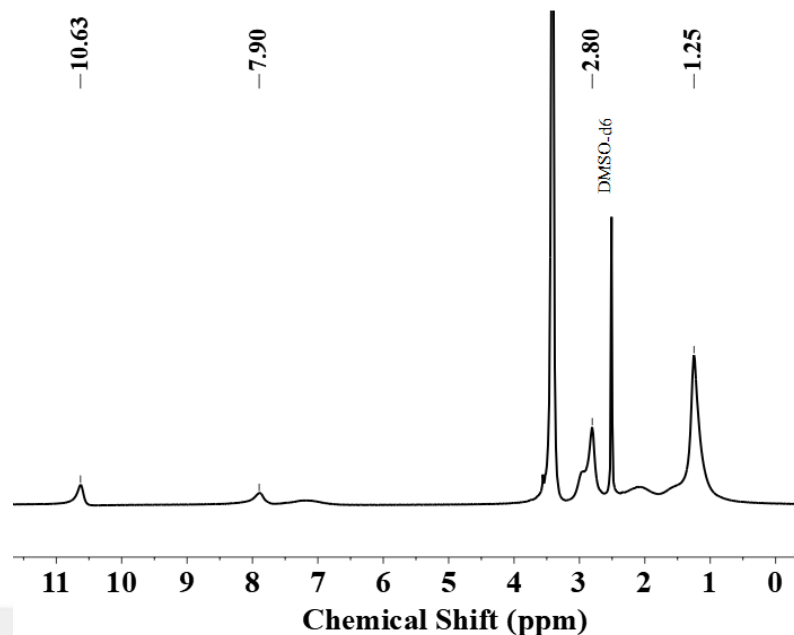


Figure 3.4 : ^1H NMR spectrum of the P(HA-co-NNDMAAm) (solvent: DMSO- d_6) FTIR spectra of the synthesized copolymers (7:3 mmol) of HA with NTBAAm, NIPAAm, and NNDMAAm were given with the homopolymer of HA (HP) to confirm the copolymer formations. As seen in Figure 3.5, the signals at 2973, 2928, 1458, and 1367 cm^{-1} being characteristic for the methyl group, confirming the occurrence of NTBAAm in the copolymer structure. Besides, the aromatic stretching of C-C band at 1407 cm^{-1} was overlapped by 1393 cm^{-1} band of the symmetrical C-H bending vibration of the methyl group in the comonomer structure.

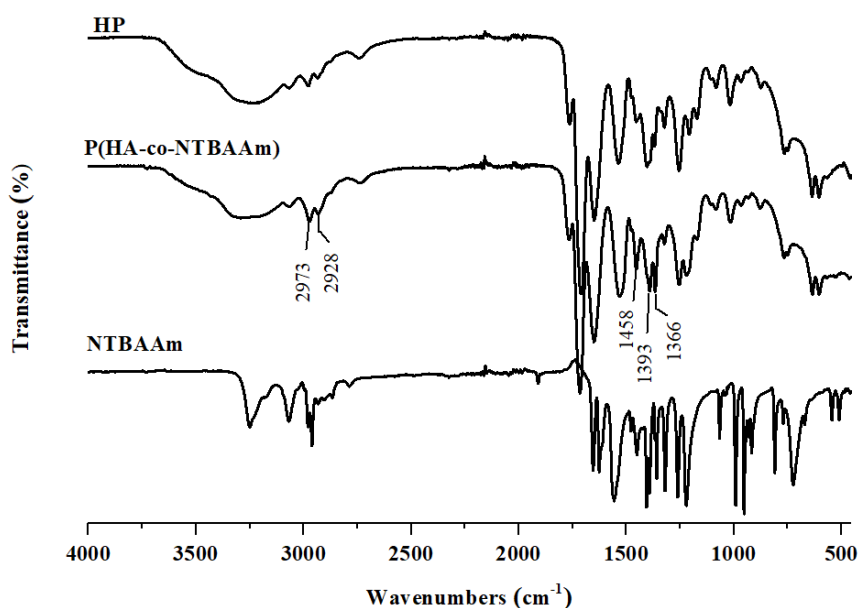


Figure 3.5 : FTIR spectra of the HP, P(HA-co-NTBAAm), and NTBAAm

FTIR spectra of the HP, its copolymer with the NIPAAm (P(HA-co-NIPAAm)), and NIPAAm monomer were given in Figure 3.6. As seen in the figure, similar to the P(HA-co-NTBAAm) spectrum with addition of NIPAAm to the polymer structure the intensities of 2973 and 2928 cm^{-1} bands were increased. The intensity of the band at 1540 cm^{-1} being characteristic for the N-H bending, increased with the addition of NIPAAm to the polymer structure. Besides, the addition of NIPAAm to the polymer structure caused the appearance of two new bands at 1392 and 1132 cm^{-1} being corresponding to the C-H bending of methyl group and asymmetric stretching of C-N-C, respectively.

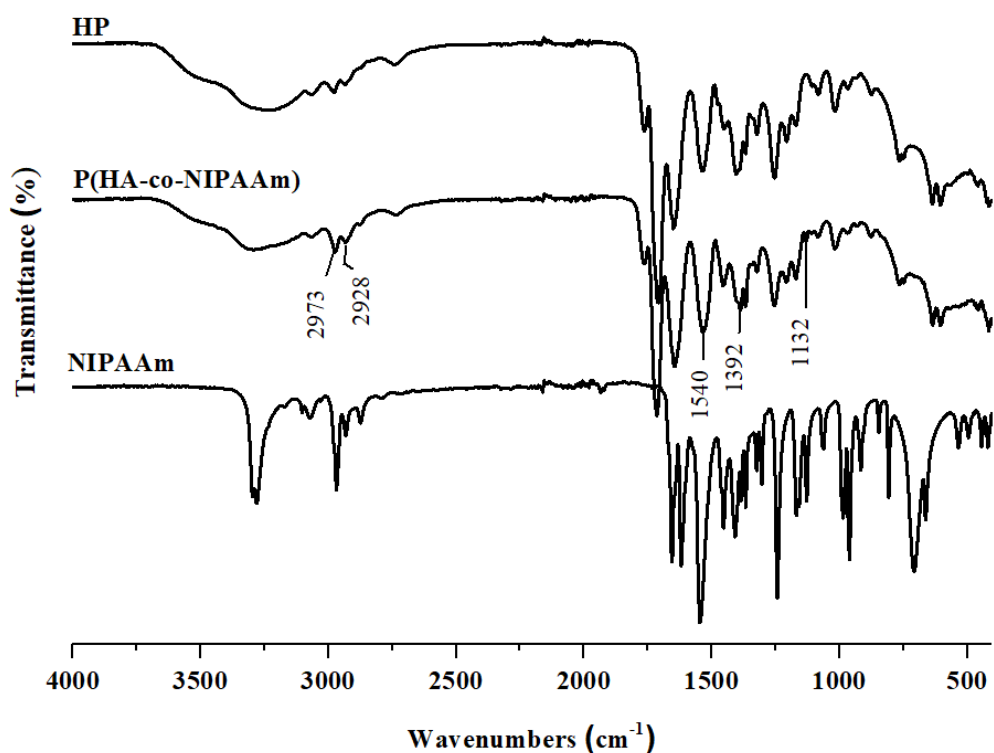


Figure 3.6 : FTIR spectra of the HP, P(HA-co-NIPAAm), and NIPAAm

FTIR spectra of the synthesized HP, its copolymer with NNDMAAm (P(HA-co-NNDMAAm)-7), and NNDMAAm were given in Figure 3.7. Similar to the other two copolymers spectrums, the band intensities at 2973 and 2928 cm^{-1} being characteristic to methyl group, increased with the addition of NNDMAAm in the polymer structure. The additional band at 1614 cm^{-1} in the copolymer spectrum was corresponding to the tertiary amide -C=O group of the comonomer.

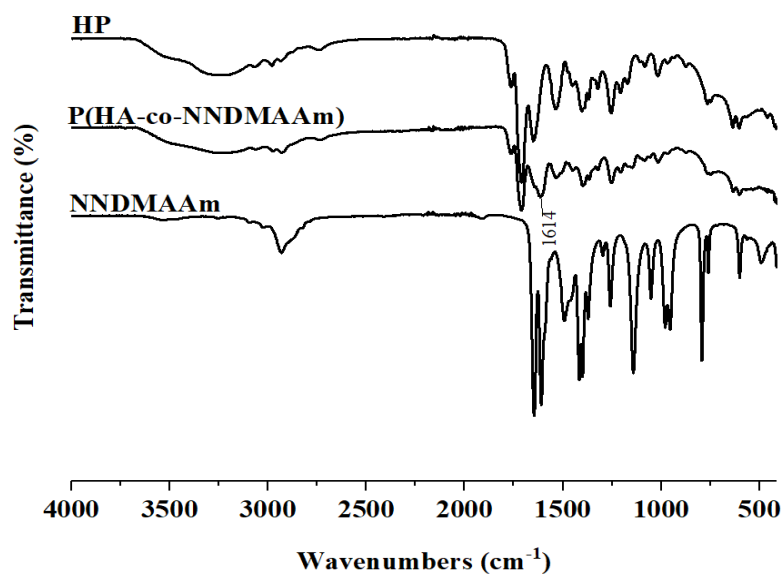


Figure 3.7 : FTIR spectra of the HP, P(HA-co-NNDMAAm), and NNDMAAm

3.3.2 Characterization of the produced membranes

3.3.2.1 Ternary phase diagrams of polymer / NMP / water systems

Ternary phase diagrams of the novel synthesized polymers were given in Figure 3.8 with the ternary phase diagrams of the polymers in the previous section. When the SEM images and the ternary phase diagrams of the HP and CP were evaluated together, it was observed that with the increase in thermodynamic stability of polymer causing delayed demixing according to PVDF, the surface roughness of the membrane was increase. To verify this observation, as seen in Figure 3.8, novel polymers with higher and lower thermal stability than HP and CP were synthesized. It was confirmed that the surface roughness of the membranes directly related to the coagulation behavior difference of the PVDF and additive polymer. However, as it was evident from both the permeability test results and the SEM images, number and size of the pores on the membrane surface are not fully related to the coagulation rate difference. As seen in Figure 3.9 ternary phase diagrams of the casting solutions including both PVDF and polymers were prepared in order to obtain more information about the membrane surface porosity and coagulation behavior of the polymers. Even though thermodynamic stability of the P(HA-co-NTBAAm) was the lowest, its mixed solution with PVDF gave the highest thermodynamic stability. López-Pérez et al. (2010) explained that lower NTBAAm added copolymers demonstrated a sharp macroscopic phase separation. Although this sharp phase separation cannot be observed during the formation of P(HA-co- NTBBAm) ternary

phase diagram, it caused a clear gelation in the ternary phase diagram of PVDF-P(HA-co-NTBAAm) mixture containing very low amount of NTBAAm. This rapid macroscopic phase separation caused an increase the number and size of the pores on the membrane surface. While a small amount of gelation was also observed during the formation of P(HA-co-NIPAAm) containing mixture phase diagram, the P(HA-co-NDMAAm) formed the most compatible mixture with PVDF. As a result, the P(HA-co-NNDMAAm) added membranes formed the lowest number and smallest sized pores compared to the other copolymers incorporated membranes.

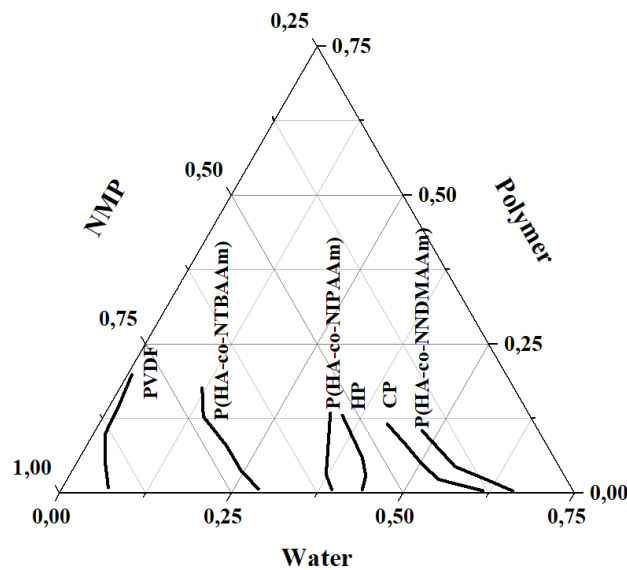


Figure 3.8 : Ternary phase diagram of Polymer / NMP / Water systems at 30 °C

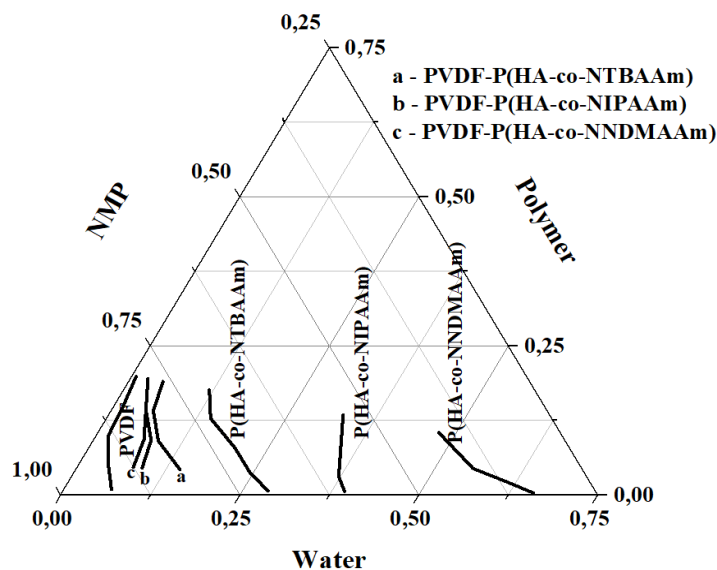


Figure 3.9 : Ternary phase diagram of polymer incorporated PVDF / NMP / Water systems at 30 °C

3.3.2.2 Filtration and BSA rejection performances of the produced membranes

Membranes were tested both before and after chlorination since chlorinated backwashing was applied on membranes in industrial applications. On the other hand these backwashings also will provide re-chlorination of the *N*-halamine for biocidal activity. The pure water flux of the unchlorinated and chlorinated membranes at 1, 3, and 5 bar pressures were given in Figure 3.10 and Figure 3.11, respectively. The pure water flux of the membranes increased with chlorination due to the cleaning of the membrane surfaces. The water flux of the membranes increased with addition of the synthesized polymers, P(HA-co-NTBAAm), P(HA-co-NIPAAm), and P(HA-co-NNDMMAm). The addition of PVP to the membrane structure with the synthesized polymers both increase the pore size, pore size distribution and water flux of the membranes especially at high pressures. But, as seen in Figure 3.12, there was a huge decrease of BSA rejection performance of the membranes with PVP addition. An increase in the membrane flux without addition of PVP could be increase the lifetime of membranes as mentioned in the previous section.

While M-P(HA-co-NTBAAm) exhibits the highest water flux performance, its BSA rejection performance was even lower than M-0. On the other hand, M-P(HA-co-NNDMMAm) exhibited the highest BSA rejection with 94%, while its water flux performance was very low even at 5 bar. The water flux and BSA rejection performances of the membranes were in good accordance with their SEM images.

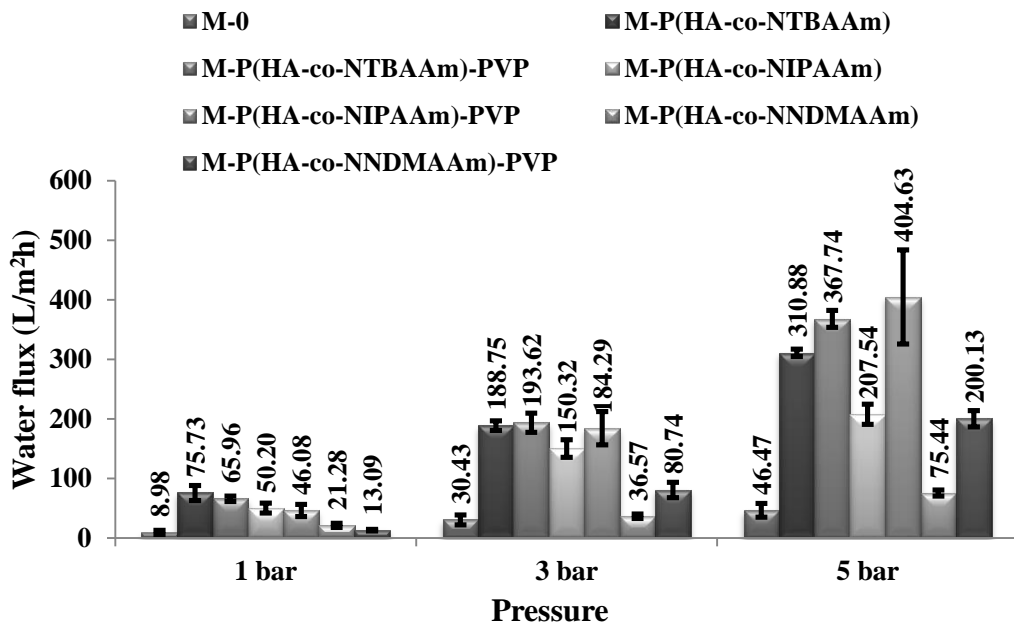
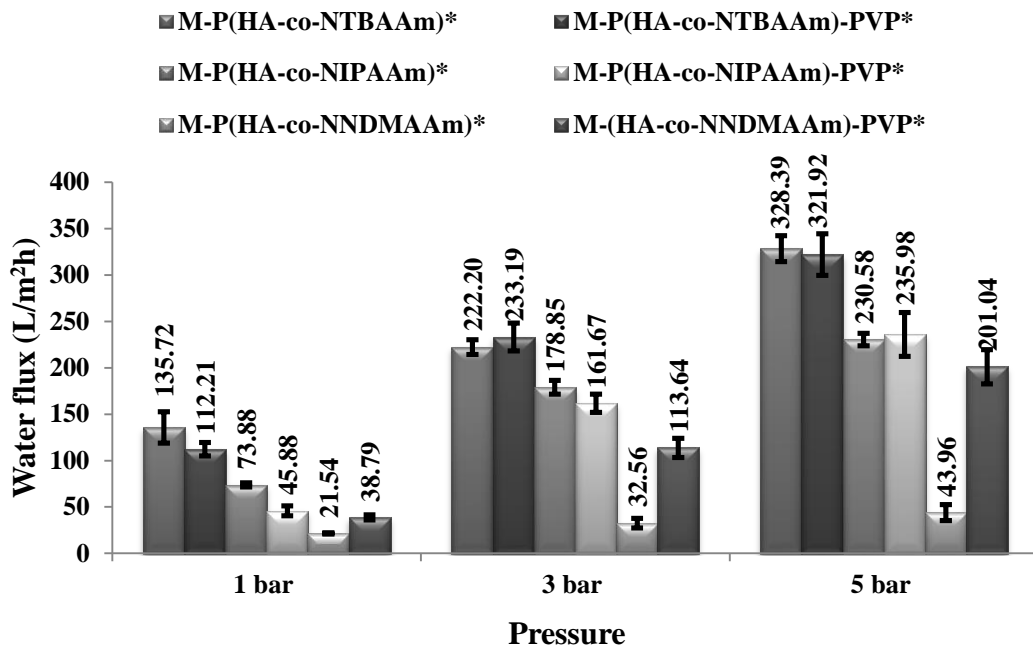
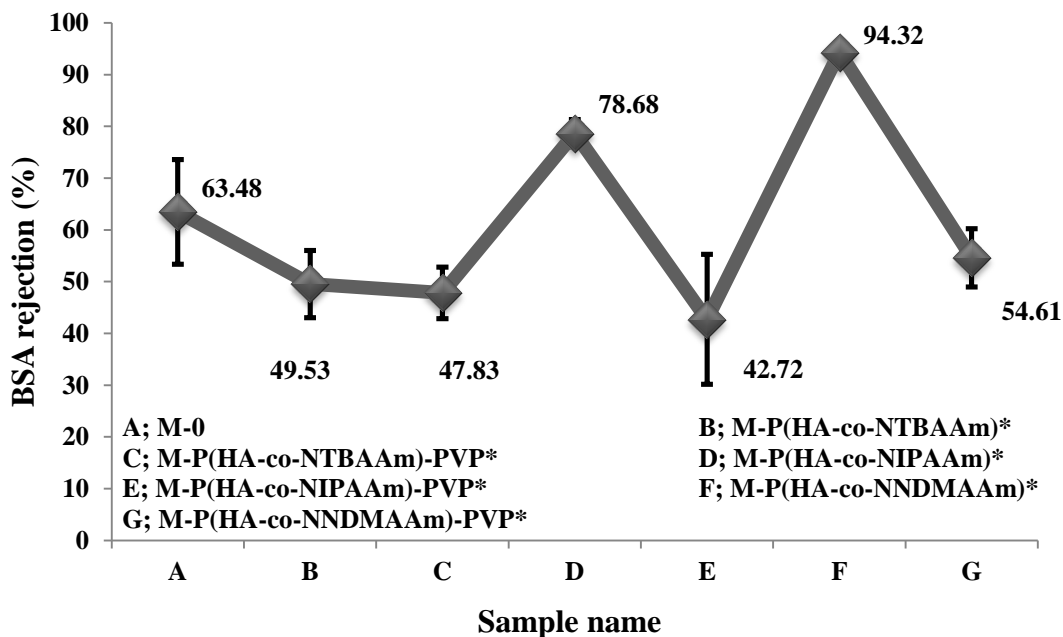


Figure 3.10 : Pure water flux performances of the unchlorinated membranes



*Chlorinated membranes

Figure 3.11 : Pure water flux performances of the chlorinated membranes



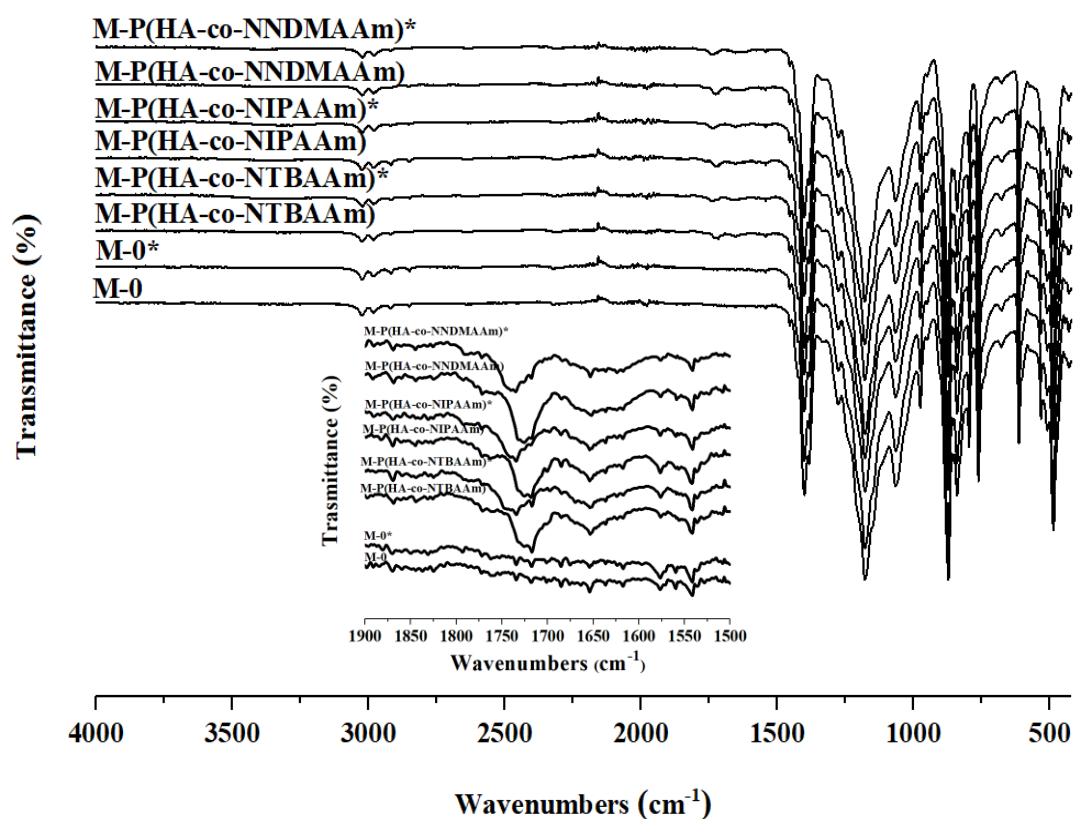
*Chlorinated membranes

Figure 3.12 : BSA rejection performances of the produced membranes

3.3.2.3 FTIR and XPS characterization of the produced membranes

FTIR spectra of the produced membranes both for chlorinated and unchlorinated were given in Figure 3.13, with full scale spectrum between 400 cm^{-1} and 4000 cm^{-1} wavenumbers and with an inlet focusing on the region between 1500 cm^{-1} and 1900 cm^{-1} wavenumbers. As seen more clearly in the P(HA-co-NTBAAm),

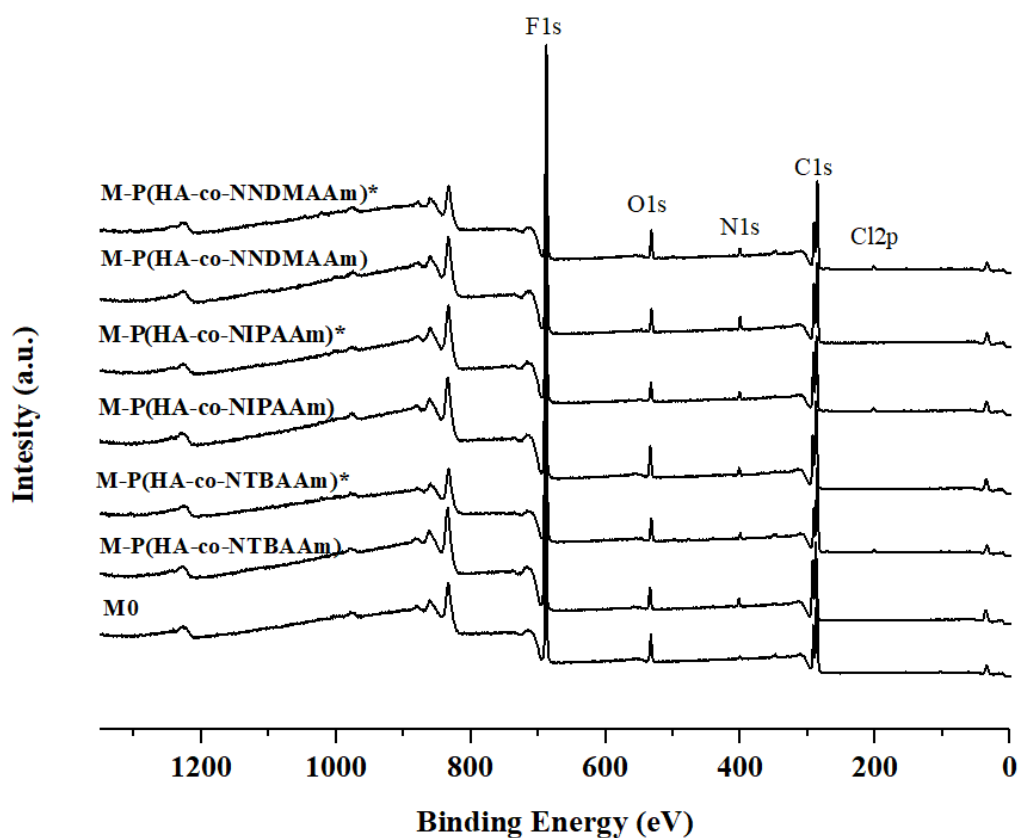
P(HA-co-NIPAAm) and P(HA-co-NNDMAAm) added membranes inlet spectra, the additional bands at 1653 cm^{-1} , 1717 cm^{-1} , and 1760 cm^{-1} showed the presence of the copolymers in the membrane structure. While the band at 1653 cm^{-1} was characteristic for the aliphatic amide carbonyl stretching mode, other two bands were corresponding to the carbonyl stretching of amide and imide groups on hydantoin ring, respectively. The bond between N-H converts to N-Cl with chlorination and that cause disruption of hydrogen bonding (N-H...O=C). This bond breakage caused by chlorination was also clearly seen in Figure 3.10 by the shift of the bands at 1717 cm^{-1} to 1734 cm^{-1} and 1760 cm^{-1} to 1790 cm^{-1} .



*Chlorinated membranes

Figure 3.13 : FTIR spectra of the synthesized polymers added membranes

The bond conversion of N-H to N-Cl was also confirmed by XPS measurement as seen in Figure 3.14. There was a new Cl2p peak appeared at 200 eV in the copolymer added and chlorinated membranes. Moreover, in contrast to M-0, the copolymer added membranes exhibited a more intensive peak of N1s at 400 eV originating from the amide groups appearing in the copolymer structure. And, this increase in peak intensity was indicating the copolymer presence in the membrane structure.



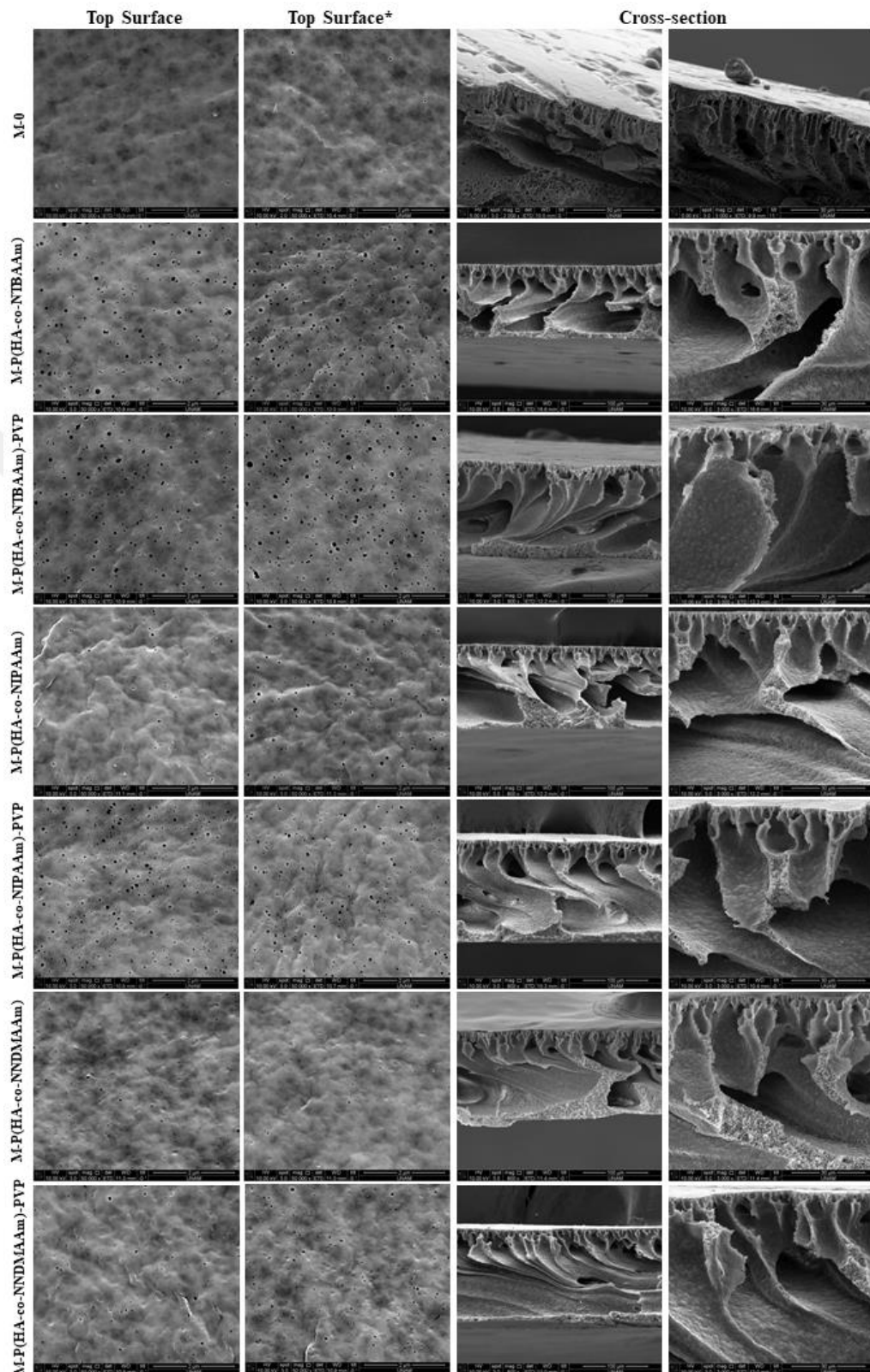
*Chlorinated membranes

Figure 3.14 : XPS spectra of the synthesized polymers added membranes

3.3.2.4 Morphology of the produced membranes

The top surface and cross-section images of the produced membranes were analyzed by SEM micrographs as seen in Figure 3.15. While the surface images of the chlorinated and unchlorinated membranes were given with 50,000x magnifications, the cross-section images of the produced membranes were given with both 800x and 3,000x magnifications. It can be observed from the top surface images, the surface of the membranes were cleaned with chlorination so that the pores become more visible. The pure water flux of the membranes was also increased with chlorination which is also confirming the cleaning on the membrane surface similar to findings in the previous section. The top surface micrographs indicated that the quantity of the pores in the M-0 was evidently less than the other produced membranes. It could be seen clearly from the Figure 3.15, PVP addition with the synthesized polymers to the membrane structure dramatically increase the pore size and porosity of the

membrane surface. On the other hand, these membranes had a wider pore size distribution and some cracks on the surfaces of the membranes.



*Chlorinated membranes

Figure 3.15 : The surface and cross-section SEM images of the produced membranes

The membrane surface homogeneity is very important to membrane filtration process, as seen in filtration results even though the membranes included both PVP and the synthesized polymers had high pure water flux; they had lower BSA rejection performance than the solely synthesized polymers added ones. This inhomogeneous membrane surface could be attributed to microphase separation between PVP and synthesized polymers. It was observed that while the P(HA-co-NTBAAM) added membrane had the lowest membrane surface roughness, the P(HA-co-NNDMAAm) added one has the highest membrane roughness. This observation was also consistent with the thermodynamic stabilities of the polymers which were ranked in the order of P(HA-co-NTBAAM) < P(HA-co-NIPAAm) < P(HA-co-NNDMMAM). However, the number and size of the pores on the membrane surface decreased with the same order.

All membranes exhibited asymmetric cross-section morphology with a thin skin layer on finger-like porous voids and a sponge layer at bottom of the membrane. As seen in ternary phase diagram the binodal curves of the synthesized polymers P(HA-co-NTBAAM), P(HA-co-NIPAAm), and P(HA-co-NNDMAAm) were at more right than PVDF causing a delayed demixing. The decrease in the demixing rate in the phase inversion process tended to suppress the formation of finger like structure (Stratmann et al., 1975). However, unexpectedly with the addition of synthesized polymers in the membrane structure, the width and the depth of the finger like voids increased. This could be related with the molecular weight of the additives, similar results were obtained in literature for PVP (Chakrabaty et al., 2008; Yoo et al., 2004;).

3.3.2.5 Biocidal performance of the produced membranes

In order to determine the biocidal effectiveness of the produced membranes against the biofilm formation on their surfaces, disk diffusion tests were applied with *S.aureus* and *E.coli* bacteria. Since the activation mechanism of *N*-halamine required a direct contact of agent with the bacterial cell to transfer of oxidative halogen to the cell, the membranes were removed from the agar disks after incubation (for 24 h, at 37 °C) and the areas under the membranes were observed. Figure 3.16 and Figure 3.17 indicated the biocidal performances of the produced membranes at 10⁵ CFU/mL and 10⁸ CFU/mL bacterial concentrations, respectively. The images in Figure 3.16

were taken immediately after the membranes were removed from the agar, but the images in Figure 3.17 were taken two weeks later than removal of the membranes from the agar. While the M0, M0*, M-P(HA-co-NTBAAm), M-P(HA-co-NIPAAm), and M-P(HA-co-NNDMAAm) did not show any inhibition effect against *S.aureus* and *E.coli*, the synthesized polymers added and chlorinated membranes showed clear surfaces at both bacteria concentrations. As seen in Figure 3.17, the M-P(HA-co-NTBAAm)*, M-P(HA-co-NIPAAm)* and M-P(HA-co-NNDMAAm)* did not lose their biocidal effectiveness up to two weeks even at 10^8 CFU/mL bacterial concentration.

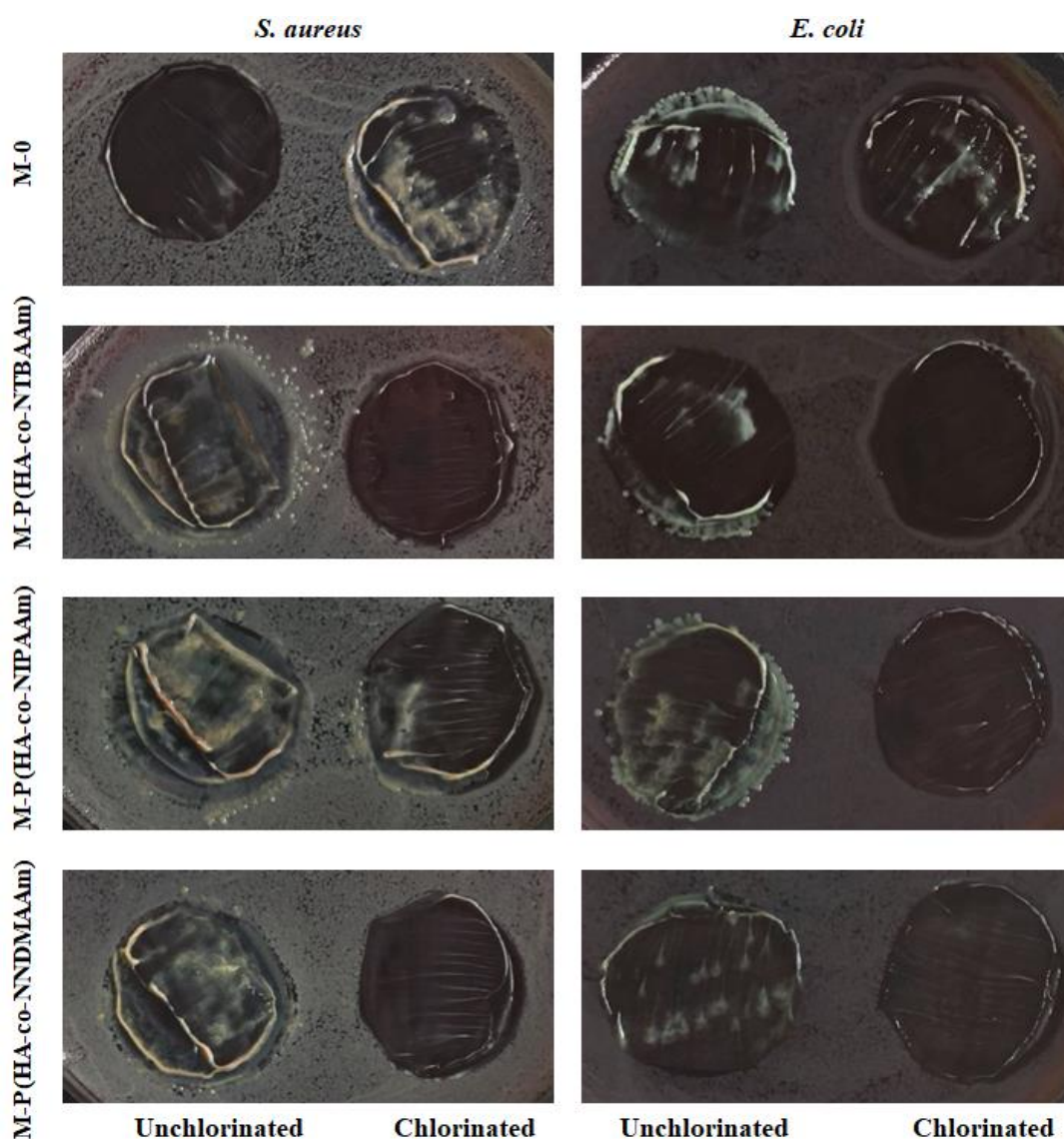


Figure 3.16 : Results of the biocidal tests by using agar diffusion method with 10^5 CFU/mL bacterial concentrations. (Chlorine loading on the chlorinated samples of M-0, M-P(HA-co-NTBAAm), M-P(HA-co-NIPAAm), and M-P(HA-co-NNDMAAm) were 0%, 0.144%, 0.135%, and 0.123%, respectively.)

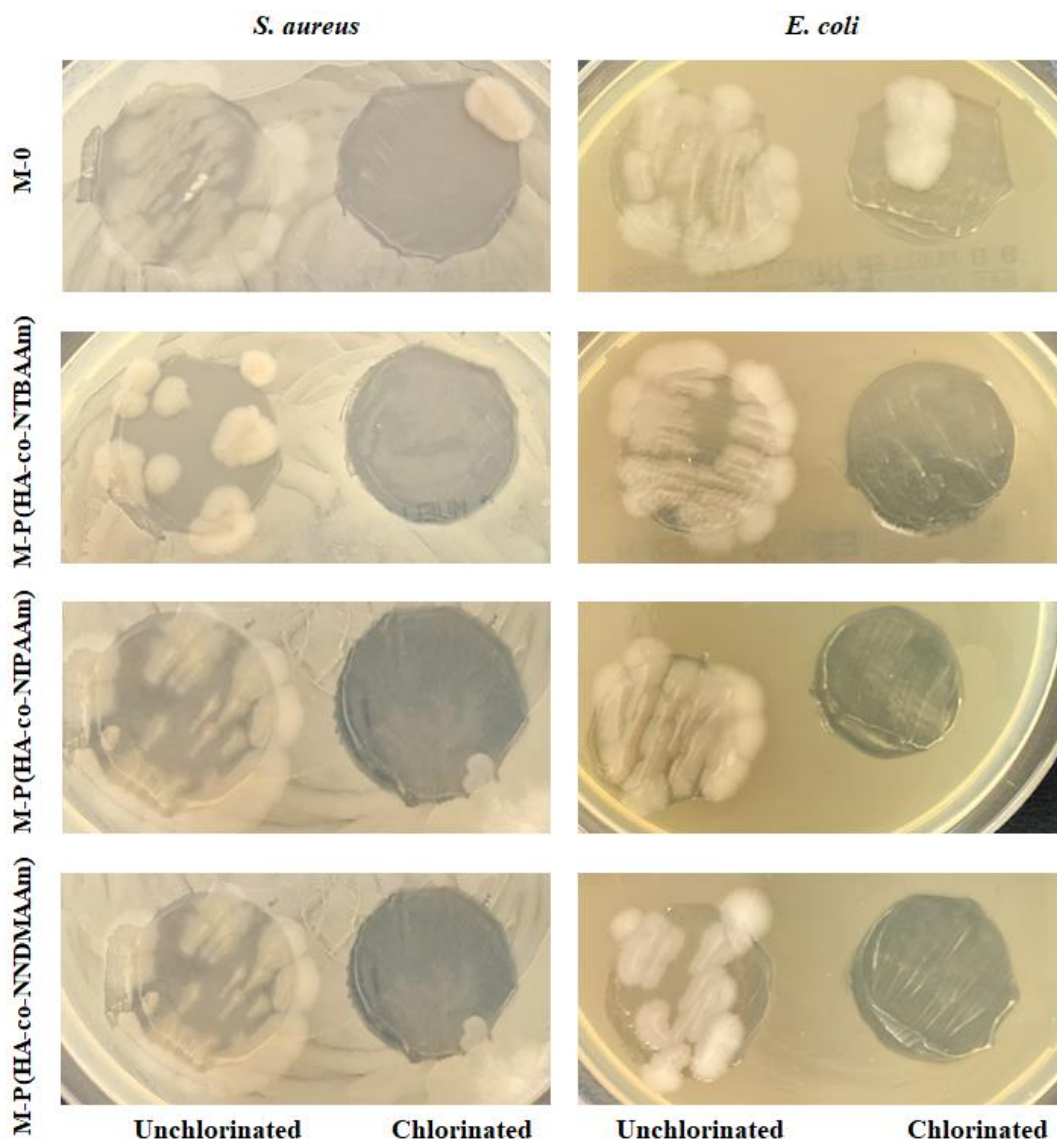
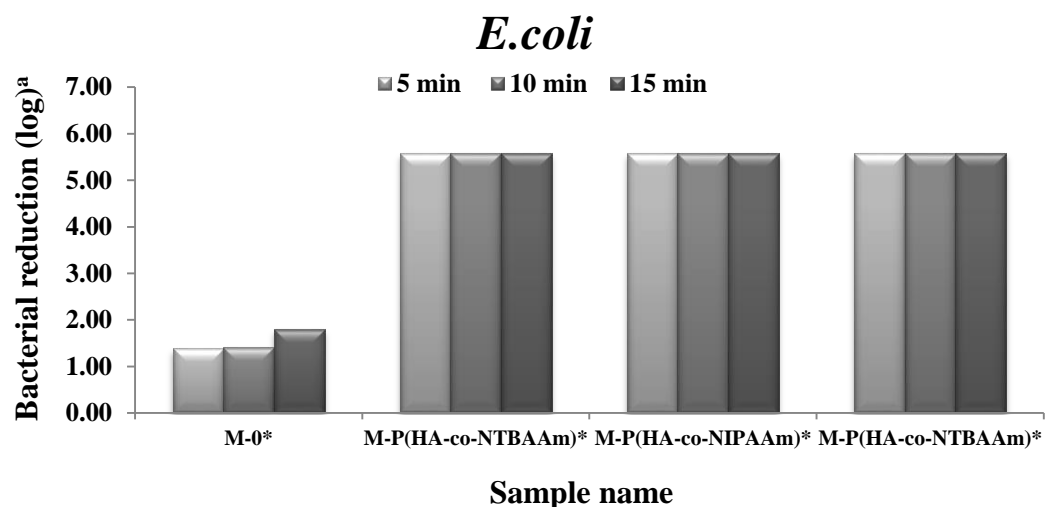


Figure 3.17 : Results of the biocidal tests by using agar diffusion method with 10^8 CFU/mL bacterial concentrations. (Chlorine loading on the chlorinated samples of M-0, M-P(HA-co-NTBAAm), M-P(HA-co-NIPAAm), and M-P(HA-co-NNDMAAm) were 0%, 0.144%, 0.135%, and 0.123%, respectively.)

After the efficacy of the membrane against biofilm formation on the membrane surface and the duration of biocidal activity were determined by the agar diffusion test, the speed of the antibacterial effectiveness of the membranes were determined with a countable test method. Approximately 10^5 CFU/mL *E.coli* was filtered through the membrane and then the membranes were divided into four parts to detect the biocidal effectiveness for various contact times as 5 min, 10 min, and 15 min. As seen in Figure 3.18, while the M-0* did not show any inactivation, all of the new synthesized polymers added and chlorinated membranes exhibited complete

inactivation against *E.coli* even at 5 min contact time. The test was repeated four times.



^aThe inoculum concentration was 5.58 log for *E.coli* (ATCC 35218).

*Chlorinated membranes

Figure 3.18 : Biocidal test results of membranes after microorganism solution filtration. (Chlorine loading on the chlorinated samples of M-0, M-P(HA-co-NTBAAm), M-P(HA-co-NIPAAm), and M-P(HA-co-NNDMAAm) were 0%, 0.144%, 0.135%, and 0.123%, respectively.)

3.4 Conclusion

Three novel *N*-halamine copolymers were designed and synthesized to improve the membrane flux performances. The synthesized polymers were characterized with FTIR and NMR analyses. Then the membranes were produced with the addition of these polymers. Ternary phase diagrams of the synthesized polymers with NMP and water were formed and compared with ternary phase diagrams of HP and CP. The ternary phase diagrams of the polymers and SEM images of the membranes were examined together and it was confirmed that as the binodal curve of the polymer move away from the binodal curve of PVDF, the deterioration on membrane surface increases. However, filtration test results and SEM images showed that the porosity on the membrane surface was not directly related to the thermodynamic stability of the polymer systems. Therefore, ternary phase diagrams of dope solutions including both PVDF and the synthesized copolymers were also formed. As a result, the importance of the compatibility of the additive polymer with PVDF was demonstrated and the findings were confirmed by the filtration test results and SEM images of the membranes. Similar to the previous section, the presence of the additive polymers in the membrane structure has been proven by FTIR and XPS

analyses. In particular, while the BSA rejection performances were similar, the flux values of the M-P(HA-co-NIPAAm) were approximately 10 times higher at 1 bar pressure, 7 times higher at 3 bar pressure, 2 times higher at 5 bar pressure than the M-HP1. Besides, while the water flux performances of the M-P(HA-co-NNDMAAm) and the M-HP1 were approximately same, the BSA rejection performance of the M-P(HA-co-NNDMAAm) was 16% higher than the M-HP1. On the other hand, the biocidal performances of the produced membranes were tested with two different test methods and it was shown that all the polymer added membranes provided a rapid and long-term antibacterial activity against *S.aureus* and *E.coli* bacteria at both 10^5 and 10^8 CFU/mL bacterial concentrations. All these results indicated that the correct polymer structures were designed in accordance with the results obtained in the previous section and these polymers were successfully synthesized and incorporated into the membrane structure.

4. ESTABLISHMENT OF A HOLLOW FIBER SPINNING UNIT AND PRODUCTION OF HOLLOW FIBER MEMBRANES WITH ADDITION OF ANTIBACTERIAL *N*-HALAMINE COPOLYMERS

4.1 Introduction

Membrane separation technologies are very fast developing systems; especially HFMs have been subject of research because they are used in industrially important areas such as drinking water treatment, wastewater treatment, gas separation, and liquid filtration (Feng et al., 2013). In this part of the study, firstly, a hollow fiber spinning system was designed and established to produce HFMs having intensive use in water treatment industry.

Hollow fiber structures are very advantageous because of their high surface area, low pressure loss, high material transfer rate, easy production and the ability to process liquids in the same bed (Peng et al., 2012). In the majority of the membrane water filtration systems, HFM modules are used. Therefore, the novel *N*-halamine copolymers synthesized and incorporated into the flat-sheet membranes in the third section were targeted to add into the HFMs in this section. Between the synthesized three copolymers, P(HA-co-NIPAAm) and P(HA-co-NNDMAAm) highly improved the water flux and BSA rejection performances of the flat-sheet membranes, respectively, were used in this section. In addition, the air gap effect on the membrane structure was also investigated. The hypothesis of this section of the thesis is “Direct incorporation of P(HA-co-NIPAAm) and P(HA-co-NNDMAAm) into hollow fibers would exhibit performances similar to the flat sheet membranes as investigated in the previous section”.

After production of hollow fibers, fibers were packed into modules to perform the permeability tests. Modules were designed to allow outside-in flow as used in industrial water treatment applications. The effects of the copolymers addition and air gap distances to the membrane morphology were determined with SEM analyses. Lastly, the biocidal performances of the hollow fibers were tested.

4.2 Experimental

4.2.1 Materials

Polyvinylidene fluoride (PVDF) (Alfa Aesar) and N-Methyl-2-pyrrolidone (NMP) was used as based polymer and solvent in HFM spinning solution, respectively. P(HA-co-NIPAAm) and P(HA-co-NNDMAAm) copolymers synthesized in the previous section were used as additive in the hollow fiber spinning dope solutions.

Disodium phosphate ($\text{Na}_2\text{HPO}_4 \cdot 2\text{H}_2\text{O}$) (Merck) and sodium dihydrogen phosphate (NaH_2PO_4) (Merck) were used for the preparation of protein feed solution. Bovine Serum Albumin (BSA) (Fisher Scientific) was used for the estimation of the protein rejection performance of the membranes.

4.2.2 Design and production of the hollow fiber spinning spinneret

As seen in Figure 4.1, a two-part spinneret was designed for hollow fiber spinning. Aluminum was chosen as the spinneret material. The two-parts were fixed with four bolts being around the bore liquid spinning hole. As shown clearly in the cross-section view of the spinneret, the inner solvent spinning hole ($D = 6.6$ mm) was designed to be inserted into a syringe needle. By inserting a needle into the spinneret, a spinneret with 1.5 mm outer diameter and 0.5 mm inner diameter was obtained. As shown in the Figure 4.1a, a 2 mm hole was drilled at the side face of the lower part, which was compatible with syringe. The spinneret was produced as inclined to apply shear force to the polymer dope solution (Figure 4.1b). The technical drawings of the spinneret were attached in the Appendix A.

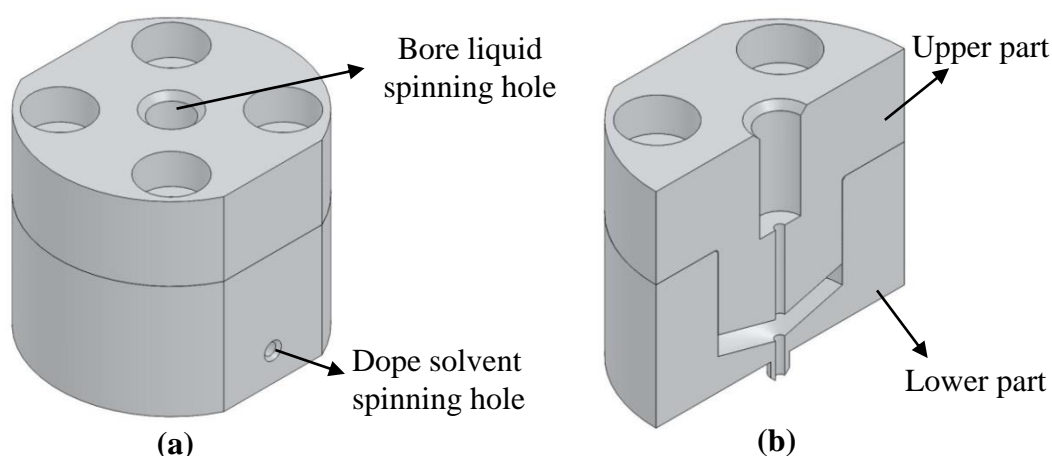


Figure 4.1 : Schematic view of the spinneret; (a) isometric, (b) cross-section

4.2.3 Design and establishment of the hollow fiber spinning unit

Two baths were prepared in the size of 500 x 150 x 150 mm and 200 x 150 x 150 mm (l x w x h) for coagulation and winding, respectively. Feed and drain valves were fitted to these baths for water circulation, which is important to remove all residual solvent in the fiber structure. Fiber spinning devices including wheels and belts were designed and manufactured (Figure 4.2). The technical drawings of the spinning device were attached in the Appendix B. As seen in the Figure 4.2, the spinning devices were designed to be easily installed to the coagulation and winding baths. DC motors and controllers, which were supplied from Robotus Corp., were adjusted on the fiber spinning devices.

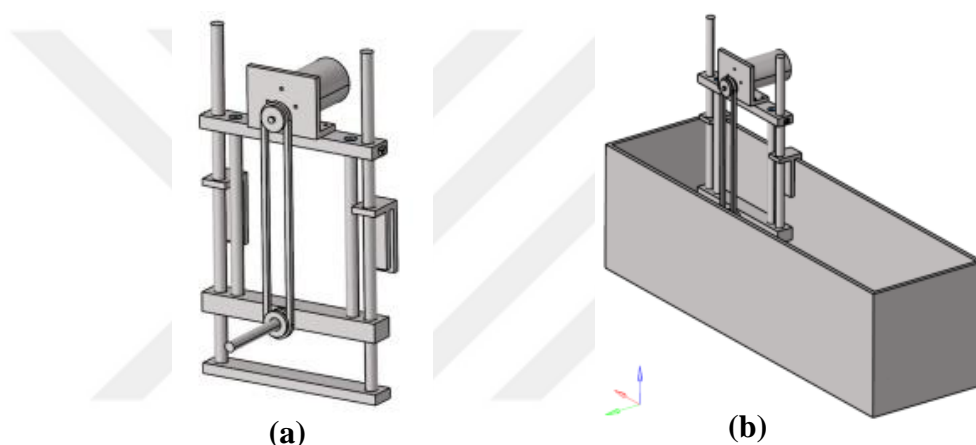


Figure 4.2 : Schematic view of the (a) designed spinning device, (b) spinning device with coagulation bath

Two NEW ERA-NE300 syringe pumps were used to pump the bore solvent and spinning dope solution. A general view of the installed hollow fiber spinning system was given in Figure 4.3.

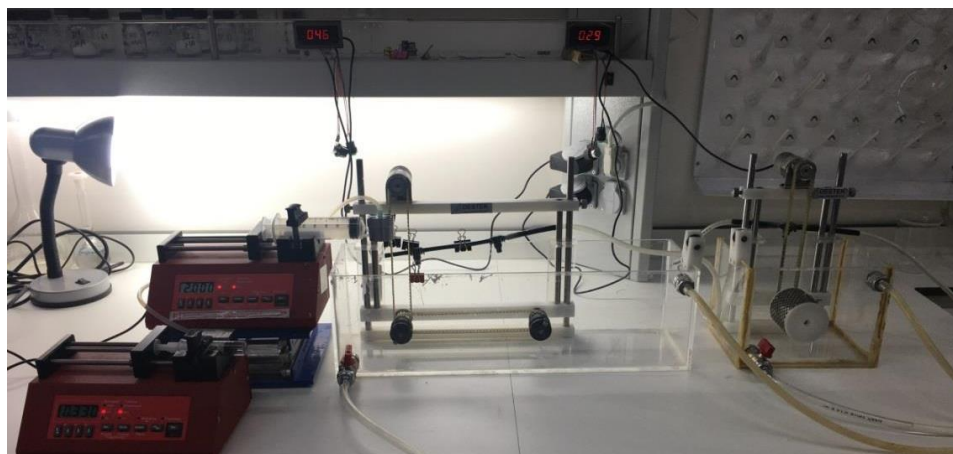


Figure 4.3 : General view of the hollow fiber spinning system

4.2.4 Preparation of the dope solutions

Pristine PVDF (HFM-0) and synthesized polymers added (HFM-P(HA-co-NIPAAm) and HFM-P(HA-co-NNDMAAm)) membranes were prepared as seen in Table 4.1. While preparing membrane dope solutions, firstly, P(HA-co-NIPAAm) or P(HA-co-NNDMAAm) was dissolved in NMP by stirring at 60 °C for 2 h, then PVDF addition was made and stirring was continued for an extra 4 h, and the mixture was stirred overnight at 40 °C to obtain a homogeneous solution.

Table 4.1 : Dope solution compositions of the HFM.

Membranes	Component Compositions			
	PVDF (wt%)	P(HA-co-NIPAAm) (wt%)	P(HA-co-NNDMAAm) (wt%)	NMP (wt%)
HFM-0	18.00	-	-	82.00
HFM-P(HA-co-NIPAAm)	17.82	0.18	-	82.00
HFM-P(HA-co-NNDMAAm)	17.82	-	0.18	82.00

4.2.5 Spinning of the HFMs

HFMs were produced with established spinning line by phase inversion method. The polymer dope and bore liquid solutions were pumped into the spinneret by the help of syringe pumps. Distilled water was used as liquid dope solution. The pumping speeds of the polymer dope and bore liquid solutions were 2 mm/min and 0.33 mm/min, respectively. Three different air gap distances (50 mm, 100 mm, and 150 mm) between the spinneret and coagulation bath were used. After the fiber entered the coagulation bath (tap water), it was passed through the six spinning wheels (with 30 mm diameter), and wrapped around a perforated drum (with 61 mm diameter) in the winding bath. The fibers were kept in winding bath for 2 h in order to remove all solvent in the fiber structure, and then the produced HFMs were kept in distilled water. The spinning conditions of the produced HFMs were given in Table 4.2. As seen in the table, while the all other parameters were kept constant, the change in the membrane morphology with addition of the synthesized polymers and air gap distances were investigated.

Table 4.2 : Spinning conditions of the HFMs

Dope composition (wt %)	PVDF/synthesized polymers/NMP
Bore fluid component	Distilled water
External coagulant	Tap water
Dope flow rate (mL/min)	2.00
Bore fluid flow rate (mL/min)	0.33
Air gap distances (cm)	5 – 10 – 15
Spinneret outer diameter/inner diameter (mm)	1.55 / 0.55
Spinning velocity (cm/min)	175
Take-up velocity (cm/min)	185

4.2.6 Chlorination of the HFMs

A 10% aqueous solution of 6% sodium hypochlorite (household bleach) was prepared and the pH of the solution was adjusted to 7 with 6 N HCl. After the produced HFMs were waited in this solution for 1h, the unbonded chlorine on the membrane was removed by washing with tap and distilled water, and 1 h drying at 45 °C. Iodometric/thiosulfate titration was applied to determine the loaded chlorine concentration onto the samples (Kocer et al., 2010). A solution of ethanol with 0.1 N acetic acid (90/10; v/v) was prepared and 0.25 g potassium iodide was dissolved in this solution, then the dried membrane sample was added to the solution. Titration was made with 0.005 N sodium thiosulfate solution until the color of the solution is yellow to clear. The weight percent of the loaded chlorine (Cl^+) on the membrane samples were calculated according to the equation 2.1.

4.2.7 Preparation of the hollow fiber test modules

Preparation of the hollow fiber test modules was given step by step in Figure 4.4. A hollow fiber bundle was created with 6 fibers. The bundle was wrapped with a paste and placed in a syringe as seen in the Figure 4.4a and b, respectively. Then, the syringe was filled with water in order to prevent drying of the fibers. After that, as seen in the Figure 4.4c, epoxy was poured on the paste and waited until the epoxy resin was cured. SR 8100 epoxy resin (Sicomin) and SD 882x hardener (Sicomin)

were used with a ratio of 100/22 (wt/wt). Modules were made ready to outside-in type dead-end filtration test by cutting the fibers from the ends.

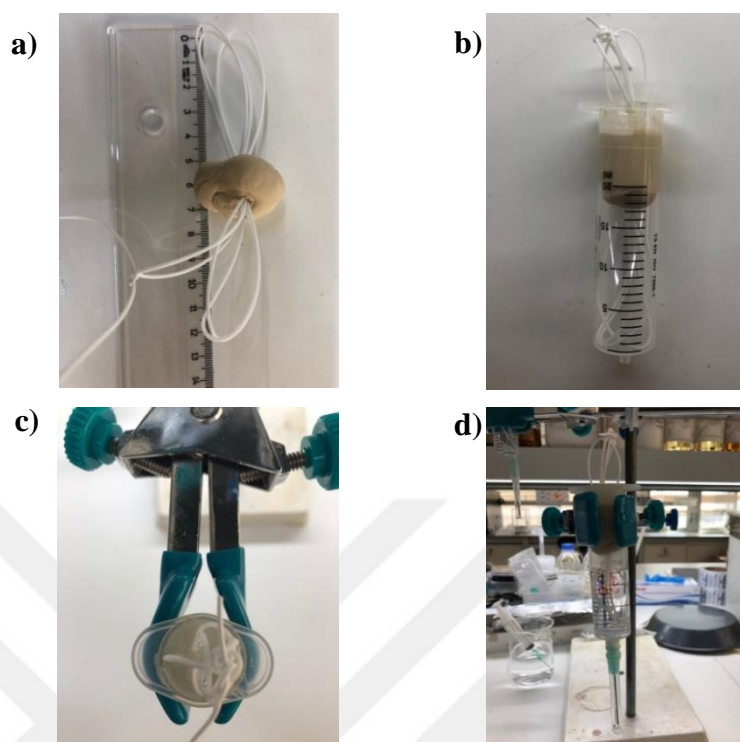


Figure 4.4 : Preparation of the HFM test modules

4.2.8 Permeability tests of the HFMs

Dead-end filtration test method with outside-in flow was used to determine water flux performances of the HFMs. The installed dead-end filtration system with HP4750 Sterlitech stirred cell was modified for HFM module tests as seen in Figure 4.5. The HFM modules were connected to the stirred cell with help of a hose. The effective membrane filtration area was calculated for each module separately. Water filtration experiments were performed under two different constant pressures of 1 and 2 bars. The pure water fluxes (L/m^2h) of the produced membranes were calculated according to the equation 2.2.

A phosphate buffer solution (0.1 M, pH 7) containing 1 g/L BSA was prepared to perform BSA rejection tests. The protein content in filtrated solution after one hour filtration was determined with UV-Visible spectrophotometer at 280 nm wavelength. Scinco-NEOSYS200 UV-Visible spectrophotometer was used for analysis and the rejection ratios of the produced membranes were calculated according to the equation 2.3. For the pure water flux and BSA rejection performances, two test modules were

prepared and tested, then the results were given as mean value along with the standard deviations.



Figure 4.5 : HFM module filtration test system

4.2.9 Characterization of the HFMs

FTIR and XPS analyses were not applied to HFMs since the presence of the synthesized polymers (P(HA-co-NIPAAm) and P(HA-co-NNDMAAm)) in the membrane structure had been proven in the section 3.

The surface morphology and cross-section of the HFMs were characterized with FEI, QUANTA 200F Field Emission scanning electron microscope. Images of gold-palladium coated (10 nm) membranes were obtained at 175x and 600x magnifications for cross-section, 5,000x and 50,000x magnifications for surface.

Biocidal performances of the HFMs were determined according to the ASTM E 2149. *Staphylococcus aureus* (ATCC 6538) and *Escherichia coli* (ATCC 35218) bacteria were used for tests. Bacteria suspension with 5.80×10^5 CFU/mL concentration were treated to the chlorinated (M*) and unchlorinated membrane samples. The 1 g of membrane samples were put in 50 mL bacteria suspension and shaken for three different contact times as 15 min, 30 min, and 60 min. Then serial dilutions with PBS were prepared and spread onto Muller-Hilton II agar plates. Before colonies were counted, the agar media was waited at 37 °C for 24 h and the bacterial reduction was determined as logarithmic.

4.3 Results and Discussion

4.3.1 Morphologies of the produced HFMs

SEM surface images of the HFMs produced with the copolymer additions and different air-gaps (a.g.) were given in Figure 4.6 with 5,000x and 50,000x magnifications. As seen in the Figure 4.6a the surface roughness of the HFMs were increase with the increase in air gap distance from 5 cm to 10 cm. When the air gap was further increased, the surface roughness was again decreased. For 5 cm air gap distance, the polymer chains entered the coagulation bath without finding time to be oriented. The membrane surface formation occurred like flat sheet membranes for 5 cm air gap distance. When the air gap distance increased to 10 cm, the elongational stress on the fiber also increased due to the gravity force. This increased stress on the fiber cause polymer chain orientation. The increase in the surface roughness of the fibers (produced with 10 cm air gap distance) could be caused by the water entering between the partially oriented polymer chains. On the other hand, when the air gap distance was increased to 15 cm, the polymer chains were more oriented with the increasing elongational force and formed a more stronger outer surface before entering the coagulation bath. As the coagulation fluid (tap water) could not easily penetrate between the polymer chains, the membrane surface roughness reduced with the increase air gap distance.

The SEM surface images of the HFMs with 50,000x magnification showed the pore size and pore size distribution on the membrane surface more clearly. As seen in the Figure 4.6b, the surface porosity of HFMs were increased when the air gap distance increase to 10 cm from 5 cm. However, when the air gap distance was further increased; the pore number on the HFM-P(HA-co-NIPAAm) surface decreased, the porosity of the HFM-0 and HFM-P(HA-co-NNDMAAm) increased. Chung and Hu (1997) explained that molecular chains oriented by a high elongational stress create porosity. The porosity changes observed on the membrane surface were confirmed by the water flux and BSA rejection performances of the HFMs.

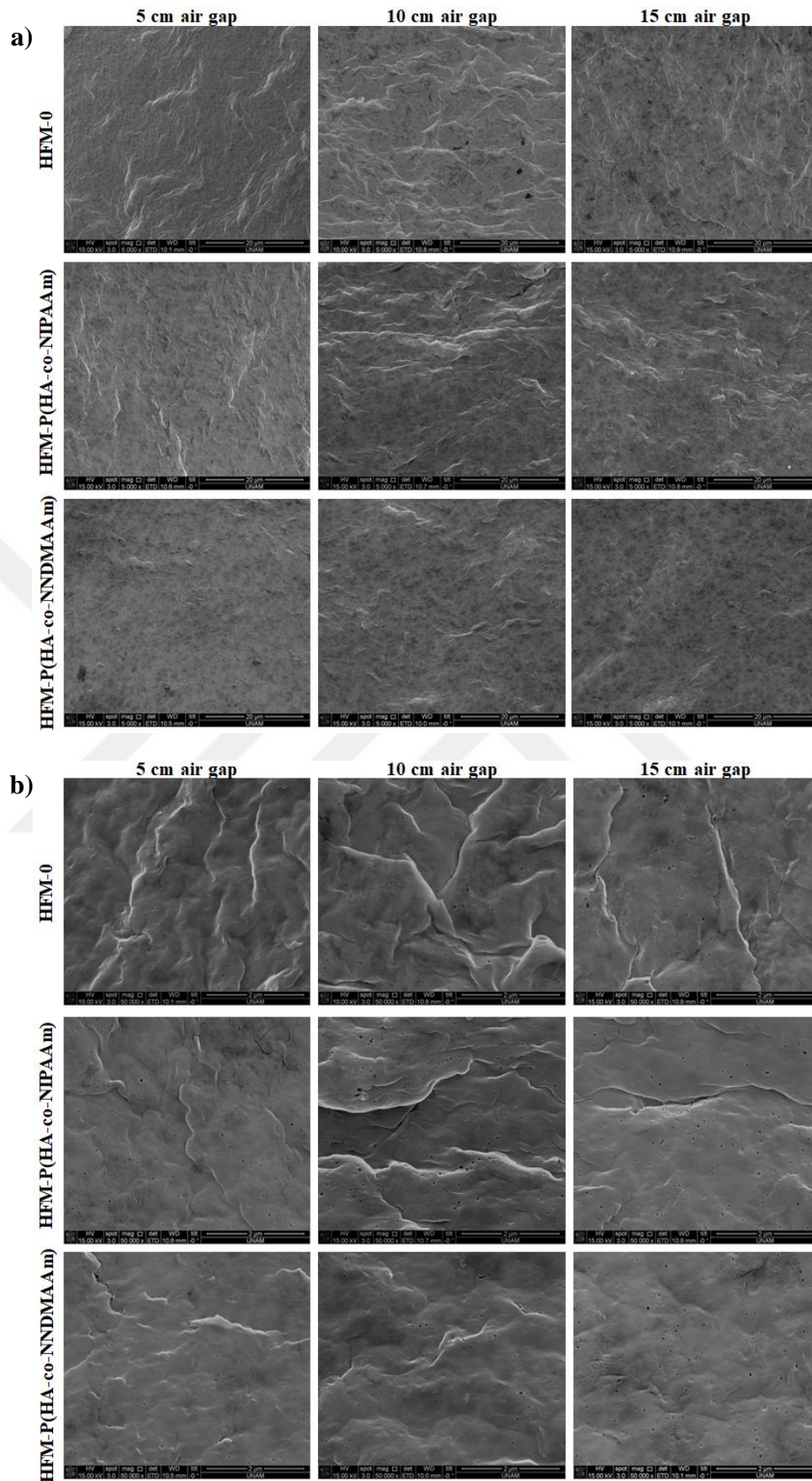


Figure 4.6 : Surface SEM images of the produced HFMs with a) 5,000x and b)50,000x magnifications

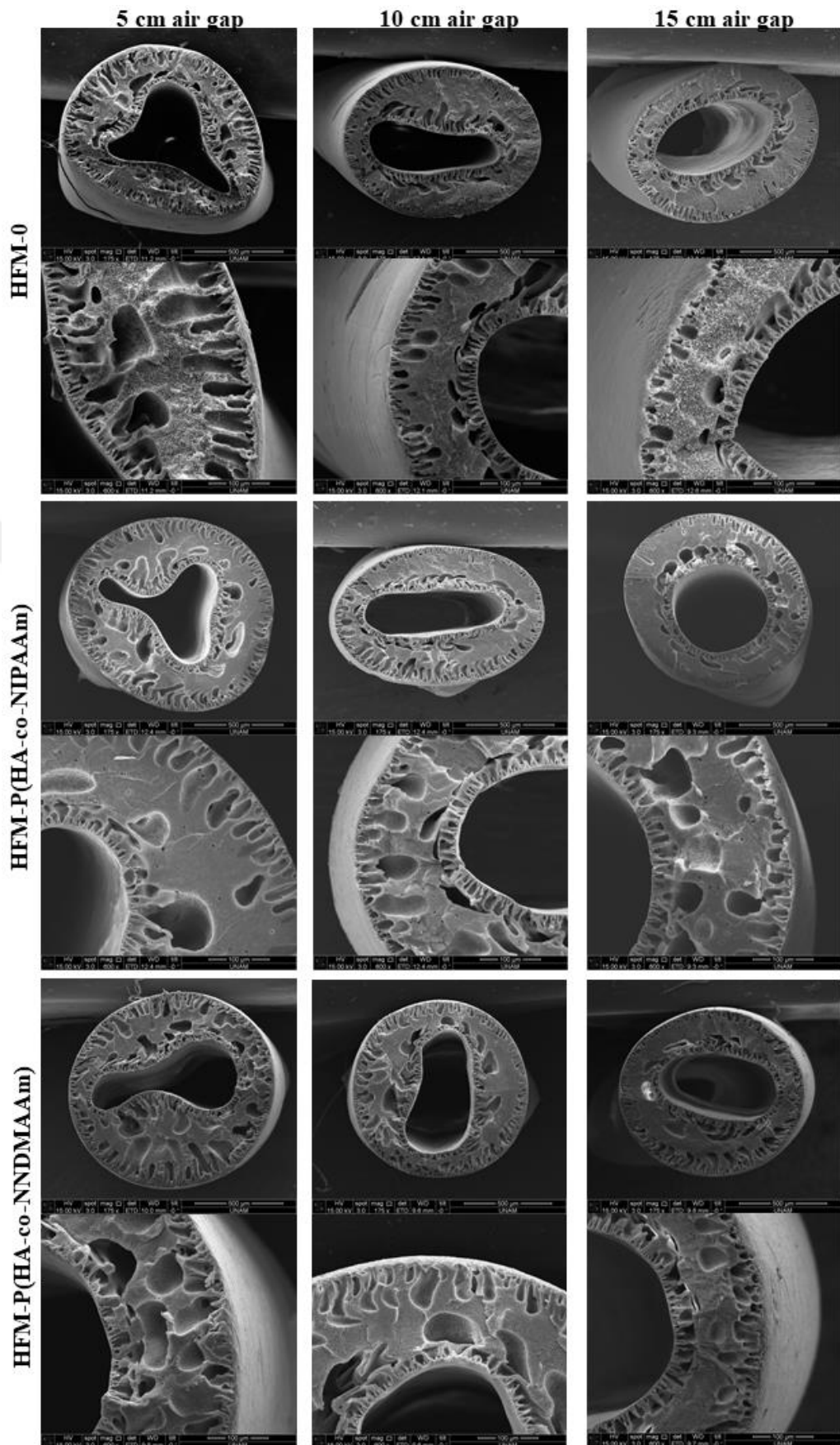


Figure 4.7 : Cross-section SEM images of the produced HFMs at 175x and 600x magnifications

The cross-section images of the produced HFMs were given in Figure 4.7 with 175x and 600x magnifications. As can be easily understood from the images, the irregular inner shape of the HFMs gained a circular form with increased air gap distance. All of the produced HFMs had approximately 1 mm diameter as intended to be similar to commercial water treatment HFMs. The hollow fibers produced with 5 cm air gap had finger like pores at both inner and outer sides of the fiber. These finger like pore formation was caused by the fast phase separation. The coagulation at inner side of the fiber began immediately without being affected by the air gap distance. Therefore, finger like pores were formed at the inner side of the all hollow fibers. However, finger like pore formation at the outer side of the fiber decreased as the air gap increased. The stronger outer layer formed by the elongational stress delayed the solvent-nonsolvent exchange on the outer surface of the fiber, so the formation of sponge like pore began to be observed instead of the finger like pores. An inhomogeneity was observed at the outer side pores of the hollow fibers produced with 10 cm and 15 cm air gap distances. This inhomogeneity could be due to one side of the fiber coming into contact with the wheel without being fully coagulated. This problem can be eliminated by increasing the length of the coagulation bath.

4.3.2 Filtration and BSA rejection performances of the HFMs

The pure water flux performances of the HFMs at 1 and 2 bar pressures were given in Figure 4.8. The water flux of the membranes were increased with addition of the synthesized polymers, P(HA-co-NIPAAm) and P(HA-co-NNDMAAm). The water flux performances of the HFM-0 and HFM-P(HA-co-NNDMAAm) increased with increasing air gap distance. However, the water flux performance of the HFM-P(HA-co-NIPAAm) was firstly increased with increasing air gap distance (from 5 cm to 10 cm), but then decreased with further increase in air gap distance. These results were consistent with the SEM images of the HFMs.

According to the hypothesis of this section, we expected to see a trend similar to the flat sheet membranes in the HFMs with the synthesized copolymers additions. However, while the P(HA-co-NIPAAm) added flat sheet membranes showed higher water flux performance (73.88 L/m²h) than the P(HA-co-NNDMAAm) added membranes (21.54 L/m²h) at 1 bar pressure, in the HFM form, an opposite trend was observed. The HFM-P(HA-co-NNDMAAm) (produced with 15 cm air gap distance)

showed 26.52 L/m²h at 1 bar being even higher than its flat sheet form. On the other hand, the water flux of the HFM-P(HA-co-NIPAAm) (produced with 15 cm air gap) was 10.04 L/m²h at 1 bar which was lower than the P(HA-co-NNDMAAm) added membrane.

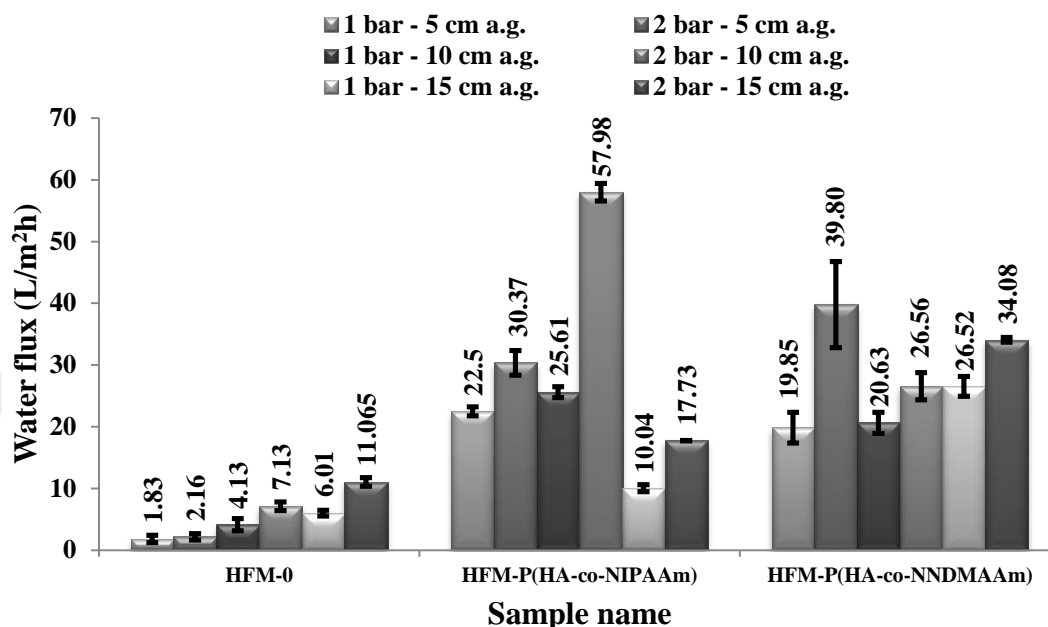


Figure 4.8 : Pure water flux performances of the produced HFMs

The BSA rejection performances of the produced HFMs were given in Figure 4.9. The BSA rejection performance of the M-0 was unable to determine due to the very low BSA solution flux. As seen in the Figure 4.9, the BSA rejection values of the HFMs were also consistent with SEM images similar to the water flux performances.

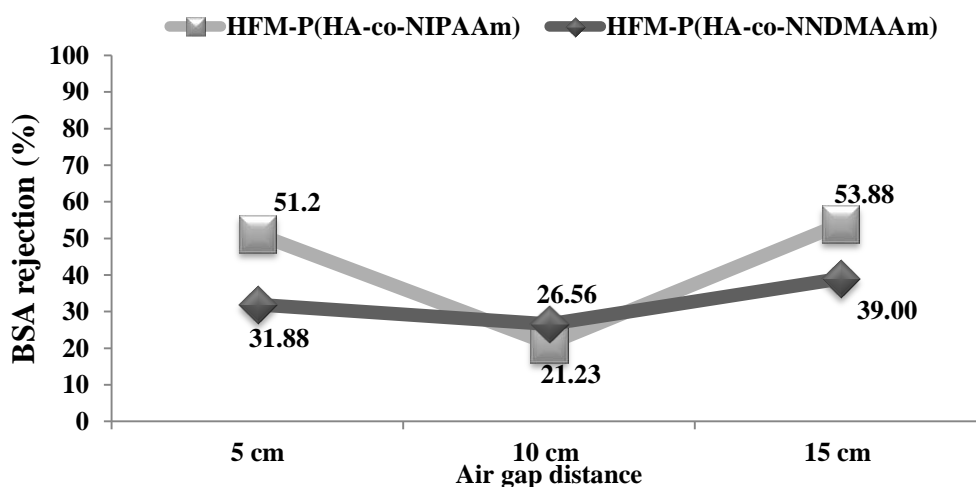


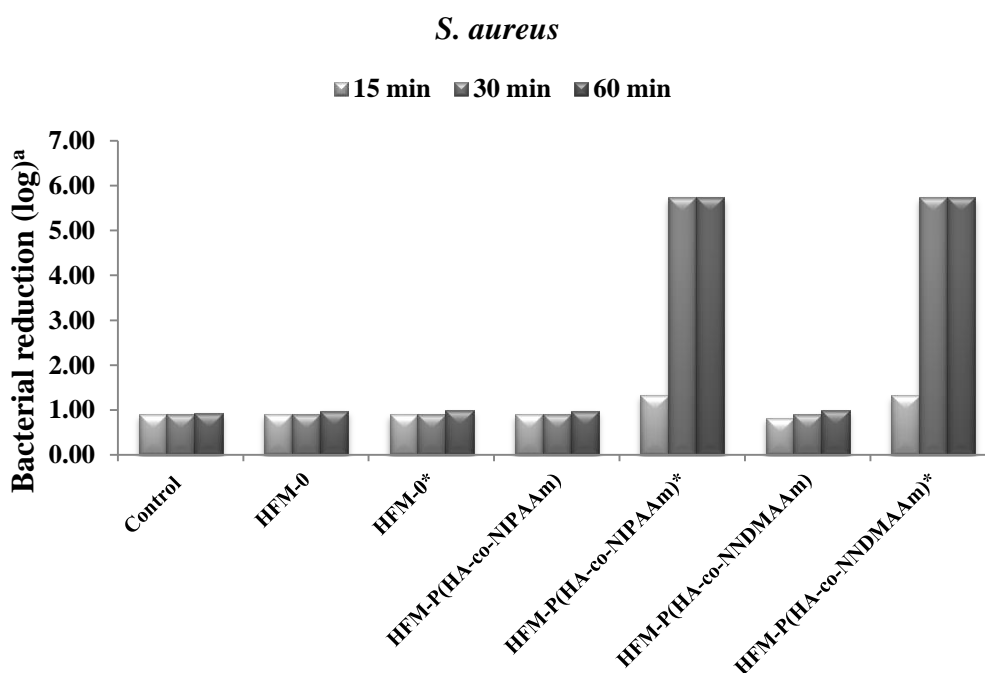
Figure 4.9 : BSA rejection performances of the produced HFMs

The BSA rejection performances of the P(HA-co-NIPAAm) and P(HA-co-NNDMAAm) added HFMs were not as good as their flat sheet analogs. The P(HA-

co-NNDMAAm) added flat sheet membranes showed the highest BSA rejection performance with 94.32%, however, there was a 55% decrease in its HFMs form. On the other hand, even the HFM-P(HA-co-NIPAAm) added membrane demonstrated the highest BSA rejection performance with 53.88%, it also showed approximately 20% reduction according to the its flat sheet membrane form.

4.3.3 Biocidal performances of the produced HFMs

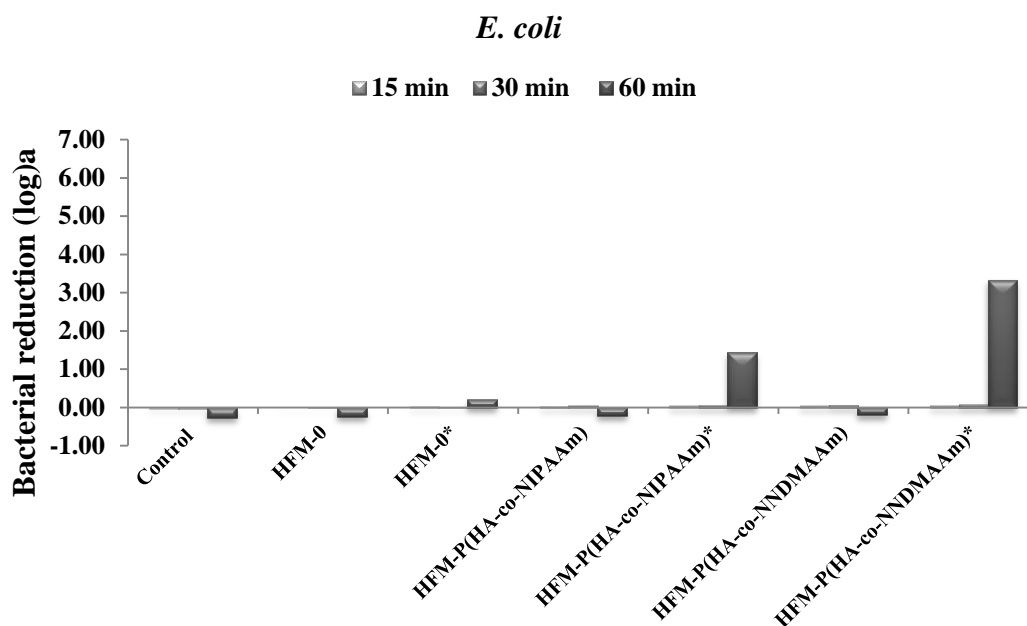
The biocidal performances of produced HFMs (both chlorinated and unchlorinated samples) were tested against *S.aureus* and *E.coli* at concentrations of about 10^5 CFU/mL, for various contact times as 15 min, 30 min, and 60 min. As seen in Figure 4.10, the control sample that was not include any membrane, the unchlorinated samples, and chlorinated sample of pristine PVDF membrane (HFM-0*) did not show inactivation even at the end of the 60 min. All of the synthesized polymers added membranes exhibited complete inactivation against *S.aureus* in a contact time of 30 min. But, for inactivation of *E.coli* more contact time was needed as seen in Figure 4.11.



^aThe inoculum concentration was 5.74 log for *S.aureus* (ATCC 6538)

*Chlorinated membranes

Figure 4.10 : Biocidal test against *S. aureus*



^aThe inoculum concentration was 5.76 log for *E. coli* (ATCC 35218)

*Chlorinated membranes

Figure 4.11 : Biocidal test against *E. coli*

4.4 Conclusion

A hollow fiber spinning line and a spinneret were designed and produced in this section of the study. HFMs were successfully produced with addition of the P(HA-co-NIPAAm) and P(HA-co-NNDMAAm) which showed the better water flux and BSA rejection performance in the previous section, respectively. The effects of the synthesized polymers addition and the air gap distance on the HFMs morphology was investigated with SEM images. It was found that both the polymers addition and the air gap distance caused a huge change on membrane morphology. With the increase in air gap distance irregular inner structure of the fiber changed to circular form. Also, the increase in air gap distance increase the elongational stress on the fiber causing orientation of the polymer chains and decreasing the coagulation rate of the membrane outer surface.

Since, the dead-end outside-in flow modules are used in the industrial water treatment applications; HFM modules were prepared which allow to the outside-in flow. Water filtration and BSA rejection performances of the HFMs were tested with the help of prepared modules. To check the accuracy of our hypothesis, the water flux and BSA rejection performances of the synthesized polymers added HFMs were compared with their flat sheet forms. The results showed that the additives did not

show the same effects in these two membrane forms. It was thought that the different effects of the polymers additives on these membrane performances could be resulted from the complexity of the HFMs formation according to the flat sheet form. While it was easy to explain the coagulation behavior of the flat sheet membranes with ternary phase diagram, some fiber spinning parameters such as the air-gap distance and take-up speed also affect the thermodynamic stability of the polymer solution in the hollow fiber form membrane production.

Lastly, biocidal effectiveness of the produced HFMs was tested against *S.aureus* and *E.coli*. Biocidal test results showed that addition of minute amount of the synthesized polymers can significantly improve the antibacterial performances of the produced HFMs.



5. CONCLUSIONS AND RECOMMENDATIONS

Ultrafiltration membranes have a large scale application in water treatments. Especially HFMs with high surface area to a certain volume are preferred in this application area. PVDF has received tremendous attentions in ultrafiltration membrane applications due to its good mechanical and film-forming properties, strong thermal and hydrolytic stabilities, outstanding anti-oxidation activities, excellent chemical resistance, and good solubility in many organic solvents. In contrast to all these advantages, the hydrophobic nature of the PVDF restricts its usage in water treatments. Even though this restriction is negotiated with hydrophilic additions, to overcome the biofouling, production of membranes having antibacterial properties is essential.

In this study, firstly suitable *N*-halamine polymers, which could be rechlorinated in every backwashing cycle, were chosen from literature. It was thought that, with addition of these polymers into the membrane, the biofilm formation on membrane surface would be reduced and the filtration performance of the membrane would be increased without hydrophilic additives. The changes in the membrane structure were observed by applying these agents. It was found that the water flux performance of the membranes could be improved without hydrophilic additions. The performances of the produced membranes were compared with a commercial membrane. While the water flux performances of the produced membranes were not as good as the commercial membrane, the BSA rejection performances of the M-HP1 was higher than the commercial membrane.

As a result of the observations in the second section, three novel *N*-halamine copolymers were designed to improve the water flux performance of the membrane and successfully synthesized in the third section. Between the synthesized three polymers, the P(HA-co-NIPAAm) improved the water flux performance of the membrane without changing the BSA rejection performance according to the M-HP1, on the other hand the P(HA-co-NDMAAm) slightly increased the water flux performance of the membrane but caused a huge increase in the BSA rejection

performance of the membrane. So these two polymers were chosen to incorporate into the HFM structure.

In the last section, a hollow fiber spinning line and spinneret were designed and produced. The chosen two *N*-halamine copolymers were added into the HFMs and the hollow fibers were produced as similar diameter with industrial applications. On the other hand, the air gap distances effects on the membrane morphology and performance were investigated. For filtration tests, the produced HFMs were packed in modules. The water flux performances of the produced HFMs were compared with their flat sheet forms and it was shown that due to the spinning parameters effects on the thermodynamic stability of the polymer solution in HMF spinning, the additives effect on the membrane performances were different for two membrane forms.

Although this study is expected to make significant contribution to solve membrane fouling problems and improve the membrane filtration performances, membrane performances can be more improved in future studies. Recommendations about these future studies are given below;

- New copolymers can be designed and synthesized to improve the membrane performances.
- Spinning parameters effects on the membrane morphology and performances can be studied.
- Polymer solution composition can be changed and the effect of the dope solution viscosity on HFM structure can be studied.
- Compositions of the inner fluid and coagulation bath can be changed to obtain different membrane morphologies.
- Coagulation bath length can be increased to obtain homogeneous pore structure on the outer side of the HFMs.
- The effect of the coagulation bath temperature can be studied.

REFERENCES

Akdag, A., Okur, S., McKee, M. L., Worley, S. D. (2006). The stabilities of N– Cl bonds in biocidal materials, *Journal of Chemical Theory and Computation*, 2(3), 879-884.

Antimicrobial Agents I. (2018). *Wikiversity*. Date retrieved: September 19, 2018, https://en.wikiversity.org/wiki/Antimicrobial_Agents_I

Aryanti, P. T. P., Hakim, A. N., Widodo, S., Widiasa, I. N., Wenten, I. G. (2018). Prospect and challenges of tight ultrafiltration membrane in drinking water treatment, *IOP Conference Series: Materials Science and Engineering*, 395(1), 012012.

Avlonitis, S., Hanbury, W. T., Hodgkiess, T. (1992). Chlorine degradation of aromatic polyamides, *Desalination*, 85(3), 321-334.

Baker, R. W. (2004). *Membrane Technology and Applications*. Hoboken, NJ.: John Wiley & Sons.

Bennett, A. (2012). Membrane technology: Developments in ultrafiltration technologies, *Filtration + Separation*, 49(6), 28-33.

Biocide. (2018). *Wikipedia*. Date retrieved: September 17, 2018, <https://en.wikipedia.org/wiki/Biocide>

Block, S. S. (2001). *Disinfection, sterilization, and preservation*. Philadelphia, PA.: Lippincott Williams & Wilkins.

Bogati, R., Goodwin, C., Marshall, K., Leung, K. T., Liao, B. Q. (2015). Optimization of chemical cleaning for improvement of membrane performance and fouling control in drinking water treatment, *Separation Science and Technology*, 50(12), 1835-1845.

Boributh, S., Chanachai, A., Jiratananon, R. (2009). Modification of PVDF membrane by chitosan solution for reducing protein fouling, *Journal of Membrane Science*, 342(1-2), 97-104.

Booshehri, A. Y., Wang, R., Xu, R. (2013). The effect of re-generable silver nanoparticles/multi-walled carbon nanotubes coating on the antibacterial performance of hollow fiber membrane, *Chemical Engineering Journal*, 230, 251-259.

Capelli, C. C. (1990). U.S. Patent No. 4,933,178. Kenosha, U.S. Patent and Trademark Office.

Causserand, C., Pellegrin, B., Rouch, J. C. (2015). Effects of sodium hypochlorite exposure mode on PES/PVP ultrafiltration membrane degradation, *Water Research*, 85, 316-326.

Chakrabarty, B., Ghoshal, A. K., Purkait, M. K. (2008). Preparation, characterization and performance studies of polysulfone membranes using PVP as an additive, *Journal of Membrane Science*, 315(1-2), 36-47.

- Chang, X., Wang, Z., Quan, S., Xu, Y., Jiang, Z., Shao, L.** (2014). Exploring the synergetic effects of graphene oxide (GO) and polyvinylpyrrolidone (PVP) on poly (vinylidene fluoride)(PVDF) ultrafiltration membrane performance, *Applied Surface Science*, 316, 537-548.
- Chapman, J. S.** (2003). Biocide resistance mechanisms, *International Biodeterioration & Biodegradation*, 51(2), 133-138.
- Chen, G. E., Sun, W. G., Kong, Y. F., Wu, Q., Sun, L., Yu, J., Xu, Z. L.** (2018). Hydrophilic Modification of PVDF Microfiltration Membrane with Poly (Ethylene Glycol) Dimethacrylate through Surface Polymerization, *Polymer-Plastics Technology and Engineering*, 57(2), 108-117.
- Chen, Y., Deng, Q., Xiao, J., Nie, H., Wu, L., Zhou, W., Huang, B.** (2007). Controlled grafting from poly (vinylidene fluoride) microfiltration membranes via reverse atom transfer radical polymerization and antifouling properties, *Polymer*, 48(26), 7604-7613.
- Chindera, K., Mahato, M., Sharma, A. K., Horsley, H., Kloc-Muniak, K., Kamaruzzaman, N. F., Kumar, S., McFarlane, A., Stach, J., Bentin, T., Good, L.** (2016). The antimicrobial polymer PHMB enters cells and selectively condenses bacterial chromosomes, *Scientific Reports*, 6, 23121.
- Chou, W. L., Yu, D. G., Yang, M. C.** (2005). The preparation and characterization of silver-loading cellulose acetate hollow fiber membrane for water treatment, *Polymers for Advanced Technologies*, 16(8), 600-607.
- Chung, T. S. & Hu, X.** (1997). Effect of air-gap distance on the morphology and thermal properties of polyethersulfone hollow fibers, *Journal of Applied Polymer Science*, 66(6), 1067-1077.
- Damodar, R. A., You, S. J., Chou, H. H.** (2009). Study the self cleaning, antibacterial and photocatalytic properties of TiO₂ entrapped PVDF membranes, *Journal of Hazardous Materials*, 172(2-3), 1321-1328.
- De Paula, G. F., Netto, G. I., Mattoso, L. H. C.** (2011). Physical and chemical characterization of poly(hexamethylene biguanide) hydrochloride, *Polymers*, 3(2), 928-941.
- Denyer, S. P.** (1995). Mechanisms of action of antibacterial biocides, *International Biodeterioration & Biodegradation*, 36(3-4), 227-245.
- Denyer, S. P., & Stewart, G. S. A. B.** (1998). Mechanisms of action of disinfectants, *International Biodeterioration & Biodegradation*, 41(3-4), 261-268.
- Dizman, B., Elasri, M. O., Mathias, L. J.** (2004). Synthesis and antimicrobial activities of new water-soluble bis-quaternary ammonium methacrylate polymers, *Journal of Applied Polymer Science*, 94(2), 635-642.
- Ettori, A., Gaudichet-Maurin, E., Schrotter, J. C., Aimar, P., Causserand, C.** (2011). Permeability and chemical analysis of aromatic polyamide based membranes exposed to sodium hypochlorite, *Journal of Membrane Science*, 375(1-2), 220-230.
- Fadilah, N. I. & Hassan, A. R.** (2016). Preparation, characterization and performance studies of active PVDF ultrafiltration-surfactants membranes containing PVP as additive, *Malasian Journal of Analytical Science*, 20(2), 335-341.

- Fakhru'l-Razi, A., Pendashteh, A., Abdullah, L. C., Biak, D. R. A., Madaeni, S. S., Abidin, Z. Z.** (2009). Review of technologies for oil and gas produced water treatment, *Journal of Hazardous Materials*, 170(2-3), 530-551.
- Feng, C. Y., Khulbe, K. C., Matsuura, T., Ismail, A. F.** (2013). Recent progresses in polymeric hollow fiber membrane preparation, characterization and applications, *Separation and Purification Technology*, 111, 43-71.
- Fontananova, E., Jansen, J. C., Cristiano, A., Curcio, E., Drioli, E.** (2006). Effect of additives in the casting solution on the formation of PVDF membranes, *Desalination*, 192(1-3), 190-197.
- Fraiese, A. P.** (1999). Choosing disinfectants, *Journal of Hospital Infection*, 43(4), 255-264.
- Gao, Y., & Cranston, R.** (2008). Recent advances in antimicrobial treatments of textiles, *Textile Research Journal*, 78(1), 60-72.
- Gram stain.** (2018). *Wikipedia*. Date retrieved: September 15, 2018, https://en.wikipedia.org/wiki/Gram_stain
- Gunawan, P., Guan, C., Song, X., Zhang, Q., Leong, S. S. J., Tang, C., Chen, Y., Chan-Park, M. B., Chang, M. W., Wang, K., Xu, R.** (2011). Hollow fiber membrane decorated with Ag/MWNTs: toward effective water disinfection and biofouling control, *Acs Nano*, 5(12), 10033-10040.
- Hammel, H. T. & Scholander, P. F.** (1976). *Perspectives on the Mechanism of Osmosis and Imbibition. In: Osmosis and Tensile Solvent*. Berlin, Heidelberg: Springer-Verlag.
- Hanafi, Y., Szymczyk, A., Rabiller-Baudry, M., Baddari, K.** (2014). Degradation of poly (ether sulfone)/polyvinylpyrrolidone membranes by sodium hypochlorite: insight from advanced electrokinetic characterizations, *Environmental Science & Technology*, 48(22), 13419-13426.
- Hilal, N., Kochkodan, V., Al-Khatib, L., Levadna, T.** (2004). Surface modified polymeric membranes to reduce (bio) fouling: a microbiological study using E. coli, *Desalination*, 167, 293-300.
- Hou, S., Dong, X., Zhu, J., Zheng, J., Bi, W., Li, S., Zhang, S.** (2017). Preparation and characterization of an antibacterial ultrafiltration membrane with N-chloramine functional groups, *Journal of Colloid and Interface Science*, 496, 391-400.
- Huang, Y. W., Wang, Z. M., Yan, X., Chen, J., Guo, Y. J., Lang, W. Z.** (2017). Versatile polyvinylidene fluoride hybrid ultrafiltration membranes with superior antifouling, antibacterial and self-cleaning properties for water treatment, *Journal of Colloid and Interface Science*, 505, 38-48.
- Idris, A., Man, Z., Maulud, A. S., Khan, M. S.** (2017). Effects of phase separation behavior on morphology and performance of polycarbonate membranes, *Membranes*, 7(2), 21-39.
- Ismail, A. F., Khulbe, K. C., Matsuura, T.** (2015). *Gas Separation Membranes, Polymeric and Inorganic*. Cham: Springer.
- Jeon, S., Rajabzadeh, S., Okamura, R., Ishigami, T., Hasegawa, S., Kato, N., Matsuyama, H.** (2016) The effect of membrane material and surface pore size on the fouling properties of submerged membranes, *Water*, 8(12), 602-613.

- Jönsson, A. S., & Trägårdh, G.** (1990). Ultrafiltration applications, *Desalination*, 77, 135-179.
- Kakahana, Y., Cheng, L., Fang, L. F., Wang, S. Y., Jeon, S., Saeki, D., Rajabzadeh, S., Matsuyama, H.** (2017). Preparation of positively charged PVDF membranes with improved antibacterial activity by blending modification: Effect of change in membrane surface material properties, *Colloids and Surfaces A: Physicochemical and Engineering Aspects*, 533, 133-139.
- Kaminski, J. J., Bodor, N., Higuchi, T.** (1976). N-halo derivatives III: Stabilization of nitrogen-chlorine bond in N-chloroamino acid derivatives, *Journal of Pharmaceutical Sciences*, 65(4), 553-557.
- Kang, B., Li, Y. D., Liang, J., Yan, X., Chen, J., Lang, W. Z.** (2016). Novel PVDF hollow fiber ultrafiltration membranes with antibacterial and antifouling properties by embedding *N*-halamine functionalized multi-walled carbon nanotubes (MWNTs), *RSC Advances*, 6(3), 1710-1721.
- Kang, G. & Cao, Y.** (2014). Application and modification of poly(vinylidene fluoride) (PVDF) membranes – A review, *Journal of Membrane Science*, 463, 145-165.
- Kocer, H. B., Worley, S. D., Broughton, R. M., Acevedo, O., Huang, T. S.** (2010). Effect of phenyl derivatization on the stabilities of antimicrobial *N*-chlorohydantoin derivatives, *Industrial & Engineering Chemistry Research*, 49(22), 11188-11194.
- Kocer, H. B., Worley, S. D., Broughton, R. M., Huang, T. S.** (2011a). A novel *N*-halamine acrylamide monomer and its copolymers for antimicrobial coatings, *Reactive and Functional Polymers*, 71(5), 561-568.
- Kocer, H. B., Cerkez, I., Worley, S. D., Broughton, R. M., Huang, T. S.** (2011b). Polymeric antimicrobial *N*-halamine epoxides, *ACS Applied Materials & Interfaces*, 3(8), 2845-2850.
- Koros, W. J., Ma, Y. H., Shimidzu, T.** (1996). Terminology for membranes and membrane processes (IUPAC Recommendations 1996), *Pure and Applied Chemistry*, 68(7), 1479-1489.
- Kou, L.** (2009). *Preparation and Application of Regenerable N-Halamine Biocidal Materials*, (Ph.D. Thesis). Graduate Faculty of Auburn University, Auburn, Alabama.
- Li, J. S., Liang, Y., Wang, H. Y., Sun, X. Y., Wang, L. J.** (2004). Preparation and characterization of TiO₂/PVDF composite hollow fiber membrane, *Acta Polymerica Sinica*, 5, 709–712.
- Li, N. N., Fane, A. G., Ho, W. S. W., Matsuura, T.** (2008). *Advanced Membrane Technology and Applications*. Hoboken, NJ.: John Wiley & Sons.
- Liang, S., Kang, Y., Tiraferri, A., Giannelis, E. P., Huang, X., Elimelech, M.** (2013). Highly hydrophilic polyvinylidene fluoride (PVDF) ultrafiltration membranes via postfabrication grafting of surface-tailored silica nanoparticles, *ACS Applied Materials & Interfaces*, 5(14), 6694-6703.
- Liu, B., Chen, C., Li, T., Crittenden, J., Chen, Y.** (2013). High performance ultrafiltration membrane composed of PVDF blended with its derivative copolymer PVDF-g-PEGMA, *Journal of Membrane Science*, 445, 66-75.

Liu, F., Hashim, N. A., Liu, Y., Abed, M. M., Li, K. (2011). Progress in the production and modification of PVDF membranes, *Journal of Membrane Science*, 375(1-2), 1-27.

Loeb, S. & Sourirajan, S. (1963). Sea Water Demineralization by Means of an Osmotic Membrane, *Advances in Chemistry*, 38, 117-132.

López-Pérez, P. M., da Silva, R. M., Pashkuleva, I., Parra, F., Reis, R. L., San Roman, J. (2009). Hydrophobic–electrostatic balance driving the LCST offset aggregation–redissolution behavior of N-Alkylacrylamide-based ionic terpolymers, *Langmuir*, 26(8), 5934-5941.

Lv, J., Zhang, G., Zhang, H., Zhao, C., Yang, F. (2018). Improvement of antifouling performances for modified PVDF ultrafiltration membrane with hydrophilic cellulose nanocrystal, *Applied Surface Science*, 440, 1091-1100.

Ma, Y., Shi, F., Ma, J., Wu, M., Zhang, J., Gao, C. (2011). Effect of PEG additive on the morphology and performance of polysulfone ultrafiltration membranes, *Desalination*, 272(1-3), 51-58.

Macedonio, F., Drioli, E., Gusev, A. A., Bardow, A., Semiat, R., Kurihara, M. (2012). Efficient technologies for worldwide clean water supply, *Chemical Engineering and Processing: Process Intensification*, 51, 2-17.

Maillard, J. Y. (2002). Bacterial target sites for biocide action, *Journal of Applied Microbiology*, 92, 16S-27S.

Mansouri, J., Simon, D., Ramaswamy, A. P., Chen, V., Weiss, T. (2009). Patent No. WO2009047154. European Patent Office.

McBain, A. J., Ledder, R. G., Moore, L. E., Catrenich, C. E., Gilbert, P. (2004). Effects of quaternary-ammonium-based formulations on bacterial community dynamics and antimicrobial susceptibility, *Applied and Environmental Microbiology*, 70(6), 3449-3456.

McDonnell, G. & Russell, A. D. (1999). Antiseptics and disinfectants: activity, action, and resistance, *Clinical Microbiology Reviews*, 12(1), 147-179.

Membrane technology. (2018). *Wikipedia*. Date retrieved: July 01, 2018, https://en.wikipedia.org/wiki/Membrane_technology

Meng, J. Q., Chen, C. L., Huang, L. P., Du, Q. Y., Zhang, Y. F. (2011). Surface modification of PVDF membrane via AGET ATRP directly from the membrane surface, *Applied Surface Science*, 257(14), 6282-6290.

Meyer, J. & Ulbricht, M. (2018). Poly (ethylene oxide)-block-poly (methyl methacrylate) diblock copolymers as functional additive for poly(vinylidene fluoride) ultrafiltration membranes with tailored separation performance, *Journal of Membrane Science*, 545, 301-311.

Mohammad, A. W., Teow, Y. H., Ang, W. L., Chung, Y. T., Oatley-Radcliffe, D. L., Hilal, N. (2015). Nanofiltration membranes review: recent advances and future prospects, *Desalination*, 356, 226-254.

Moch Jr, I. (2005). Membranes, hollow-fiber, Kirk-Othmer Encyclopedia of Chemical Technology. doi:10.1002/0471238961.0815121213150308.a01.pub2

- Morato, J., Mir, J., Codony, F., Mas, J., Ribas, F.** (2003). Microbial response to disinfectants. In Mara, D. Horan, N. J. (Ed.). *Handbook of Water and Wastewater Microbiology* (pp. 657-694). London: Academic Press.
- Mulder, M.** (1996). *Basic Principles of Membrane Technology*. Norwell, MA.: Kluwer Academic Publishers.
- Ngang, H. P., Ahmad, A. L., Low, S. C., Ooi, B. S.** (2014). The influence of PEG additive on the morphology of PVDF ultrafiltration membranes and its antifouling properties towards proteins separation, *Jurnal Teknologi*, 70(2), 23-27.
- Nguyen, S. T. & Roddick, F. A.** (2011). Chemical cleaning of ultrafiltration membrane fouled by an activated sludge effluent, *Desalination and Water Treatment*, 34(1-3), 94-99.
- Nunes, S. P., Sforça, M. L., Peinemann, K. V.** (1995). Dense hydrophilic composite membranes for ultrafiltration, *Journal of Membrane Science*, 106(1-2), 49-56.
- Osmosis.** (2018). *Wikipedia*. Date retrieved: July 03, 2018, <https://en.wikipedia.org/wiki/Osmosis>
- Oxidizing Agents.** (2018). *Merc Manual*. Date retrieved: September 19, 2018, <https://www.merckvetmanual.com/pharmacology/antiseptics-and-disinfectants/oxidizing-agents>
- Pearce, G. K.** (2010). SWRO pre-treatment: Integrity and disinfection. *Filtration & Separation*, 47(1), 32-35.
- Pellegrin, B., Prulho, R., Rivaton, A., Thérias, S., Gardette, J. L., Gaudichet-Maurin, E., Causserand, C.** (2013). Multi-scale analysis of hypochlorite induced PES/PVP ultrafiltration membranes degradation, *Journal of Membrane Science*, 447, 287-296.
- Peng, N., Widjojo, N., Sukitpaneenit, P., Teoh, M. M., Lipscomb, G. G., Chung, T. S., Lai, J. Y.** (2012). Evolution of polymeric hollow fibers as sustainable technologies: past, present, and future, *Progress in Polymer Science*, 37(10), 1401-1424.
- Porter, M. C.** (1990). *Handbook of Industrial Membrane Technology*. Westwood, NJ.: Noyes Publications.
- Puspitasari, V., Granville, A., Le-Clech, P., Chen, V.** (2010). Cleaning and ageing effect of sodium hypochlorite on polyvinylidene fluoride (PVDF) membrane, *Separation and Purification Technology*, 72(3), 301-308.
- Rahimi, S., Milani, A. S., Ghasemi, N., Shahi, S.** (2012). Antibacterial Agents in Dental Treatments. In Bobbarala, V. (Ed.). *Antimicrobial Agents* (pp. 333-344). Croatia: InTech.
- Rahimpour, A., Madaeni, S. S., Zereshki, S., Mansourpanah, Y.** (2009). Preparation and characterization of modified nano-porous PVDF membrane with high antifouling property using UV photo-grafting, *Applied Surface Science*, 255(16), 7455-7461.
- Rahimpour, A., Jahanshahi, M., Rajaeian, B., Rahimnejad, M.** (2011). TiO₂ entrapped nano-composite PVDF/SPES membranes: Preparation, characterization, antifouling and antibacterial properties, *Desalination*, 278(1-3), 343-353.

- Regula, C., Carretier, E., Wyart, Y., Sergent, M., Gésan-Guiziu, G., Ferry, D., Vincent, A., Boudot, D., Moulin, P.** (2013). Ageing of ultrafiltration membranes in contact with sodium hypochlorite and commercial oxidant: experimental designs as a new ageing protocol, *Separation and Purification Technology*, 103, 119-138.
- Resosudarmo, A., Razmjou, A., Li, H., Gunawan, A., Chen, V.** (2011). The effect of surface functionalization of TiO₂ nanoparticles on PES ultrafiltration hollow fibre membranes, *Chemeca 2011: Engineering a Better World: Sydney Hilton Hotel*, (pp. 199-208). NSW, Australia, 18-21 September.
- Russell, A. D.** (1999). Bacterial resistance to disinfectants: present knowledge and future problems, *Journal of Hospital Infection*, 43, S57-S68.
- Sadrzadeh, M. & Bhattacharjee, S.** (2013). Rational design of phase inversion membranes by tailoring thermodynamics and kinetics of casting solution using polymer additives, *Journal of Membrane Science*, 441, 31-44.
- Safarpour, M., Khataee, A., Vatanpour, V.** (2014). Preparation of a novel polyvinylidene fluoride (PVDF) ultrafiltration membrane modified with reduced graphene oxide/titanium dioxide (TiO₂) nanocomposite with enhanced hydrophilicity and antifouling properties, *Industrial & Engineering Chemistry Research*, 53(34), 13370-13382.
- Sawada, I., Fachrul, R., Ito, T., Ohmukai, Y., Maruyama, T., Matsuyama, H.** (2012). Development of a hydrophilic polymer membrane containing silver nanoparticles with both organic antifouling and antibacterial properties, *Journal of Membrane Science*, 387, 1-6.
- Serra, C., Clifton, M. J., Moulin, P., Rouch, J., Aptel, P.** (1998). Dead-end ultrafiltration in hollow fiber modules: Module design and process simulation, *Journal of Membrane Science*, 145(2), 159-172.
- Shi, H., Liu, F., Xue, L.** (2013). Fabrication and characterization of antibacterial PVDF hollow fiber membrane by doping Ag-loaded zeolites, *Journal of Membrane Science*, 437, 205-215.
- Simoncic, B., & Tomsic, B.** (2010). Structures of novel antimicrobial agents for textiles-a review, *Textile Research Journal*, 80(16), 1721-1737.
- Sun, X., Cao, Z., Porteous, N., Sun, Y.** (2010). Amine, melamine, and amide *N*-halamines as antimicrobial additives for polymers, *Industrial & Engineering Chemistry Research*, 49(22), 11206-11213.
- Susanto, H. & Ulbricht, M.** (2009). Characteristics, performance and stability of polyethersulfone ultrafiltration membranes prepared by phase separation method using different macromolecular additives, *Journal of Membrane Science*, 327(1-2), 125-135.
- Strathmann, H.** (2001). Membrane separation processes: current relevance and future opportunities, *AIChE Journal*, 47(5), 1077-087.
- Strathmann, H., Kock, K., Amar, P., Baker, R. W.** (1975). The formation mechanism of asymmetric membranes, *Desalination*, 16(2), 179-203.
- Timofeeva, L. & Kleshcheva, N.** (2011). Antimicrobial polymers: mechanism of action, factors of activity, and applications, *Applied Microbiology and Biotechnology*, 89(3), 475-492.

- Tsai, H. A., Kuo, C. Y., Lin, J. H., Wang, D. M., Deratani, A., Pochat-Bohatier, C., Lee, K. R., Lai, J. Y.** (2006). Morphology control of polysulfone hollow fiber membranes via water vapor induced phase separation, *Journal of Membrane Science*, 278(1-2), 390-400.
- Wang, H., Wang, Z. M., Yan, X., Chen, J., Lang, W. Z., Guo, Y. J.** (2017). Novel organic-inorganic hybrid polyvinylidene fluoride ultrafiltration membranes with antifouling and antibacterial properties by embedding *N*-halamine functionalized silica nanospheres, *Journal of Industrial and Engineering Chemistry*, 52, 295-304.
- Wang, P., Tan, K. L., Kang, E. T., Neoh, K. G.** (2002). Plasma-induced immobilization of poly (ethylene glycol) onto poly (vinylidene fluoride) microporous membrane, *Journal of Membrane Science*, 195(1), 103-114.
- Wang, Z., Yu, H., Xia, J., Zhang, F., Li, F., Xia, Y., Li, Y.** (2012). Novel GO-blended PVDF ultrafiltration membranes, *Desalination*, 299, 50-54.
- WHO.** (2017). Progress on drinking water, sanitation and hygiene: 2017 update and SDG baselines. Geneva: World Health Organization and the United Nations Children's Fund.
- Windler, L., Height, M., Nowack, B.** (2013). Comparative evaluation of antimicrobials for textile applications, *Environment International*, 53, 62-73.
- Witte, P. V. D., Dijkstra, P. J., Berg, J. W. A., Feijen, J.** (1996). Phase Separation Processes in Polymer Solutions in Relation to Membrane Formation, *Journal of Membrane Science*, 117(1-2), 1-31.
- Wu, R.** (2004). *Preparation, Bioactivity, and Application of Novel Biocidal Materials*, (Ph.D. Dissertation). Graduate Faculty of Auburn University, Auburn, Alabama.
- WWAP (World Water Assessment Programme).** (2012). The United Nations World Water Development Report 4: Managing Water under Uncertainty and Risk (Volume 1). Paris: UNESCO.
- WWAP (United Nations World Water Assessment Programme).** 2016. The United Nations World Water Development Report 2016: Water and Jobs. Paris: UNESCO
- Yan, L., Li, Y. S., Xiang, C. B., Xianda, S.** (2006). Effect of nano-sized Al₂O₃-particle addition on PVDF ultrafiltration membrane performance, *Journal of Membrane Science*, 276(1-2), 162-167.
- Yang, L., Wei, J. F., Zhao, K. Y., Luo, Z. A.** (2013). Preparation of a hydrophilic PVDF membranes by electron beam induced grafting polymerization of acrylic acid, *Advanced Materials Research* 625, 273-276.
- Yao, F., Fu, G. D., Zhao, J., Kang, E. T., Neoh, K. G.** (2008). Antibacterial effect of surface-functionalized polypropylene hollow fiber membrane from surface-initiated atom transfer radical polymerization, *Journal of Membrane Science*, 319(1-2), 149-157.
- Yoo, S. H., Kim, J. H., Jho, J. Y., Won, J., Kang, Y. S.** (2004). Influence of the addition of PVP on the morphology of asymmetric polyimide phase inversion membranes: effect of PVP molecular weight, *Journal of membrane science*, 236(1-2), 203-207.

- Yoshimura, S. Minami, H.** (1998). U.S. Patent No. 5,709,870. Sakai-gun, U.S. Patent and Trademark Office.
- Yu, H., Zhang, X., Zhang, Y., Liu, J., Zhang, H.** (2013). Development of a hydrophilic PES ultrafiltration membrane containing SiO₂@ N-Halamine nanoparticles with both organic antifouling and antibacterial properties, *Desalination*, 326, 69-76.
- Yuliwati, E., Ismail, A. F., Matsuura, T., Kassim, M. A., Abdullah, M. S.** (2011). Effect of modified PVDF hollow fiber submerged ultrafiltration membrane for refinery wastewater treatment, *Desalination*, 283, 214-220.
- Zhang, X., Zhang, T., Ng, J., Sun, D. D.** (2009). High-performance multifunctional TiO₂ nanowire ultrafiltration membrane with a hierarchical layer structure for water treatment, *Advanced Functional Materials*, 19(23), 3731-3736.
- Zhang, X., Wang, D. K., Lopez, D. R. S., da Costa, J. C. D.** (2014). Fabrication of nanostructured TiO₂ hollow fiber photocatalytic membrane and application for wastewater treatment, *Chemical Engineering Journal*, 236, 314-322.
- Zhang, X., Ma, J., Tang, C. Y., Wang, Z., Ng, H. Y., Wu, Z.** (2016). Antibiofouling polyvinylidene fluoride membrane modified by quaternary ammonium compound: direct contact-killing versus induced indirect contact-killing, *Environmental Science and Technology*, 50(10), 5086-5093.
- Zhao, C., Xu, X., Chen, J., Yang, F.** (2013). Effect of graphene oxide concentration on the morphologies and antifouling properties of PVDF ultrafiltration membranes, *Journal of Environmental Chemical Engineering*, 1(3), 349-354.
- Zhao, X., Xuan, H., Chen, Y., He, C.** (2015). Preparation and characterization of superior antifouling PVDF membrane with extremely ordered and hydrophilic surface layer, *Journal of Membrane Science*, 494, 48-56.
- Zhao, Y. H., Qian, Y. L., Zhu, B. K., & Xu, Y. Y.** (2008). Modification of porous poly(vinylidene fluoride) membrane using amphiphilic polymers with different structures in phase inversion process, *Journal of Membrane Science*, 310(1-2), 567-576.
- Zhao, Z., Zheng, J., Wang, M., Zhang, H., Han, C. C.** (2012). High performance ultrafiltration membrane based on modified chitosan coating and electrospun nanofibrous PVDF scaffolds, *Journal of Membrane Science*, 394, 209-217.
- Zuo, D., Xu, Y., Xu, W., Zou, H.** (2008). The influence of PEG molecular weight on morphologies and properties of PVDF asymmetric membranes, *Chinese Journal of Polymer Science*, 26(4), 405-414.

APPENDICES

APPENDIX A: The technical drawings of the spinneret

APPENDIX B: The technical drawings of the spinning device



APPENDIX A

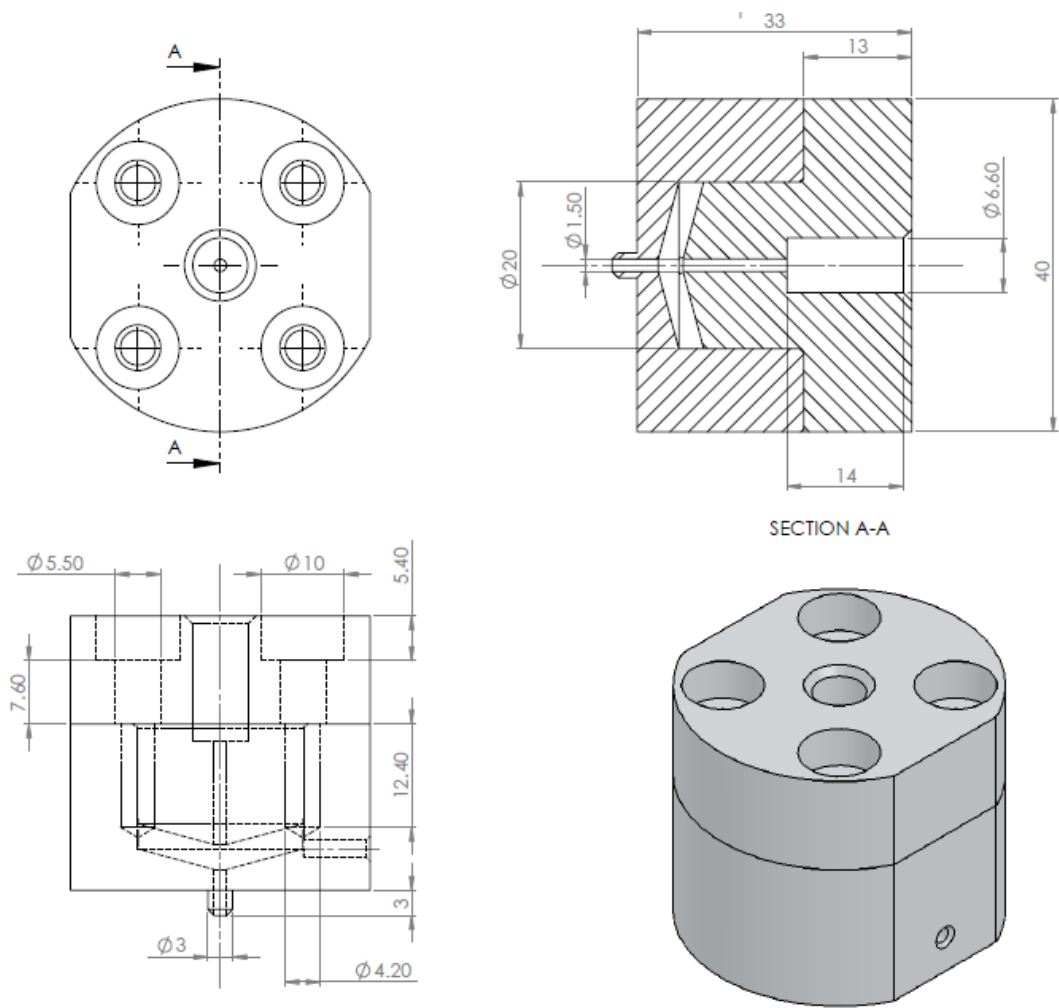


Figure A.1 : The technical drawings of the spinning device

APPENDIX B

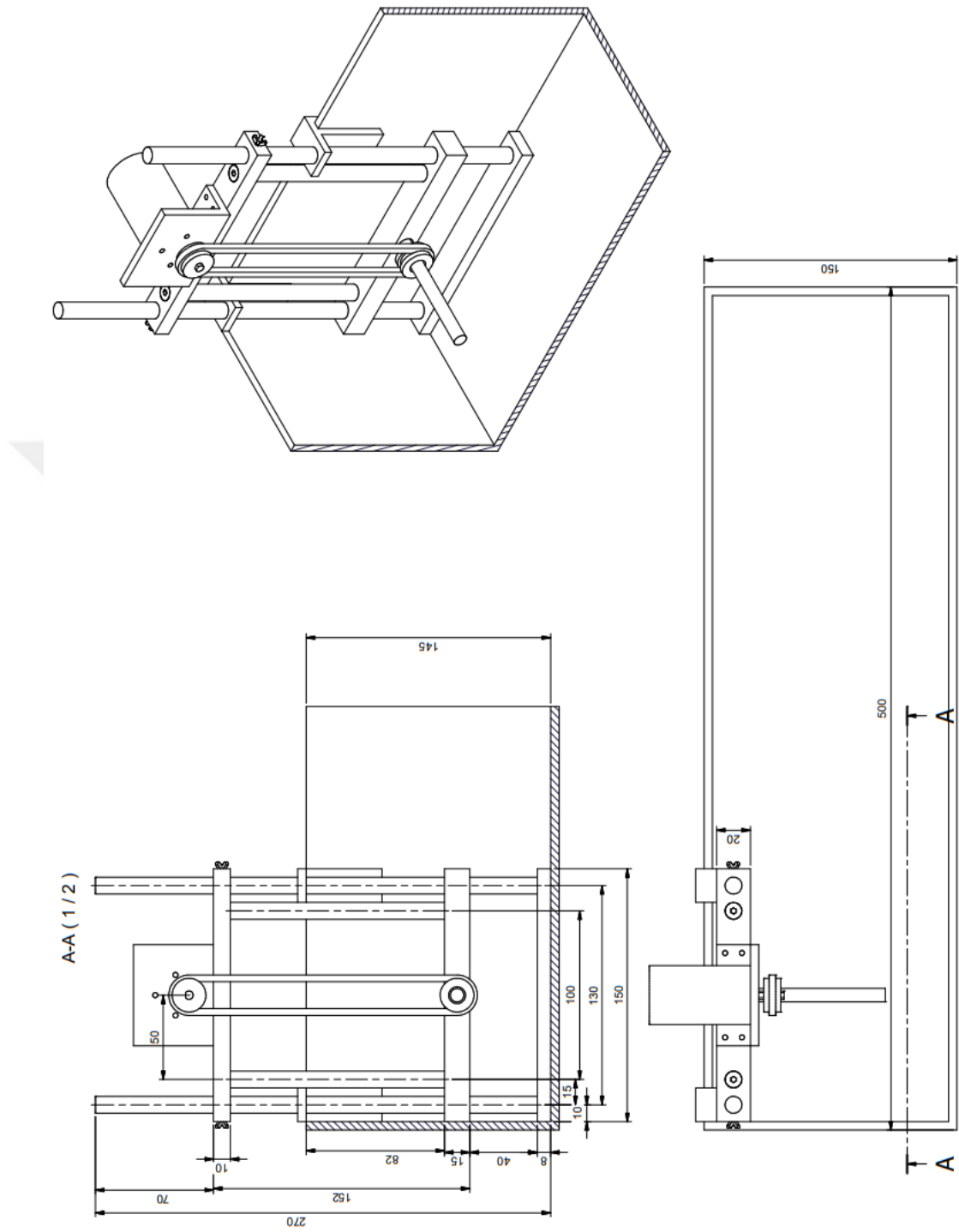


Figure B.2 : The technical drawings of the spinning device

CURRICULUM VITAE



Name Surname : Fatma DEMİRCİ
Date and Place of Birth : 10.03.1989 - Bursa
E-Mail : fatma.demirci@btu.edu.tr

EDUCATION:

- **B.Sc.** : 2012, Uludağ University, Faculty of Engineering, Textile Engineering
- **M.Sc.** : 2014, Bursa Technical University, Fiber and Polymer Engineering

PROFESSIONAL EXPERIENCE AND REWARDS:

- 2013 – Present Research Assistant, Fiber and Polymer Engineering, Bursa Technical University

PUBLICATIONS, PRESENTATIONS AND PATENTS ON THE THESIS:

- **Demirci, F., & Kocer, H. B.** (2018). Preparation of antibacterial polyvinylidene fluoride (PVDF) ultrafiltration membranes with direct addition of *N*-halamine polymers, *Separation Science and Technology*, doi: 10.1080/01496395.2018.1512622

OTHER PUBLICATIONS, PRESENTATIONS AND PATENTS:

- Aydin, A., **Demirci, F.**, Orhan, F., Kocer, H. B. (2018). Preparation of breathable polyurethane membranes with quaternary ammonium salt diols providing durable antibacterial property, *Journal of Applied Polymer Science*, doi: 10.1002/app.47133
- **Demirci, F.**, Yildirim, K., & Kocer, H. B. (2018). Antimicrobial open-cell polyurethane foams with quaternary ammonium salts, *Journal of Applied Polymer Science*, 135(9), 45914.

- Karahan, M., **Ozkan, F.**, Yildirim, K., & Karahan, N. (2016). Investigation of the Properties of Natural Fibre Woven Fabrics as a Reinforcement Materials for Green Composites, *Fibres & Textiles in Eastern Europe*, 4(118), 98-104.
- Kocer, H. B., **Ozkan, F.**, Broughton, R. M., & Worley, S. D. (2015). Treatment of melamine formaldehyde fibers for decontaminating biological and chemical warfare agents, *Journal of Applied Polymer Science*, 132(46), 42799.

